

R-08-65

Thermal properties Forsmark Modelling stage 2.3

Complementary analysis and verification of the thermal bedrock model, stage 2.2

Jan Sundberg, John Wrafter, Märta Ländell
Geo Innova AB

Pär-Erik Back, Lars Rosén
SWECO AB

November 2008

Svensk Kärnbränslehantering AB

Swedish Nuclear Fuel
and Waste Management Co
Box 250, SE-101 24 Stockholm
Tel +46 8 459 84 00



Thermal properties Forsmark Modelling stage 2.3

Complementary analysis and verification of the thermal bedrock model, stage 2.2

Jan Sundberg, John Wrafter, Märta Ländell
Geo Innova AB

Pär-Erik Back, Lars Rosén
SWECO AB

November 2008

This report concerns a study which was conducted for SKB. The conclusions and viewpoints presented in the report are those of the authors and do not necessarily coincide with those of the client.

A pdf version of this document can be downloaded from www.skb.se.

Preface

This report presents the thermal site descriptive model for the Forsmark area, stage 2.3. In stage 2.2 /Back et al. 2007/ a thermal model was presented for two rock domains, namely RFM029 and RFM045. Stage 2.3 focuses on a re-modelling of rock domain RFM045, which has a more heterogeneous geology comprising a significant proportion of low-conductive rock of mafic composition. Thermal modelling is based on the strategy reported in /Back and Sundberg 2007/.

John Wrafter had responsibility for the intensive discussions with the geologists in the Forsmark modelling team, in particular Michael Stephens, regarding the division of domain RFM045 into thermal subdomains, and for the coordination of the geological simulations. Lars Rosén has been responsible for the implementation of the geological simulations. Pär-Erik Back has among other things been responsible for verifying the analysis of the results in stage 2.2. Jan Sundberg is the editor of this report and was responsible for the internal review process.

In addition to the authors, the following persons have participated in the project: Nils Kellgren (stochastic geologic simulations) and Tommy Norberg (transformation and statistical analysis of stochastic geologic simulations) and Anders Sundberg (thermal modelling). Pär Kinnbom produced the WellCAD diagrams.

Lars O Ericsson (Chalmers University of Technology, Göteborg) reviewed an earlier draft of this report.

Summary

This report presents the results of thermal modelling work for the Forsmark area carried out during modelling stage 2.3. The work complements the main modelling efforts carried out during modelling stage 2.2 and reported in /Back et al. 2007/. A revised spatial statistical description of the rock mass thermal conductivity for rock domain RFM045 is the main result of this work.

Thermal modelling of domain RFM045 in Forsmark model stage 2.2 gave lower tail percentiles of thermal conductivity that were considered to be conservatively low due to the way amphibolite, the rock type with the lowest thermal conductivity, was modelled. New and previously available borehole data are used as the basis for revised stochastic geological simulations of domain RFM045. By defining two distinct thermal subdomains, these simulations have succeeded in capturing more of the lithological heterogeneity present. The resulting thermal model for rock domain RFM045 is, therefore, considered to be more realistic and reliable than that presented in model stage 2.2 /Back et al. 2007/.

The main conclusions of modelling efforts in model stage 2.3 are:

- Thermal modelling indicates a mean thermal conductivity for domain RFM045 at the 5 m scale of 3.56 W/(m·K). This is slightly higher than the value of 3.49 W/(m·K) derived in model stage 2.2.
- The variance decreases and the lower tail percentiles increase as the scale of observation increases from 1 to 5 m. Best estimates of the 0.1 percentile of thermal conductivity for domain RFM045 are 2.24 W/(m·K) for the 1 m scale and 2.36 W/(m·K) for the 5 m scale. This can be compared with corresponding values for domain RFM029 of 2.30 W/(m·K) for the 1 m scale and 2.87 W/(m·K) for the 5 m scale /Back et al. 2007/.
- The reason for the pronounced lower tail in the thermal conductivity distribution for domain RFM045 is the presence of large bodies of the low-conductive amphibolite.
- The modelling results for domain RFM029 presented in model stage 2.2 are still applicable.
- As temperature increases, the thermal conductivity decreases. This temperature dependence tends to decrease as the thermal conductivity decreases.
- Heat capacity: Domains RFM029 and RFM045 have a mean heat capacity of 2.06 MJ/(m³·K) and 2.12 MJ/(m³·K) respectively.
- The mean in situ temperatures at 400 m, 500 m and 600 m depth are estimated at 10.5°C, 11.6°C, and 12.8°C respectively, and are therefore unchanged compared to model stage 2.2.
- The estimates of the TRC (thermal rock class) proportions in domain RFM029 are considerably more reliable than those for domain RFM045. For the latter, the small number of boreholes in combination with the higher degree of lithological heterogeneity results in rather large uncertainties in the estimated proportions.
- The aspect of the thermal model with the highest confidence is the thermal conductivity distribution of domain RFM029, because of its higher degree of lithological and thermal homogeneity compared to domain RFM045.
- The aspect of the thermal model with the lowest confidence is the lower tail of the thermal conductivity distribution for rock domain RFM045. This uncertainty is related to the spatial and size distribution of amphibolite in domain RFM045.

Contents

1	Introduction	7
1.1	Background	7
1.2	Scope and objectives	8
1.3	Previous model versions	8
1.4	This report	8
2	Overview and assessment of investigation data	11
2.1	Databases	11
2.2	Borehole orientation data	12
2.3	Heat capacity	12
2.4	Temperature dependence in thermal properties	12
2.5	Pressure dependence in thermal conductivity	15
2.6	Thermal conductivity vs heat capacity	15
2.7	In situ temperature	16
	2.7.1 Method	16
	2.7.2 Results	18
2.8	Geology from boremap	25
2.9	WellCAD borehole plots	25
3	Modelling approach	27
3.1	Introduction	27
3.2	Outline of the methodology	27
4	Geostatistical analyses and stochastic simulations of geology in domain RFM045	29
4.1	General	29
4.2	Modelling assumptions	29
4.3	Description of geological input	30
	4.3.1 Thermal Rock Classes (TRC) – definition and properties	30
	4.3.2 Lithological borehole data: geological heterogeneity and division into thermal subdomains	30
	4.3.3 Orientation and geometry of subordinate rock types in domain RFM045	32
4.4	Spatial statistical models of lithology (TRC)	35
	4.4.1 Introduction	35
	4.4.2 Spatial analysis	36
	4.4.3 Spatial properties – results	37
4.5	Stochastic simulation of lithology (TRC)	38
	4.5.1 Introduction	38
	4.5.2 Examples and visualisation of results	38
	4.5.3 Analysis and verification of results	40
5	Thermal domain model	45
5.1	Modelling results – domain RFM045	45
5.2	Modelling results – heat capacity	48
5.3	Evaluation of modelling results – domain RFM045	50
5.4	Quality control of thermal modelling – domain RFM029	52
	5.4.1 Uncertainties	52
	5.4.2 Comparison of results after upscaling	53
6	Thermal rock class proportions and size distributions	55
6.1	Uncertainties in thermal rock class proportions	55
	6.1.1 Introduction	55
	6.1.2 Data treatment and assumptions	55

6.1.3	Method for estimating confidence intervals	57
6.1.4	Results	57
6.1.5	Conclusions	60
6.2	Size distribution of TRCs	60
7	Summary of domain thermal properties	63
8	Uncertainties	65
8.1	Major data uncertainties	65
8.2	Major model uncertainties	65
8.3	Summing up	66
9	Conclusions	69
10	References	71
Appendix A	WellCAD borehole plots	73
Appendix B	Visualisations of TRC (lithology) and thermal conductivity realisations	87
Appendix C	Histogram of simulated and observed lengths	91
Appendix D	Mathematical description of the transformation of borehole data	97
Appendix E	TRC proportions and confidence intervals	103

1 Introduction

1.1 Background

The Swedish Nuclear Fuel and Waste Management Company (SKB) is undertaking site characterisation at two different locations, the Forsmark and Simpevarp/Laxemar areas, with the objective of siting a geological repository for spent nuclear fuel.

The heat generated by the spent nuclear fuel will increase the temperature of all components of the KBS-3 repository: barriers, tunnels, seals and the host rock itself. To ensure the long-term sealing capacity and the mechanical function of the bentonite buffer surrounding each individual canister, a maximum bentonite temperature is prescribed in the design basis. This important requirement, which relates to the safety assessment, means that the canisters cannot be deposited arbitrarily close to each other. Unnecessarily large distances between the canisters, on the other hand, will mean inefficient and costly use of the rock volume considered for the repository. In order to determine the minimum canister spacing required to meet the temperature criterion for all canister positions, also those in the least conductive parts of the different rock domains where near-field temperatures will be particularly high, it is necessary to establish an adequate description, of the site rock thermal properties and their spatial variation on the relevant canister scale. In addition to being needed for the design, or layout, issue, the thermal site model will be important for predicting the thermo-mechanical evolution of the repository host rock at different scales.

The complete site investigation (CSI) work comprises three stages, concluding with a final multi-disciplinary SDM for Forsmark, SDM-Site, during model stage 2.3. The most comprehensive thermal modelling efforts within the CSI were performed within model stage 2.2 /Back et al. 2007/. The results of complementary thermal modelling in model stage 2.3 for the Forsmark site are compiled in this report. The findings from both the 2.2 modelling stage and the supplementary 2.3 analyses are summarised in the final multi-disciplinary Site Descriptive Model, SDM, Forsmark /SKB 2008/.

The target volume at Forsmark comprises the rock volume identified as suitable for hosting a final repository. Two rock domains have been identified within the target volume. Domain RFM029 makes up the major part of the target volume and will constitute the bulk of any future repository volume. The much smaller domain RFM045 is also located within the intended repository volume. Thermal properties of domains RFM029 and RFM045 were evaluated during stage 2.2 /Back et al. 2007/.

Thermal modelling of domain RFM045 in Forsmark model stage 2.2 gave lower tail percentiles of thermal conductivity that were considered to be conservatively low /Back et al. 2007/. The reason for this conclusion was that geological simulations of domain RFM045 overestimated the importance/frequency of large bodies of amphibolite, the rock type with the lowest thermal conductivity of all rock types in Forsmark. Thus, the earlier results presented in /Back et al. 2007/ are no longer considered valid for domain RFM045. However, the results for domain RFM029 are still applicable.

For purposes of thermal modelling, rock types having similar compositions and thermal properties were assigned to the same thermal rock class (TRC) /Back et al. 2007/.

1.2 Scope and objectives

This report presents the results of thermal modelling work carried out during modelling stage 2.3. The work complements the main modelling efforts performed in modelling stage 2.2 and reported in /Back et al. 2007/.

The main objective of the thermal modelling stage 2.3 for Forsmark is to provide a revised spatial statistical description of the rock mass thermal conductivity for rock domain RFM045 because of the shortcomings, referred to in section 1.1, associated with the results of previous modelling efforts.

New and previously available borehole data are used as the basis for revised stochastic geological simulations of domain RFM045.

Other objectives of this modelling stage are:

- To calculate the uncertainties in the proportions of thermal rock classes (TRC) in rock domains RFM029 and RFM045.
- To update the description of the in situ temperature and the temperature gradient.
- To further evaluate the temperature dependence in thermal properties.
- To perform domain modelling of heat capacity based on an established relationship between thermal conductivity and heat capacity.
- To evaluate the remaining uncertainties in the understanding of the thermal properties.

The data employed to support the findings presented in this model originate from the Forsmark 2.3 data freeze. Compared to the previous data freeze, the only additional data of significance are the Boremap mapping data for borehole KFM08D.

The geological setting of the rock volume for which thermal properties are investigated is described in /Back et al. 2007/. For illustration of the surface geology, see Figure 1-1. The rock domain model (version 2.2) at the surface is shown in Figure 1-2.

1.3 Previous model versions

Based on thermal modelling performed as part of model version 2.2 /Back et al. 2007/, thermal properties were reported for two rock domains, namely RFM029 and RFM045. Best estimates of the 0.1 percentile of thermal conductivity for the 5 m scale are 2.87 W/(m·K) for domain RFM029 and 2.33 W/(m·K) for domain RFM045.

One of the main uncertainties of model version 2.2 concerns the lower tail percentiles of thermal conductivity for domain RFM045 which is related to how amphibolite was modelled. Based on relatively limited data, low-conductive amphibolite rock bodies were modelled as being significantly larger than in domain RFM029, resulting in an excessively heavy lower tail of the distribution of thermal conductivity for domain RFM045.

1.4 This report

The thermal modelling work presented in this report relies heavily on the methodology described in the strategy report for thermal modelling during site investigations, version 2.0 /Back and Sundberg 2007/. Integration of geological information critical to thermal modelling was performed through close cooperation with the geology modelling team.

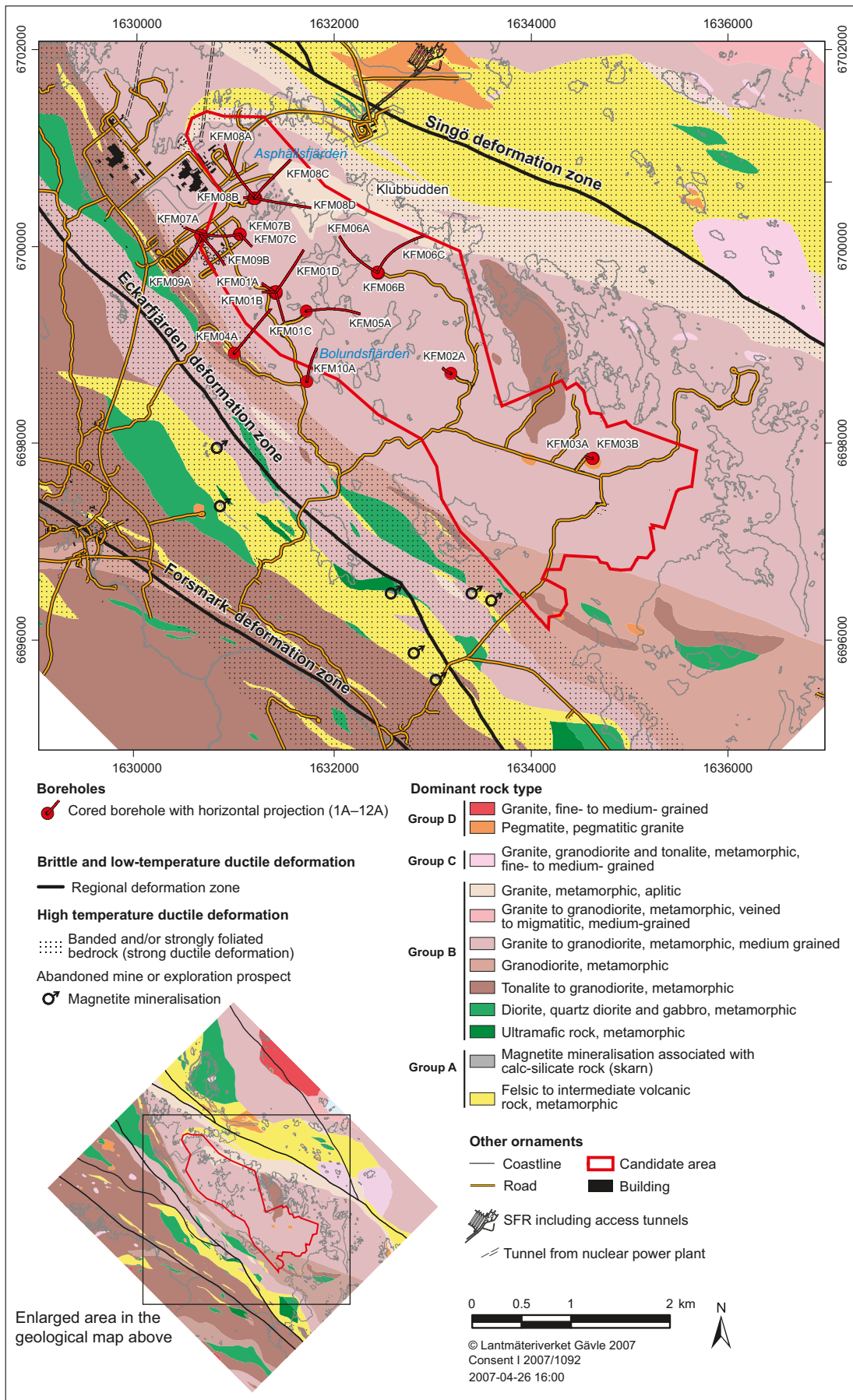


Figure 1-1. Geology of the Forsmark area and location of boreholes referred to in this report. The major groups of rocks are distinguished on the basis of their relative age, Group A being the oldest and Group D the youngest.

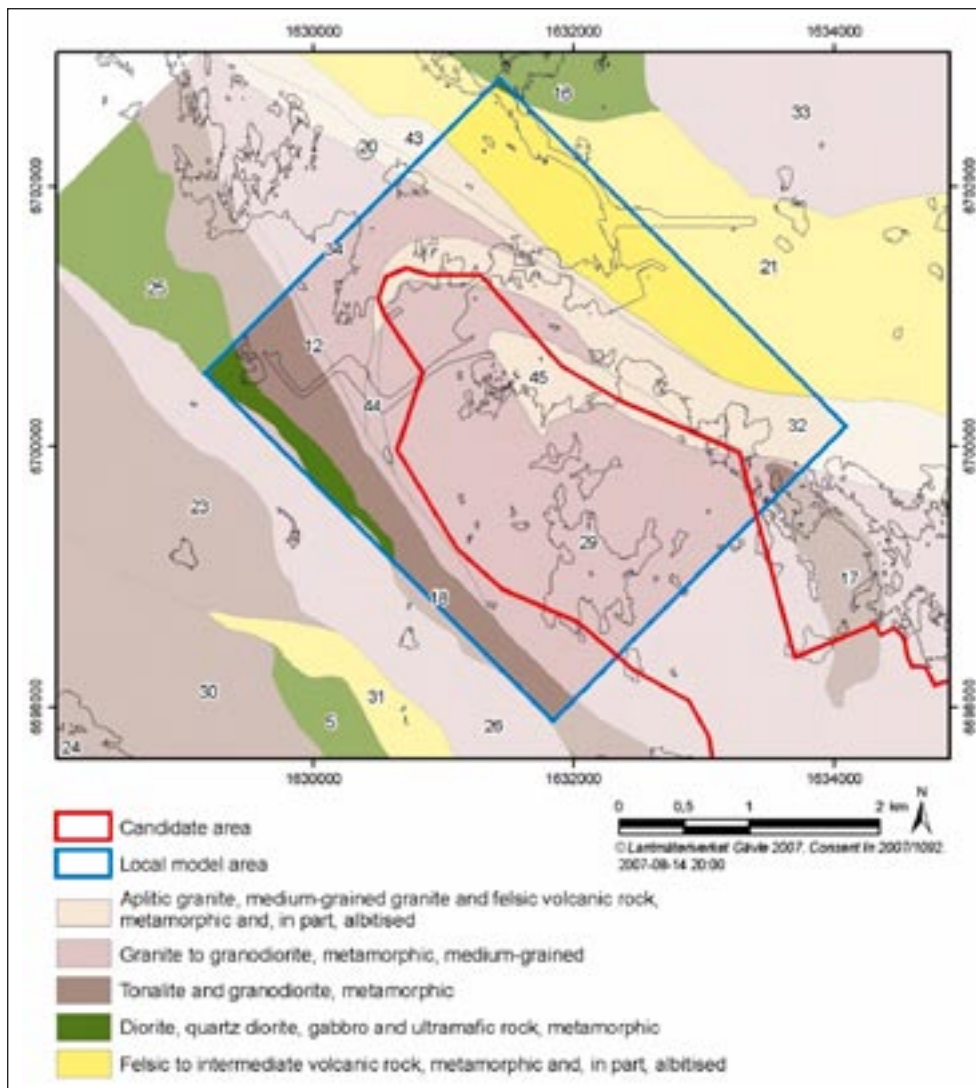


Figure 1-2. Rock domains at the surface in the Forsmark area.

Chapter 2 summarises the new primary data available for model stage 2.3. This chapter also presents complementary analysis of previously available primary data. Chapter 3 summarises the methodology employed for the thermal modelling.

The first part of Chapter 4 lists the main assumptions of the thermal modelling. This is followed by a description of aspects of the geology and the geological model that are relevant to thermal modelling. The last two sections of Chapter 4 address the spatial statistical models and simulation of lithologies for rock domain RFM045. Chapter 5 presents and evaluates the results of the thermal modelling at rock domain level. Chapter 6 deals with quantifying the uncertainties in the estimates of TRC proportions, and describing the size distribution of TRCs. Chapter 7 summarises the thermal properties at rock domain level. Chapter 8 addresses the uncertainties inherent in the thermal model. Chapter 9 summarises the conclusions of the thermal modelling work.

2 Overview and assessment of investigation data

2.1 Databases

The Forsmark thermal modelling stage 2.3 has used quality-assured primary data acquired prior to the data freeze dated 30th March, 2007. An overview of the data used in the complementary thermal modelling work conducted during stage 2.3 is compiled in Table 2-1. The main additions to the database between data freezes 2.2 and 2.3 for the purpose of thermal modelling are:

- Boremap mapping of cored borehole KFM08D.
- In situ temperature logging of borehole KFM08D.

The primary data are described and evaluated in more detail in the subsequent sections of this chapter.

Table 2-1. Primary data and their treatment in Forsmark modelling stage 2.3. Report numbers in italics show data available at data freeze 2.2.

Data specification	Reference to data report		Usage in model stage 2.3, Analysis/Modelling
Data from core-drilled boreholes			
<i>Boremap mapping</i>			
KFM06A	<i>P-05-101</i>		Major and subordinate rock type distribution. Data used as input to stochastic simulation of lithologies.
KFM06C	<i>P-06-79</i>		
KFM08A	<i>P-05-203</i>		
KFM08D	<i>P-07-103</i>		
<i>Fluid temperature logging</i>			
KFM01A	<i>P-03-103</i>	<i>P-04-80</i>	Data used for describing natural temperature variations with depth.
KFM01B	<i>P-04-145</i>	<i>P-04-80</i>	
KFM01C	<i>P-06-123</i>	<i>P-06-152</i>	
KFM01D	<i>P-06-168</i>	<i>P-06-216</i>	
KFM02A	<i>P-04-97</i>	<i>P-04-98</i>	
KFM03A	<i>P-04-97</i>	<i>P-04-98</i>	
KFM04A	<i>P-04-144</i>	<i>P-04-143</i>	
KFM05A	<i>P-04-153</i>	<i>P-04-154</i>	
KFM06A	<i>P-05-17</i>	<i>P-05-51</i>	
KFM06C	<i>P-05-276</i>	<i>P-06-84</i>	
KFM07A	<i>P-05-159</i>	<i>P-05-119</i>	
KFM07B	<i>P-06-22</i>	<i>P-06-126</i>	
KFM07C	<i>P-07-04</i>	<i>P-07-78</i>	
KFM08A	<i>P-05-159</i>	<i>P-05-202</i>	
KFM08C	<i>P-07-05</i>	<i>P-06-258</i>	
KFM08D	<i>P-07-60</i>	<i>P-07-125</i>	
KFM09B	<i>P-06-123</i>	<i>P-06-152</i>	
KFM10A	<i>P-07-05</i>	<i>P-06-258</i>	
<i>Temperature data from Posiva flow-logging</i>			
KFM02A	<i>R-04-188</i>		Description of natural temperature variations with depth. For comparison with fluid temperature loggings.
KFM03A	<i>R-04-189</i>		
KFM04A	<i>R-04-190</i>		

2.2 Borehole orientation data

SKB /Munier and Stigsson 2007/ have attempted to identify errors and quantify uncertainties in the orientation of geological features in boreholes, e.g. fractures, rock contacts, which are measured using the Boremap system. The main sources of error and uncertainties are borehole deviation measurements that constrain the position and orientation of the borehole, and the orientation of the BIPS image, which affects the orientation of geological features measured in Boremap /Munier and Stigsson 2007/. The uncertainty in the position of the boreholes translates into uncertainty in the position of boundaries between rock units. This has implications for the stochastic simulation of lithologies, which uses borehole data as input. However, this uncertainty is, for most boreholes, less than 10 m in the horizontal plane and less than 6 m in the vertical dimension /Stephens et al. 2007/. Thus, the impact of the uncertainties for the geological simulations is judged to be low.

The positions of the drill core samples used for laboratory measurement of thermal properties are also affected by uncertainties in borehole deviation measurements. However, this positional data is not used in thermal modelling.

2.3 Heat capacity

There is an error in Table 3-18, p 42 in the thermal model report for Forsmark, stage 2.2 /Back et al. 2007/. Data for 111058 (granite, fine- to medium-grained) is incorrect. In Table 2-2, the correct data is presented.

2.4 Temperature dependence in thermal properties

The temperature dependence in thermal conductivity and heat capacity has only been investigated for the dominant granite (101057) in Forsmark. However, since the temperature dependence influences the thermal properties it may be important for the thermal design of the repository. Rock types that influence the lower tail of the thermal conductivity distribution have most impact on the thermal design, e.g. amphibolite (102017) and granite, granodiorite and tonalite (101051). In order to estimate the temperature dependence for other rock types,

Table 2-2 Heat capacity, determined by the TPS and calorimetric method (direct measurement) (MJ/m³·K) on the same samples.

Rock type	Sample location	TPS		Calorimetric		Number of samples
		mean	std dev.	mean	std dev.	
Granite to granodiorite, 101057	KFM01A, KFM01C, KFM01D, KFM07A and KFM08A	2.09	0.17	2.06	0.06	14*
Granite, granodiorite and tonalite, 101051	KFM01A, KFM01C, KFM05A and KFM06A	2.23	0.13	2.15	0.05	8
Granite, metamorphic, aplitic, 101058	KFM06A	2.05	0.05	2.01	0.02	3
Amphibolite, 102017	KFM01A, KFM01C, KFM01D and KFM05A	2.43	0.05	2.41	0.11	8
Felsic to intermediate volcanic rock, 103076	KFM01C	2.33	–	2.42	–	1
Granite, fine- to medium-grained, 111058	KFM01C, KFM04A, KFM05A and KFM06A	2.14	0.10	2.06	0.05	5

* Includes three altered samples.

comparisons have been made with similar rock types in the Laxemar/Simpevarp area /Sundberg et al. 2008/ and with literature data (mainly amphibolite). In Figure 2-1 and Figure 2-2, the thermal conductivity and heat capacity versus the temperature coefficient is described. For thermal conductivity, there is a tendency towards lower temperature dependence as the thermal conductivity decreases (Figure 2-1). The literature value for low conductive amphibolite is consistent with the Laxemar and Forsmark data. The other literature data have the same tendency but the temperature dependency is larger. The measurement of high conductive amphibolite is made on dry samples /Abdulagatov et al. 2006/ and may be an explanation for the high temperature dependence.

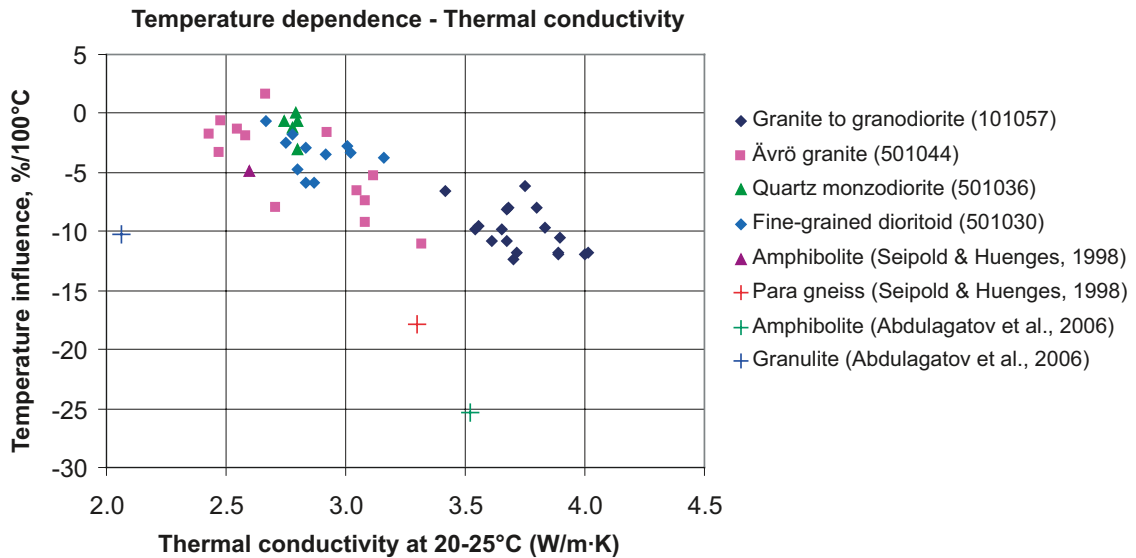


Figure 2-1. Thermal conductivity ($W/(m\cdot K)$) at 20–25°C versus the temperature coefficient ($\%/100^{\circ}C$) for the thermal conductivity in different rock types. Rock types with codes beginning with “50” are found in the Laxemar/Simpevarp area /Sundberg et al. 2008/.

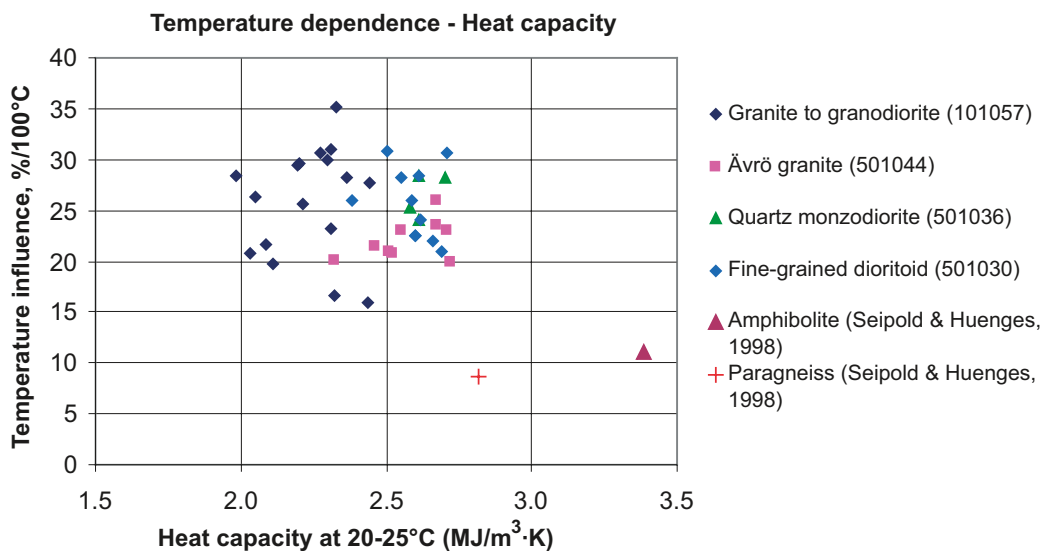


Figure 2-2. Heat capacity ($W/(m\cdot K)$) at 20–25°C versus the temperature coefficient ($\%/100^{\circ}C$) for the heat capacity in different rock types. Rock types with codes beginning with “50” are found in the Laxemar/Simpevarp area /Sundberg et al. 2008/.

For the heat capacity, there is no obvious trend in the temperature dependency related to different values of heat capacity at 20–25°C, for data from Laxemar and Forsmark. The literature heat capacity value for amphibolite is significantly higher than other data. Literature data for both amphibolite and paragneiss have a lower temperature coefficient than Laxemar and Forsmark data.

Mean temperature coefficients for thermal conductivity in different rock types are estimated in Table 2-3. The corresponding values for heat capacity are estimated in Table 2-4.

Table 2-3. Estimated mean temperature coefficients for thermal conductivity in different rock types. The thermal rock class (TRC) to which the rock type has been assigned is also given.

Rock code	Rock name	TRC	Mean thermal conductivity at approx 20°C W/(m·K)	Mean temperature dependence % per 100°C	Temperature coefficient, α_λ 1/°C	Comments
101057	Granite to granodiorite	57	3.68	-10	$-1 \cdot 10^{-3}$	Measured
101051	Granite, granodiorite and tonalite	51	2.85	-5	$-5 \cdot 10^{-4}$	Estimated from Figure 2-1
101058	Granite, aplitic	58	3.85	-11	$-1.1 \cdot 10^{-3}$	Estimated from Figure 2-1
101061	Pegmatite	61	3.33	-8	$-8 \cdot 10^{-4}$	Estimated from Figure 2-1
	Amphibolite	17	2.33	-5	$-5 \cdot 10^{-4}$	Literature data on low conductive amphibolite, see Figure 2-1

Table 2-4. Estimated mean temperature coefficients for heat capacity in different rock types. The thermal rock class (TRC) to which the rock type has been assigned is also given.

Rock code	Rock name	TRC	Mean Heat Capacity at approx 20°C MJ/(m ³ ·K)	Mean temperature dependence % per 100°C	Temperature coefficient, α_c 1/°C	Comments
101057	Granite to granodiorite	57	2.06	29	$2.9 \cdot 10^{-3}$	Measured
101051	Granite, granodiorite and tonalite	51	2.15	25	$2.5 \cdot 10^{-3}$	Estimated from Figure 2-2
101058	Granite, aplitic	58	2.01	25	$2.5 \cdot 10^{-3}$	Estimated from Figure 2-2
101061	Pegmatite	61	1.92 ¹	25	$2.5 \cdot 10^{-3}$	Estimated from Figure 2-2
	Amphibolite	17	2.41	10	$1 \cdot 10^{-3}$	Literature data on low conductive amphibolite see Figure 2-2

¹ Based on calculations from TPS data. All other based on calorimetric measurements.

Thermal conductivity and heat capacity at elevated temperature can be determined from Equation 2-1 and Equation 2-2.

$$\lambda_1 = \lambda_0(1 + \alpha_\lambda(T_1 - T_0)) \quad \text{Equation 2-1}$$

$$C_1 = C_0(1 + \alpha_C(T_1 - T_0)) \quad \text{Equation 2-2}$$

where,

- λ_0 Thermal conductivity at 20°C, T_0 , W/(m·K).
- λ_1 Thermal conductivity at elevated temperature T_1 , W/(m·K).
- C_0 Heat Capacity at room temperature T_0 , MJ/(m³·K).
- C_1 Heat Capacity at elevated temperature T_1 , MJ/(m³·K).
- α_λ Temperature coefficient for thermal conductivity, 1/°C.
- α_C Temperature coefficient for heat capacity, 1/°C.

2.5 Pressure dependence in thermal conductivity

The thermal conductivity is lower for stress-released samples compared to determinations at higher pressure (greater depths). The reason is assumed to be the closing of micro cracks. However, the pressure influence seems to be low if the samples are water saturated, approximately 1–2% /Walsh and Decker 1966/. The pressure dependence after closing of fractures can be estimated to approximately 0.5–1%/100 MPa, based on data presented in /Seipold and Huenges 1998/. All determinations of thermal conductivity in the site investigation programme have been made on water saturated samples. The pressure dependence has therefore been neglected in the evaluation.

2.6 Thermal conductivity vs heat capacity

A relationship, described by a second order equation, between heat capacity from direct measurements and thermal conductivity was established in the Forsmark thermal modelling, stage 2.2 /Back et al. 2007/.

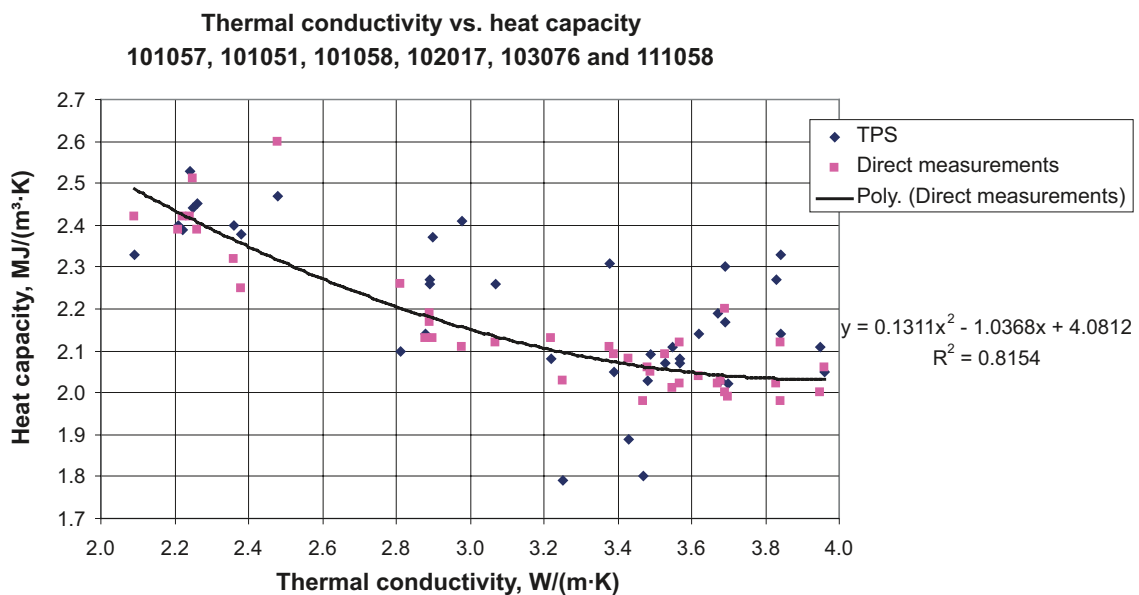


Figure 2-3. Heat capacity vs. thermal conductivity. The heat capacity is calculated from TPS-determinations and from calorimetric measurement. The second order relationship is based on calorimetric measurements only. From /Back et al. 2007/.

The heat capacity (C) is calculated from thermal conductivity (λ) by a second order linear regression equation:

$$C = 4.0812 - 1.0368 \cdot \lambda + 0.1311 \cdot \lambda^2 + \varepsilon_c \quad \text{Equation 2-3}$$

It is possible to add a random error component ε_c to C , if desired. This error is based on the uncertainty in the prediction of C from λ using the regression equation. The error component ε_c is calculated as follows (based on how a prediction interval is calculated; t -values are randomly picked from Student's t -distribution):

$$\varepsilon_c = t_{p,v} \cdot \sigma \cdot \sqrt{1 + x_0^T (X^T X)^{-1} x_0}$$

where $t_{p,v}$ is a Student's t -value for probability p and v degrees of freedom, σ is the square root of the residual variance of the regression (σ represents the standard deviation around the regression line), x_0 is the vector for the desired λ , and X is the matrix of λ -data. Vector x_0 and matrix X are defined as follows:

$$x_0 = \begin{bmatrix} 1 \\ \lambda \\ \lambda^2 \end{bmatrix} \quad ; \quad X = \begin{bmatrix} 1 & \lambda_1 & \lambda_1^2 \\ 1 & \lambda_2 & \lambda_2^2 \\ \vdots & \vdots & \vdots \\ 1 & \lambda_n & \lambda_n^2 \end{bmatrix}$$

2.7 In situ temperature

2.7.1 Method

In thermal model report, stage 2.2 /Back et al. 2007/, the results of borehole temperature logging were presented and discussed. It was discovered that the raw data were used instead of the filtered and resampled data. For this reason, the results have been re-evaluated, this time using the filtered and resampled data where available. Calculated vertical temperature gradients for 9 m sections are based on unfiltered temperature data.

Due to large differences in logged temperature for the same depth in different boreholes, the fluid temperature loggings for each borehole have been evaluated with regard to their reliability. The criteria considered, discussed more fully in /Back et al. 2007/, were 1) errors associated with logging probe and 2) time between drilling and logging. The result of this evaluation, summarised in Table 2-5, is a number of "approved" and "rejected" borehole loggings.

At least two boreholes, KFM04A and KFM05A, have been temperature logged on more than one occasion using different probes. Only one of the loggings of KFM04A is judged to be reliable, i.e. the one carried out in 2005. However, unlike most other logged data, this logging has not been resampled and filtered, so the raw data has been investigated here instead. The logging from 2003 is rejected as it was performed using a Century 9044 probe. However, it is this data that has been processed (resampled and filtered) and reported to the tables in Sicada for geophysical interpretation of borehole logging. This data has not, and should not, be used.

The temperature and gradient profiles have been investigated for the "approved" boreholes, namely KFM01A, KFM02A, KFM03A, KFM04A, KFM06C, KFM07C, KFM08C and KFM09B. The logging for KFM01C, although judged to be of good quality, extends to a depth of only 340 m, and is thus too short to be used for estimation of temperatures at repository depths.

Table 2-5. Evaluation of fluid temperature loggings.

Borehole	Probe	Risk for errors due to design/calibration faults	Core drilling: start/stop	Date of fluid temperature logging	Period between drilling stop and logging	Judgement of quality of fluid temp. logging	Comment: main reason(s) for rejecting data
KFM01A	Century 9042	Low	2002-06-25/ 2002-10-28	2003-04-25	6 months	Good	
KFM01C	Century 9042	Low	2005-11-05/ 2005-11-29	2006-02-01	2 months	Good	Vertical depth of borehole only 340 m.
KFM01D	Century 9042	Low	2005-12-18/ 2006-02-18	2006-03-07	3 weeks	Poor	Short time between drilling and logging.
KFM02A	Century 9042	Low	2003-01-08/ 2003-03-12	2003-08-05	5 months	Good	
KFM03A	Century 9042	Low	2003-04-16/ 2003-06-23	2003-08-08	6 weeks	Good	
KFM04A	Century 9044	High	2003-08-25/ 2003-11-19	2003-11-24	5 days	Poor	Unreliable probe
KFM04A	Century 9042	Low	2003-08-25/ 2003-11-19	2005-11-12	2 years	Good	
KFM05A	Century 8044	High	2003-11-25/ 2004-05-05	2004-05-18	2 weeks	Poor	Unreliable probe
KFM05A	Century 8144	Medium	2003-11-25/ 2004-05-05	2005-08-08	15 months	Poor	Unreliable probe
KFM06A	Century 8044/ 9044	High	2004-06-14/ 2004-09-21	2004-11-03	6 weeks	Poor	Unreliable probe
KFM06C	Century 9042	Low	2005-04-26/ 2005-06-30	2005-08-10	6 weeks	Good	
KFM07A	Century 8044	High	2004-06-07/ 2004-12-09	2005-02-08	2 months	Poor	Unreliable probe
KFM07C	Century 9042	Low	2006-03-30/ 2006-08-08	2006-09-19	6 weeks	Good	
KFM08A	Century 9042	Low	2005-01-25/ 2005-03-31	2005-04-27	4 weeks	Poor	Rather short time between drilling and logging.
KFM08C	Century 9042	Low	2006-01-30/ 2006-05-09	2006-07-18	10 weeks	Good	
KFM08D	Century 9042	Low	2006-12-13/ 2007-02-10	2007-02-20	10 days	Poor	Short time between drilling and logging.
KFM09B	Century 9042	Low	2005-11-16/ 2005-12-19	2006-01-30	6 weeks	Good	
KFM10A	Century 9042	Low	2006-03-14/ 2006-06-01	2006-06-08	1 week	Poor	Short time between drilling and logging. Vertical depth of borehole only 337 m.

Temperature data obtained during difference flow logging (also called Posiva flow logging or PFL) was also investigated for some boreholes. The temperatures logged in the down-borehole direction, without any pumping, were selected for comparison with the fluid temperature logs described above. Suitable data is available for three of the “approved” boreholes: KFM02A, KFM03A and KFM04A /Rouhiainen and Pöllänen 2004ab, Pöllänen and Sokolnicki 2004/. The times between end of drilling and PFL logging for these three boreholes were 6 weeks, 7 weeks, and 4 months respectively.

2.7.2 Results

Temperature-depth profiles for the “approved” boreholes are presented in Figure 2-4 to Figure 2-9. Equations were fitted to the temperature profiles for these boreholes; see Table 2-7. First-order equations were judged to be satisfactory, as higher order equations did not give better fits to the data.

In Table 2-6, the fluid temperature at vertical depths of 400 m, 500 m and 600 m in the boreholes are presented. The measured temperatures at 500 metres depth fall within the interval 11.2–12.0°C. Temperatures recorded by the Posiva flow logs (PFL) in boreholes KFM02A, KFM03A and KFM04A are also given in this table and indicate a generally good agreement between the two methods. Thus the PFL data support the conclusions made in section 2.7.1 regarding the quality of the fluid temperature data.

The calculated gradients for the boreholes are plotted in Figure 2-4 and Figure 2-5. Larger gradient anomalies often correlate with borehole sections where water bearing fractures have been identified /Follin et al. 2007/. This is evident from a study of the WellCAD plots in Appendix A. Despite the anomalies, a trend of increasing gradient with depth can be observed, from about 10°C/km at 300 m to about 13°C/km at 700 m

Mean annual air temperatures recorded at meteorological stations close to the Forsmark area are between 5°C and 5.5°C /Johansson et al. 2005/.

Table 2-6. Temperature (°C) for the “approved” boreholes at the Forsmark site, at different levels. Borehole inclinations are also included for the boreholes, given as lowest and highest angle. Temperature from Posiva flow logs are given in parentheses.

Borehole	Temperature at the depth 400 m	Temperature at the depth 500 m	Temperature at the depth 600 m	Inclination (°)
KFM01A	10.6	11.7	12.9	75–85
KFM01C*	–	–	–	46–50
KFM02A	10.8 (10.5)	11.8 (11.7)	12.9 (12.7)	80–86
KFM03A	10.8 (10.5)	12.0 (11.7)	13.1 (12.9)	83–86
KFM04A	10.4 (10.4)	11.5 (11.6)	12.7 (12.8)	44–63
KFM06C	10.2	11.3	12.5	45–60
KFM07C*	10.4	11.4**	–	84–85
KFM08C	10.1	11.2	12.5	59–60
KFM09B*	10.4	–	–	41–55
Arithmetic mean	10.5	11.6	12.8	

* Maximum vertical depth of KFM01C is about 340 m, KFM07C about 490 m, and KFM09B about 470 m.

** At 493 m (vertical depth).

Table 2-7. Equations fitted to the temperature profiles for the investigated boreholes.

Borehole	Equation (linear fit)
KFM01A	$T = -0.012057 z + 5.8706$
KFM02A	$T = -0.011315 z + 6.3212$
KFM03A	$T = -0.011566 z + 6.3852$
KFM04A	$T = -0.010425 z + 6.0654$
KFM06C	$T = -0.011010 z + 6.0013$
KFM07C	$T = -0.010466 z + 6.1887$
KFM08C	$T = -0.011064 z + 5.9005$
KFM09B	$T = -0.010834 z + 6.0946$

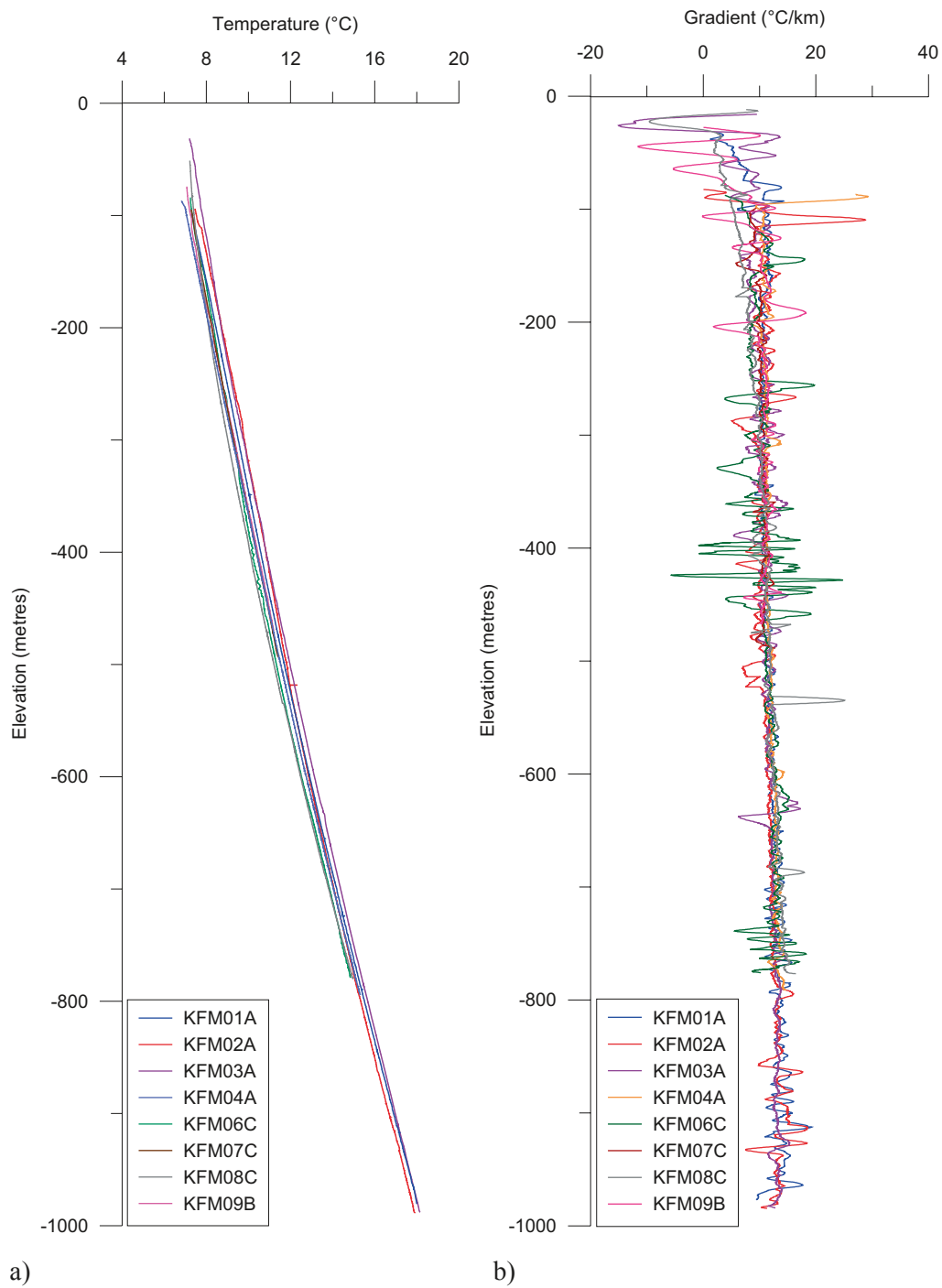


Figure 2-4. Temperature (a) and vertical temperature gradients calculated for nine metre intervals (b) for the eight “approved” boreholes at Forsmark. Results from fluid temperature loggings.

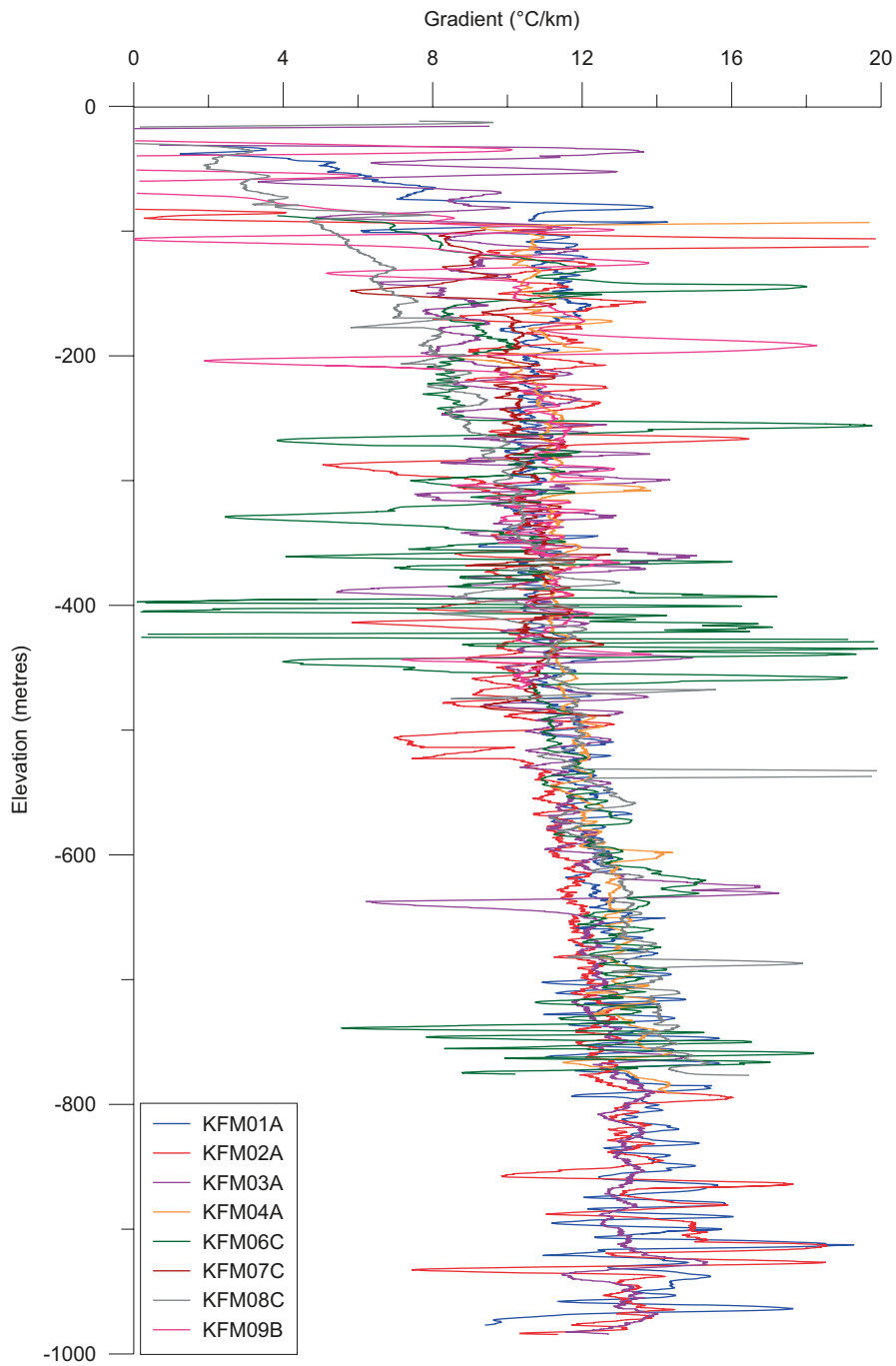


Figure 2-5. Vertical temperature gradients calculated for nine metre intervals for eight “approved” boreholes at Forsmark. Results from fluid temperature loggings.

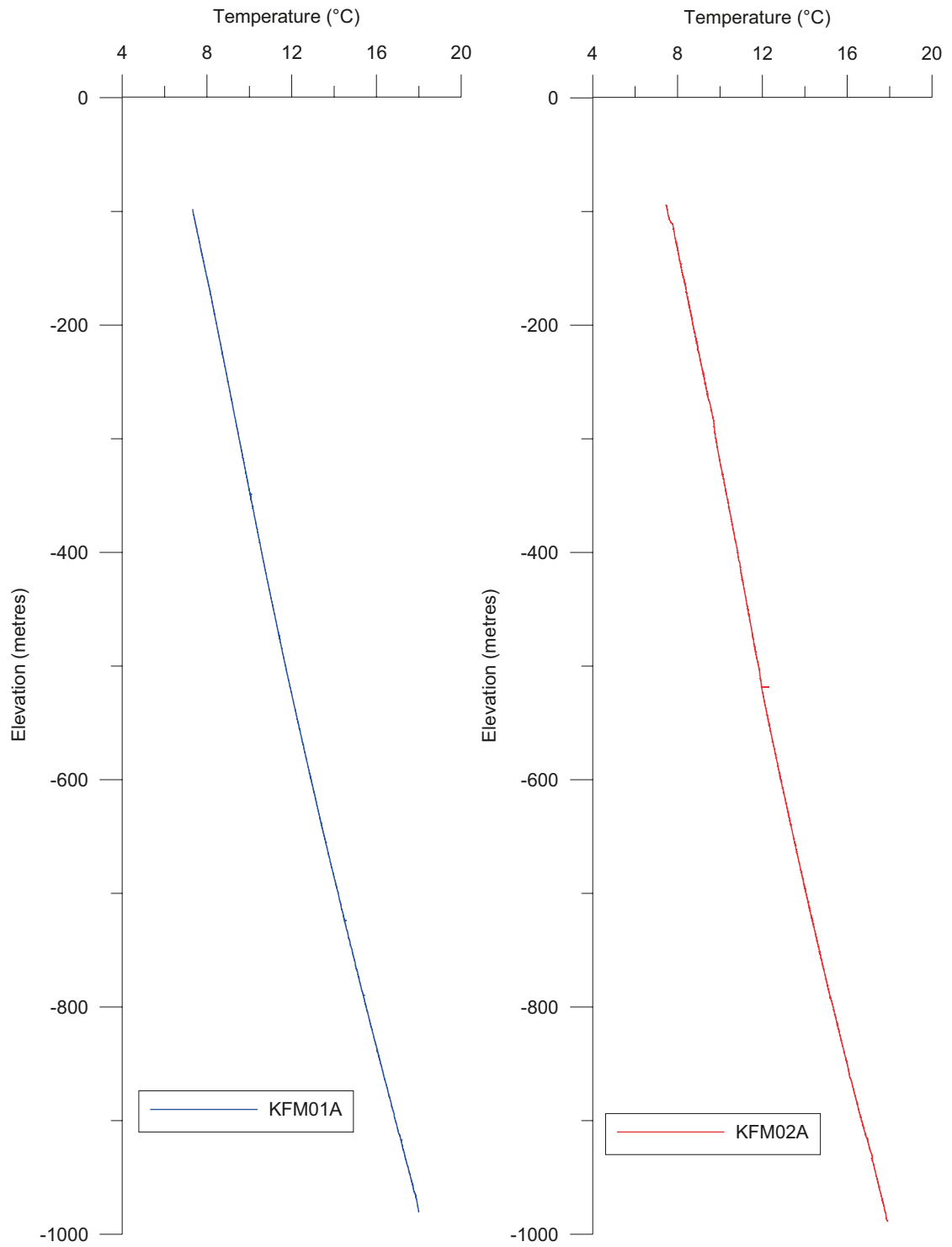


Figure 2-6. Temperature from fluid temperature loggings, for KFM01A and KFM02A.

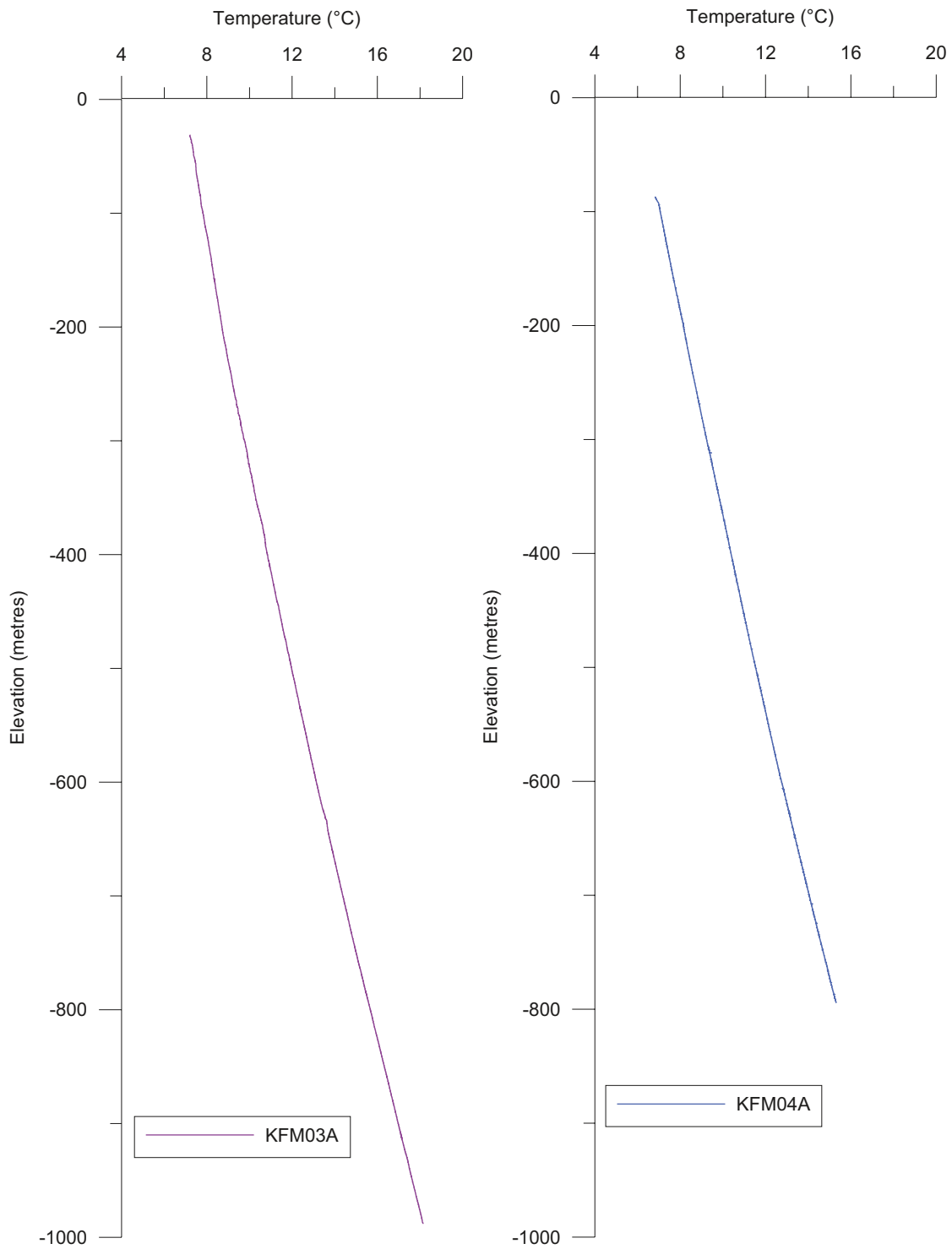


Figure 2-7. Temperature from fluid temperature loggings, for KFM03A and KFM04A. Note that data for KFM04A has not been filtered.

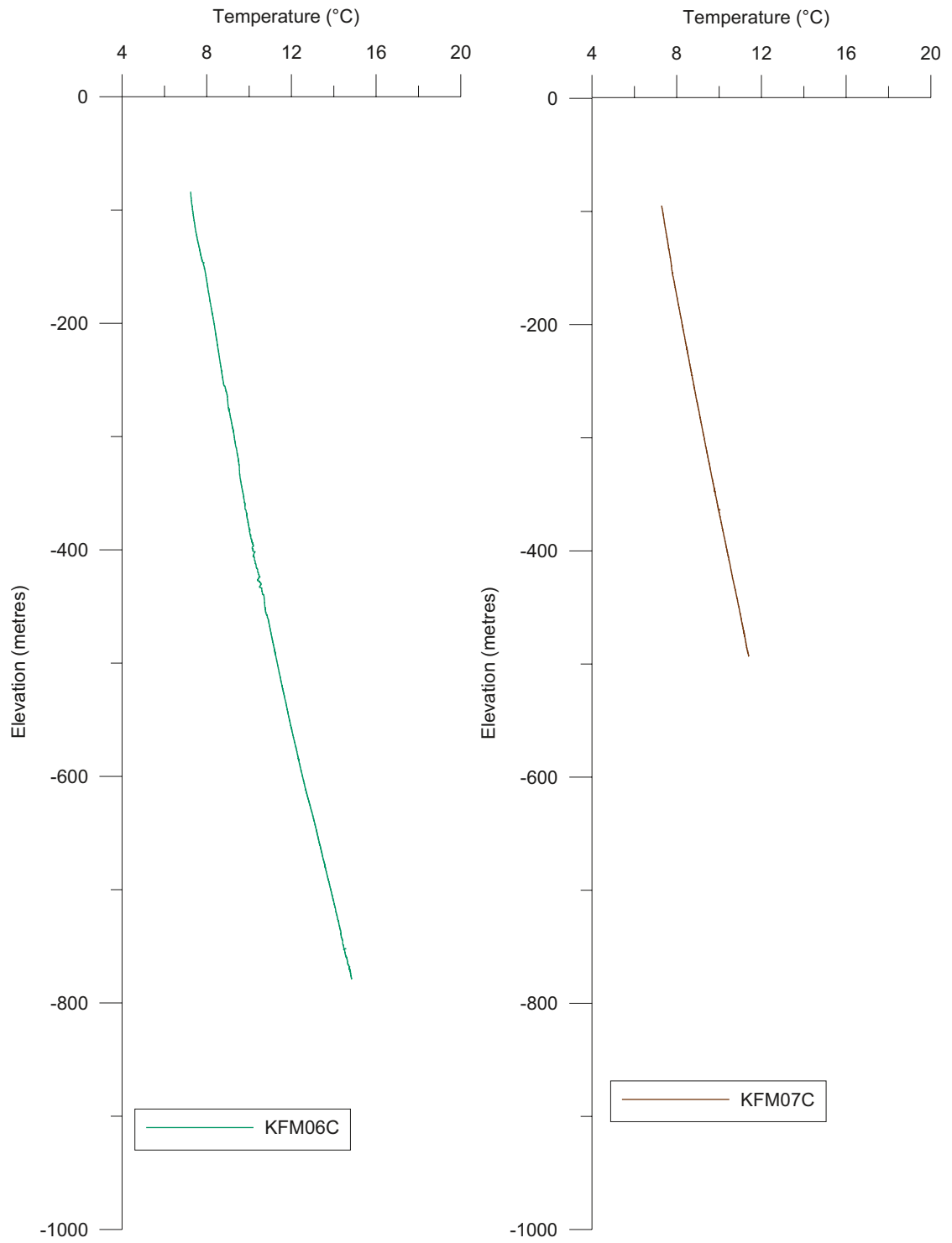


Figure 2-8. Temperature from fluid temperature loggings, for KFM06C and KFM07C.

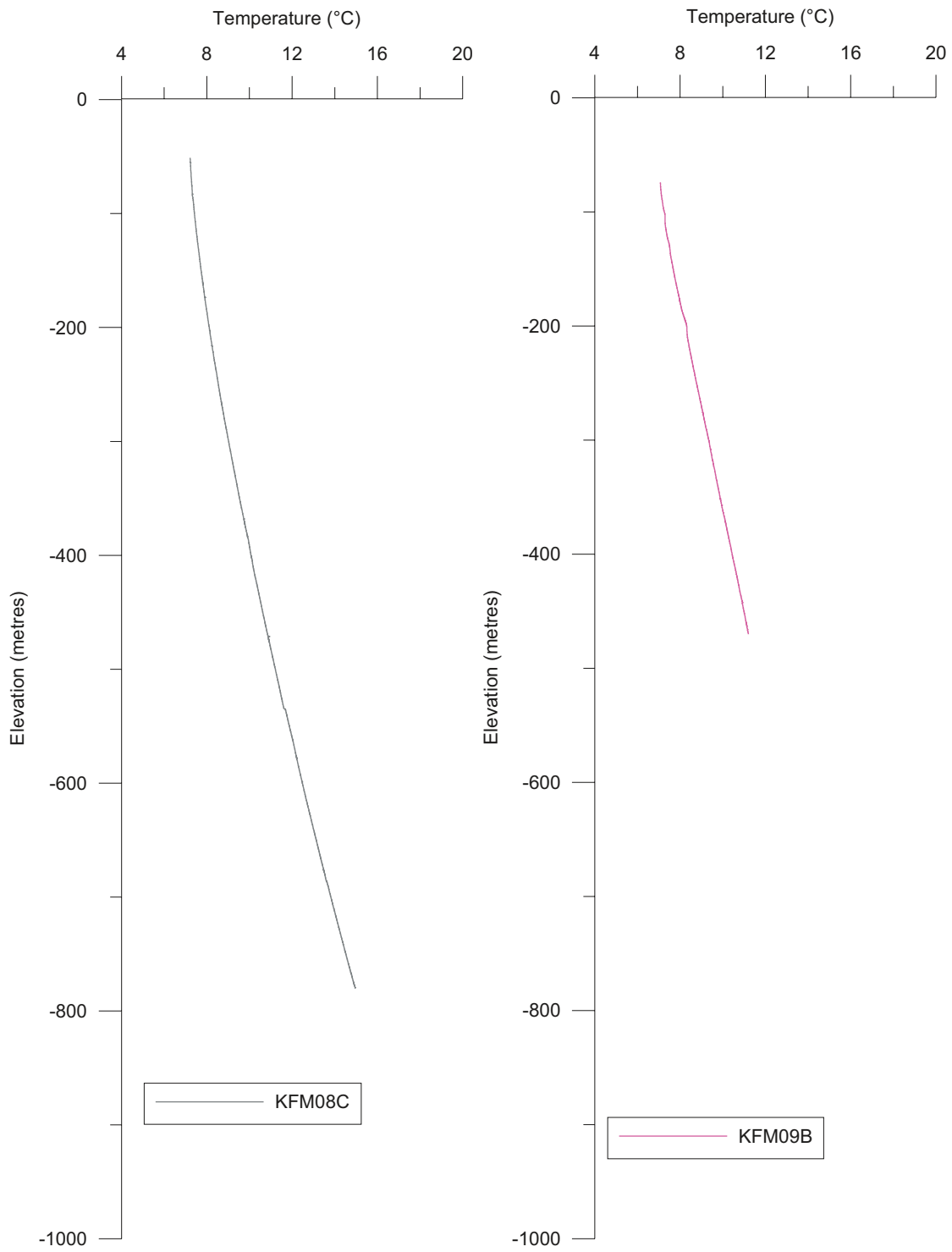


Figure 2-9. Temperature from fluid temperature loggings, for KFM08C and KFM09B.

2.8 Geology from boremap

The target volume comprises two rock domains: RFM029 and RFM045. For domain RFM045, new geological borehole data for one borehole (KFM08D) has become available in data freeze 2.3. This borehole together with existing data from boreholes KFM06A, KFM06C and KFM08C have been used as the basis for revised stochastic geological simulations of domain RFM045. The geological borehole data used are rock type (> 1 m) and rock occurrences (< 1 m), together with a lithological domain classification of boreholes.

Borehole sections assigned to domain RFM045, and which have been investigated with the purpose of using them in the geological simulation, are listed in Table 2-8.

The borehole data representing domain RFM045 have been further analysed in order to define appropriate “subdomains” for the stochastic simulation of the geology. This analysis is described in section 4.3.

2.9 WellCAD borehole plots

Geological, hydrological and thermal data relevant to the understanding of the thermal properties of the rock mass, and used in both model stage 2.2 and model stage 2.3, are presented for each cored borehole in Appendix A.

Table 2-8. Boreholes belonging to domain RFM045, and used as input for the geological simulations. The rock domain classification of boreholes is from /Stephens et al. 2007, SKB 2008/.

Domain	Borehole
RFM045	KFM06A (751–998 m), KFM06C (411–898 m), KFM08C (342–546 m), KFM08D (395–935 m)

3 Modelling approach

3.1 Introduction

The strategy for the thermal site descriptive modelling is to produce spatial statistical models of both lithologies and thermal properties and perform stochastic simulations to generate a spatial distribution of thermal properties that is representative of the modelled rock domain. The methodology is described in detail in /Back and Sundberg 2007/, and its application in Forsmark model stage 2.2 in /Back et al. 2007/.

The aim of the thermal modelling is to model the thermal properties spatially for a rock domain. There are three specific objectives for which the modelling approach can be used:

- Description: statistical description of the thermal properties of a rock domain.
- Prediction: prediction of thermal properties in a specific rock volume.
- Visualisation: visualisation of the spatial distribution of thermal properties.

In this report the focus is on description. Of special interest for the description is to:

- determine the low percentiles of thermal conductivity and the associated uncertainty,
- model how the thermal conductivity varies with scale,
- produce realisations of thermal conductivity that can be used for subsequent modelling work, such as numerical temperature simulations.

3.2 Outline of the methodology

The methodology for thermal modelling, described in detail in /Back et al. 2007/ and /Back and Sundberg 2007/, is summarised in Figure 3-1. In model stage 2.3, new lithological simulations (step 8 in the figure) are performed for rock domain RFM045. These simulations utilise models describing the spatial statistical structure of each TRC (step 7), which in turn are based on lithological data acquired from boreholes (step 2) and reclassified into thermal rock classes, TRCs (step 3). A number of equally probable realisations of the geology are created by the simulations, using the software T-PROGS /Carle 1999/.

Realisations resulting from stochastic simulations of thermal conductivity (step 10), previously performed in model stage 2.2, are merged with the realisations of TRCs (step 11), i.e. each realisation of geology is filled with simulated thermal conductivity values. The result is a set of realisations of thermal conductivity that considers both the difference in thermal properties between different TRCs, and the variability within each TRC. Upscaling of the realisations to 5 m scale is also performed (step 12).

Details of the complementary modelling of domain RFM045 can be found in Chapter 4 and 5.

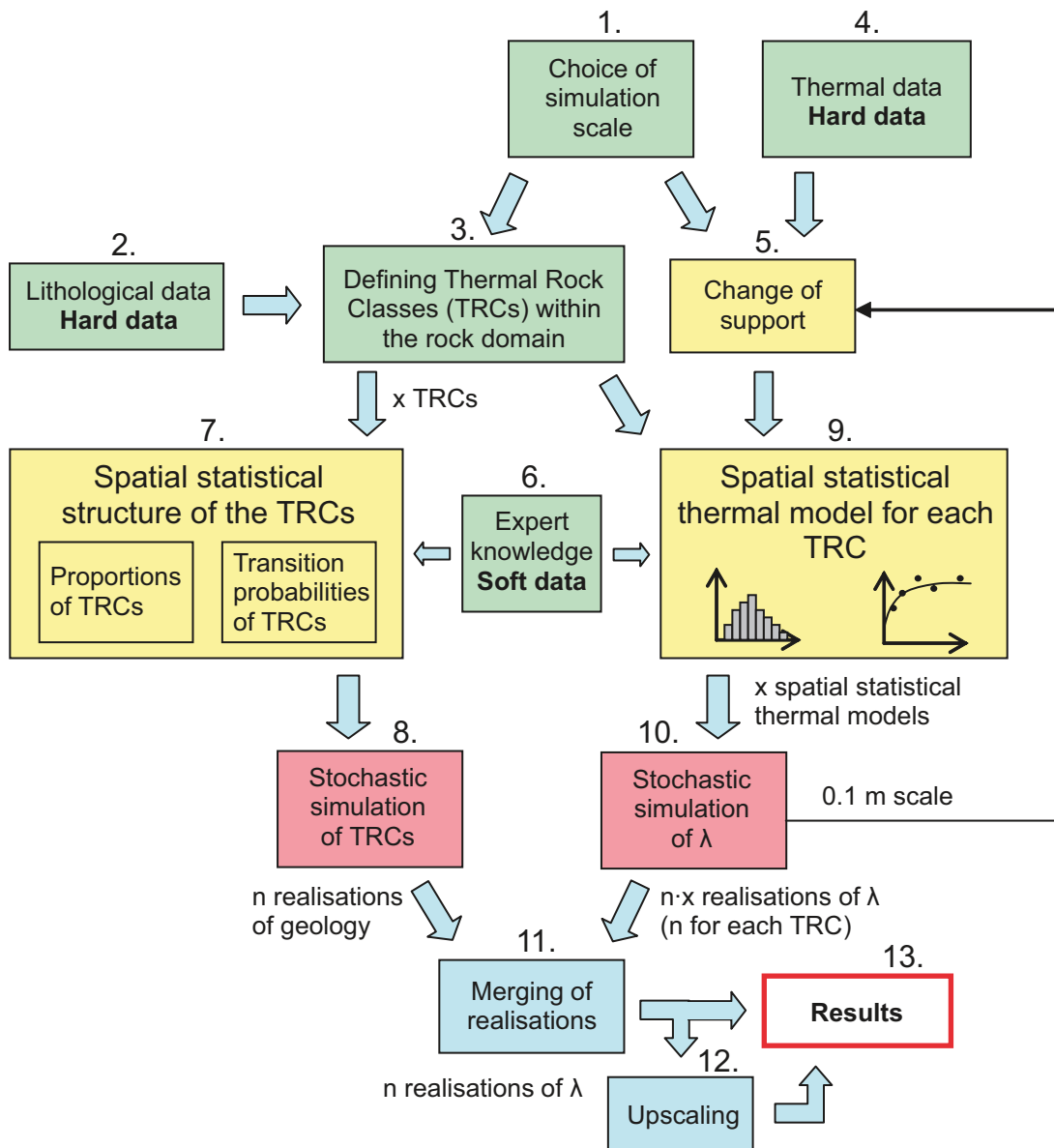


Figure 3-1. Schematic description of the approach for thermal modelling of a rock domain (λ represents thermal conductivity).

4 Geostatistical analyses and stochastic simulations of geology in domain RFM045

4.1 General

The target volume comprises the rock volume identified as suitable for hosting a final repository. Two rock domains have been identified within the target volume. Domain RFM029 makes up the major part of the target volume and will constitute the bulk of any future repository volume. The much smaller domain RFM045 is also located within the intended repository volume. Thermal properties of domains RFM029 and RFM045 were evaluated during stage 2.2 /Back et al. 2007/. A revised model for domain RFM045 is presented here.

In previous geological simulations of domain RFM045, the importance/frequency of large bodies of amphibolite, the rock type with the lowest thermal conductivity of all rock types in Forsmark was overestimated. The geological simulations were based primarily on input from borehole KFM06C, which intersects a single large body of amphibolite, with a borehole length of 35–40 m, a size not observed elsewhere within the target area. In other borehole sections assigned to domain RFM045 (KFM06A and KFM08C), as well as in all boreholes belonging to domain RFM029, amphibolite bodies are much smaller, borehole lengths only rarely exceeding a couple of metres /Stephens et al. 2007/.

The use of KFM06C to characterise domain RFM045 had a disproportionate influence on how amphibolite was modelled in the geological simulations of this domain. To correct for this in the complementary thermal modelling, new stochastic simulations of domain RFM045 have been performed. In these simulations, more of the geological heterogeneity present within domain RFM045 is captured, and the amphibolite body in KFM06C is treated so that its impact on geological simulations and thermal modelling is reduced significantly. This is achieved by using lithological data from four boreholes including new data from borehole KFM08D, dividing these borehole sections into two thermal “subdomains”, and performing simulations for each subdomain separately.

The application to domain RFM045 of the modelling steps 2, 3, 6, 7 and 8 outlined in Chapter 3 and Figure 3-1 is presented in this chapter. In section 4.3, the geological input, comprising both hard and soft data, is presented (steps 2, 3 and 6 in Figure 3-1). Next, in section 4.4 spatial statistical models of lithologies within domain RFM045 are established (step 7 in Figure 3-1). This is followed by the results of stochastic simulation of lithologies in 4.5 (step 8 in Figure 3-1).

4.2 Modelling assumptions

The assumptions made in model stage 2.2 /Back et al. 2007/ also apply to the complementary modelling of domain RFM045 in stage 2.3. However, there are new assumptions regarding the statistical heterogeneity of the geology within domain RFM045. In model stage 2.2, statistical homogeneity was assumed throughout domain RFM045, whereas in stage 2.3, the statistically heterogeneous domain is divided into thermal subdomains, each of which is assumed to be statistically homogeneous; see Section 4.3.2.

4.3 Description of geological input

4.3.1 Thermal Rock Classes (TRC) – definition and properties

The geological simulations can deal with a maximum of five lithological classes. For this reason, the rock types have been grouped into classes, called thermal rock classes (TRCs) – step 3 in Figure 3-1. Rock types with similar thermal and lithological properties were assigned to the same TRC as outlined in Table 4-1. The thermal properties considered were thermal conductivity and heat capacity and are exemplified by the mean thermal conductivity in Table 4-1. The TRCs used in the revised simulations of domain RFM045 are identical to those defined in the thermal model stage 2.2 /Back et al. 2007/.

4.3.2 Lithological borehole data: geological heterogeneity and division into thermal subdomains

Lithological data from four boreholes intersecting rock domain RFM045 have been processed into a format suitable for spatial statistical analysis (step 2 in Figure 3-1). These boreholes are KFM06A, 06C, 08C and 08D. The procedure for this processing step is described in /Back et al. 2007/. The data were prepared to match the resolution used in the simulations, which is defined as the size of a grid cell in the simulation, in this case 1 m. This required assigning a TRC to each position along a borehole at 1 m intervals.

In model stage 2.2, the boreholes characterising domain RFM029 were divided into two groups on the basis of their dominant style of deformation, characterised by either a foliation or lineation. Spatial lithological models were then erected for each of these two groups and separate simulations were performed. Lithologically, these two thermal “subdomains” are rather similar. Both are dominated by granite to granodiorite (101057) and have small amounts (< 5 %) of low conductive rocks such as amphibolite (102017) and granite, granodiorite and tonalite (101051). Domain RFM045, which is much smaller than domain RFM029, was not divided into subdomains, partly due to the small number of boreholes intersecting this rock volume, and partly because it is dominated by a single style of deformation, i.e. lineation.

Table 4-1. Division of rock types into TRCs for domain RFM045. Proportions of different rock types and geological characteristics are according to /Stephens et al. 2007/. Other rock types not belonging to any of the defined TRCs make up less than 1% of the rock volume /Stephens et al. 2007/.

TRC	Rock code	Proportion in domain RFM045, %	Mean thermal conductivity (TPS)	Composition, mode of occurrence, etc
58	Granite to granodiorite, 101057	18.0%	3.68	Both felsic group B rocks. Dominating granites commonly affected by albitization.
	Granite, aplitic, 101058	49.3%	3.85	
51	Granite, granodiorite and tonalite, 101051	9.0%	2.85	Felsic to more intermediate group A and C rocks.
	Felsic to intermediate volcanic rock, 103076	1.2%	2.54	
61	Pegmatite, pegmatitic granite, 101061	13.9%	3.33	Both felsic group D rocks. Late tectonic dykes, segregations, veins.
	Granite, 111058	1.3%	3.47	
17	Amphibolite, 102017	6.3%	2.33	Both mafic group B rocks. Dykes and small irregular bodies.
	Diorite, quartz diorite and gabbro, 101033	0.2%	2.28	

The additional data from borehole KFM08D, made available as part of data freeze 2.3, together with the previously investigated boreholes /Stephens et al. 2007/ indicate that considerable lithological heterogeneity is present in domain RFM045. Furthermore, the presence of a few large occurrences of amphibolite (as well as other mafic rocks) in the new borehole KFM08D /Carlsten et al. 2007/ indicates that such bodies may not be unusual in domain RFM045, a feature distinguishing it from domain RFM029.

Capturing this heterogeneity in the geological simulations requires sub-dividing the borehole sections intersecting domain RFM045 into two groups on the basis of their lithological characteristics. The characteristics of each type are described in Table 4-2. Sections dominated by granite (101058) and granite to granodiorite (101057) with only minor occurrences of subordinate rocks (subdomain A) can be distinguished from sections comprising larger bodies of amphibolite (102017) and granite, granodiorite and tonalite (101051) (subdomain B). Borehole sections of type A dominate the domain.

Statistical analysis of the two sets of borehole data using the software T-PROGS provide the basis for erecting spatial statistical models for each subdomain. Subsequent simulations produce a set of realisations, where the number of realisations for each subdomain is proportional to the borehole length assigned to each subdomain.

The procedure for dividing the borehole sections into two subdomains was as follows:

1. Each of the four boreholes intersecting domain RFM045 were investigated. There are no geological criteria which can be consistently used to perform the division into subdomains. For this reason, estimates of the proportion of the domain that contain large amphibolite bodies are arbitrary and were evaluated after close collaboration with the geologists in the Forsmark modelling team (M B Stephens, personal communication 2007). It was concluded that somewhere between 10% and one third of the domain volume may include large amphibolite bodies. To ensure that transitions between the different subordinate rocks and the dominant background granitic rocks are captured in the simulations of this subordinate subdomain, the upper limit of this estimate was chosen. This implies that 1/3 of the total borehole length is assigned to subdomain B and the remaining 2/3 to subdomain A. We emphasise again that this is an arbitrary choice, since it is impossible to estimate the relative volumes of rock that are typical of each subdomain with any certainty. Fortunately, for the purposes of modelling thermal properties, how this division is made has only a minor impact on the results.
2. Using the selected proportions of the rock volume assigned to each subdomain, the borehole length used to define each subdomain can be calculated. Of a total of approximately 1,500 m borehole length intersecting domain RFM045, 1,000 m (two-thirds) is assigned to subdomain A, and 500 m (one-third) is assigned to subdomain B.
3. There are three large occurrences of amphibolite/mafic rock in the investigated boreholes, one in KFM06C and two in KFM08D. Borehole sections centred about these bodies are selected so that they sum to 500 m. Taken individually, the length of these borehole sections are proportional to the size (borehole length) of the amphibolite bodies. These sections make up subdomain B.
4. The remaining borehole sections are assigned to subdomain A. It is important to point out that the exact boundaries between the boreholes sections assigned to each subdomain have no geological significance.

Borehole sections assigned to the two subdomains are described in Table 4-3 and Table 4-4.

Table 4-2. Description of subdomains in domain RFM045.

Subdomain	Proportions of 102017 and 101051	True thickness of amphibolite bodies
A	Low proportions of both TRC 17 (mainly amphibolite; 2%) and TRC 51 (mainly granite, granodiorite and tonalite; 6%)	Thin (< 1 m)
B	High proportions of both TRC 17 (18%) and TRC 51 (19%)	Thick (c. 5–30)

Table 4-3. Borehole sections assigned to subdomain A.

Borehole	Borehole section (m)	Borehole length (m)
KFM06A	751–998	247
KFM06C	411–664	253
KFM08C	342–546	204
KFM08D	395.6–532, 635–781	282
Total		986

Table 4-4. Borehole sections assigned to subdomain B.

Borehole	Borehole section (m)	Borehole length (m)
KFM06C	664–898	234
KFM08D	532–635, 781–935	257
Total		491

4.3.3 Orientation and geometry of subordinate rock types in domain RFM045

The orientation and geometry of subordinate rock types are modelled in the geological simulations of domain RFM045. Interpretations of orientation and geometry rely heavily on an understanding of the ductile deformation within the tectonic lens at Forsmark. These interpretations constitute the soft data (step 6 in Figure 3-1) that are used to improve the models describing the spatial statistical structure of TRCs.

In the geological model, domain RFM045 has been modelled as a constricted rod in the hinge of a major synform that plunges moderately to steeply to the south-east, close to the mineral stretching lineation in this part of the Forsmark site /Stephens et al. 2007/. Domain RFM045 is considered to possess a deformation style typical of the internal part of the tectonic lens at Forsmark /Stephens et al. 2007/, which means that, while a foliation is present, lineation is assumed to be the dominant form of ductile deformation. The orientation of some subordinate rocks, in particular amphibolite, follows that of the ductile deformation. Thus, they have a strike and dip parallel to the foliation, and have their maximum extension in the direction of the lineation.

Amphibolite contacts, which are commonly parallel to the foliation, show different orientations along the limbs, close to and within the hinge of the synform /Stephens et al. 2007/. Typical orientations (strike and dip) of amphibolite contacts in KFM06A, KFM06C, KFM08C and KFM08D were based on interpretations of the poles to mafic rock contacts and foliations on equal area stereographic projections including contoured Fisher concentrations (Figure 4-1 and Figure 4-2), as well as consultations with the geological modelling team. The strike and dip considered typical for each borehole are presented in Table 4-5. It is emphasized that the selected values are a simplification of the true situation. For example, there is a large variation in strike/dip in KFM08D; the dominant cluster with its midpoint at about 125/70 (equivalent

plane, right-hand-rule) was selected. According to /Stephens et al. 2007/, lineation directions are rather consistent throughout the target volume, i.e. the lineation does not appear to be affected by folding. Orientation data from domain RFM045 is scarce, whereas the more plentiful data from domain RFM029 indicate a mean trend and plunge for the mineral stretching lineation of 141/42 /Stephens et al. 2007/. Since the lineation is assumed to lie within the foliation plane, this direction (trend and plunge) was modified slightly to fit the foliation direction characterising each borehole Table 4-5.

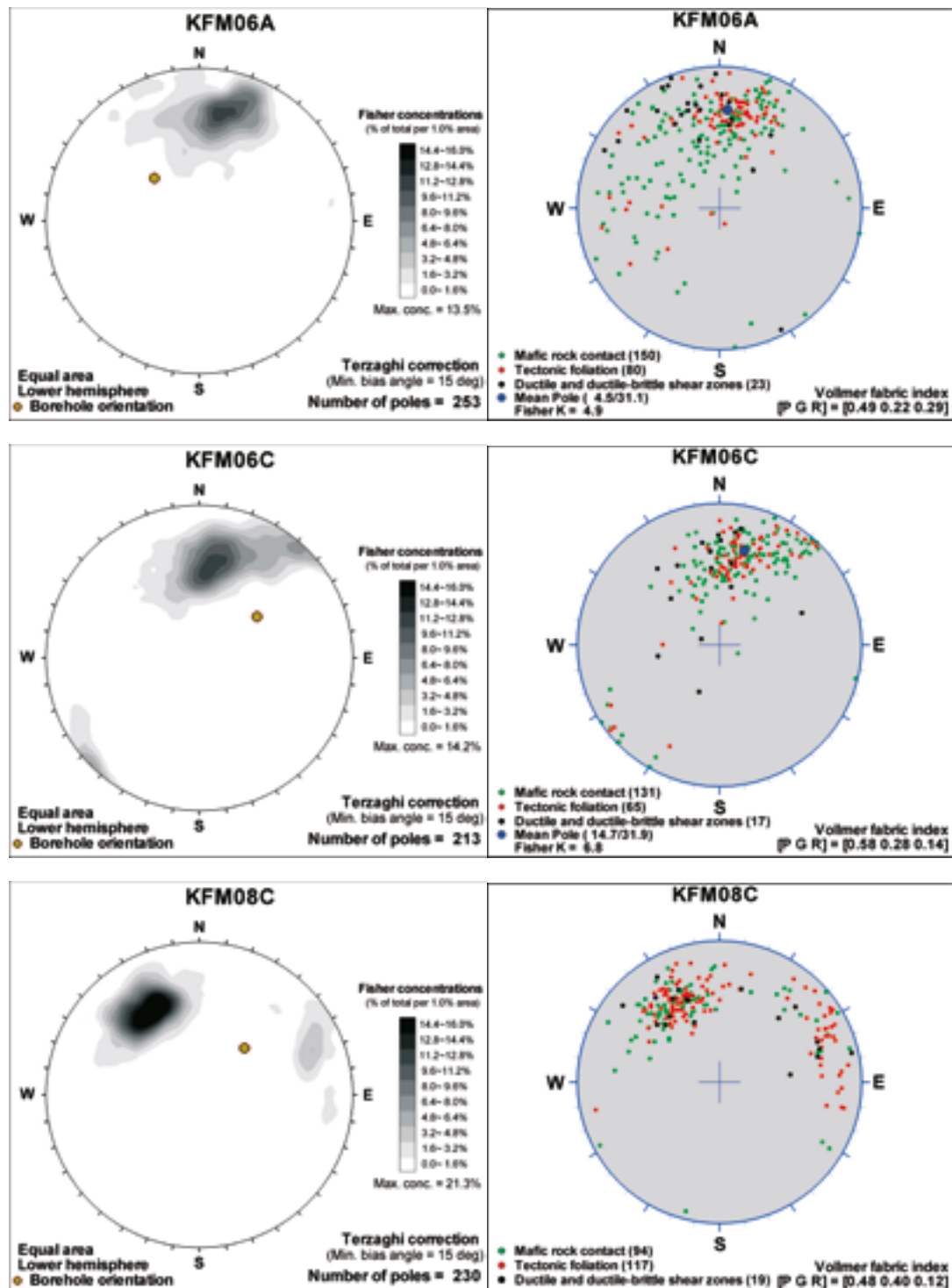


Figure 4-1. Equal area stereographic projections and Fisher concentrations of foliation and mafic rock contacts for boreholes KFM06A, KFM06C and KFM08A. Based on /Stephens et al. 2007/ with minor revision in connection with data analysis during modelling stage 2.3 (M B Stephens, personal communication 2007).

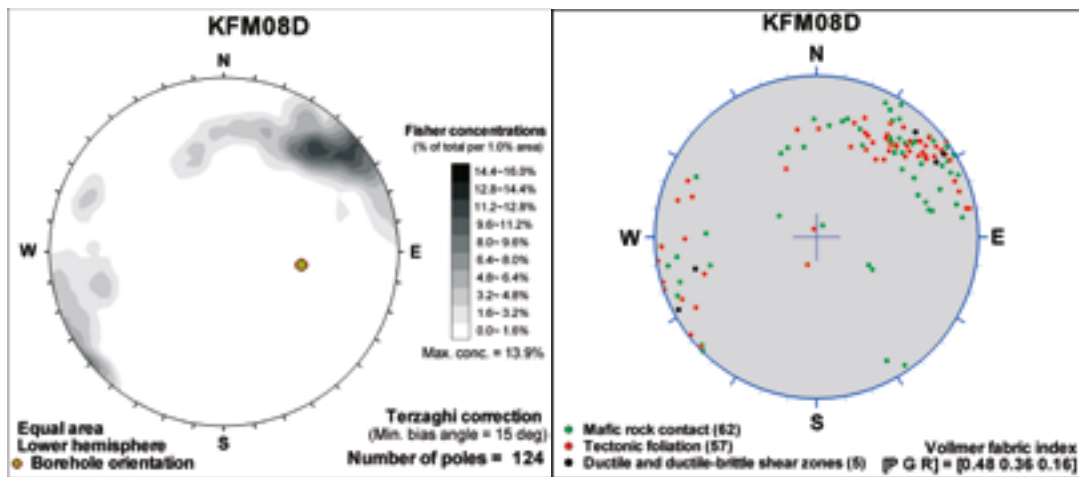


Figure 4-2. Equal area stereographic projection and Fisher concentrations of foliation and mafic rock contacts for boreholes KFM08D, based on data analysis during modelling stage 2.3 (M B Stephens, personal communication 2007).

Table 4-5. Assumed orientation of amphibolite bodies in boreholes belonging to domain RFM045.

Boreholes in domain RFM045	Orientation of foliation and amphibolite contacts		Orientation of lineation and longest axis of amphibolite bodies	
	strike	dip	trend	plunge
KFM06A	112.5°	60°S	145°	42°
KFM06C	112.5°	60°S	145°	42°
KFM08C	60°	60°S	145°	60°
KFM08D	125°	70°S	145°	42°

Interpretations of the geometry of amphibolite bodies (TRC 17) are identical to those made in model stage 2.2 /Back et al. 2007/. They are modelled as somewhat flattened, rod-like bodies with a maximum extension four times that of the thickness, and twice that of their width.

The assumptions regarding the orientation and geometries of TRC51 and TRC61 (granite, granodiorite and tonalite [101051] and pegmatite [101061], respectively), are also identical to those made in model stage 2.2 /Back et al. 2007/. For TRC51, this means a similar orientation and geometry to amphibolite. Pegmatites (101061), the main rock type in TRC61, are assumed to be dyke or disc-like bodies lying parallel to the foliation and having a diameter five times their thickness. It is emphasised here that judgements regarding the geometry of different rock types are not based on any hard data, but rather on an understanding of the ductile deformation within the tectonic lens at Forsmark, as well as on the impressions gained by geologists in the field (M B Stephens, personal communication 2007). Table 4-6 summarizes the assumptions regarding the geometry of subordinate rocks.

Table 4-6. Assumed geometries of subordinate rock/TRCs in domain RFM045.

TRC	Main rock type	Ratio between longest, intermediate and shortest axes
TRC17	Amphibolite	4:2:1
TRC51	Granite, granodiorite and tonalite	4:2:1
TRC61	Pegmatite	5:5:1

4.4 Spatial statistical models of lithology (TRC)

4.4.1 Introduction

Models of the spatial statistical structure of the thermal rock classes (TRC) for each of the two thermal subdomains defined in 4.3.2 are estimated from the borehole data characterising each subdomain (step 8 in Figure 3-1). Subdomain A required further division into two groups, A1 and A2, for the purpose of simulation, due to the variable orientations of boreholes with respect to the axes of anisotropy. For example, KFM06A lies close to the maximum axis of anisotropy (x-axis), whereas other boreholes are oriented close to the intermediate y-axis. Because of limitations of the method used, boreholes oriented at a high angle to one of the principal axes of anisotropy are not suitable for use in simulations, see Table 4-7. This was judged to be the case for KFM08C only. The omitted borehole section has nevertheless contributed to estimations of the TRC proportions. Typical lens length and interactions of TRCs were calculated by transition probability analysis of the borehole data using T-PROGS software /Carle 1999, Carle and Fogg 1997/. Anisotropy in the geometry of subordinate rocks is modelled by using different transition probability matrices for different directions based on the interpretations given in Table 4-6. The principles for establishing these models are described in detail in /Back et al. 2007/.

Coordinate transformations are performed in such a way that the principal directions of anisotropy are aligned to the axes of the simulation volume.

Table 4-7. Borehole data for each subdomain.

Thermal subdomain	Borehole name	Borehole section (length interval, m)	Anisotropy direction (x, y, z)*	Used for simulations (yes/no)*
A1	KFM06A	751–998	x	Yes
A2	KFM06C	411–664	y	Yes
	KFM08C	342–546		No
	KFM08D	395–532		Yes
	KFM08D	635–781		Yes
B	KFM06C	664–898	y	Yes
	KFM08D	532–635		Yes
	KFM08D	781–935		Yes

* For further explanation see section 4.4.2.

4.4.2 Spatial analysis

The spatial analysis was made stepwise for each subdomain as follows:

1. Initial transition probability analysis of TRCs from borehole data, see Table 4-7. This initial analysis is based on **all** borehole data selected to characterise each subdomain, and without any consideration of anisotropy.
2. Transformation of borehole data into the anisotropy orientation of the TRCs. This means that anisotropy of typical lengths, and thus also continuous-lag transition probabilities, was accounted for. The proportions of TRCs were assumed to be isotropic. The simulations need to be oriented in the principal direction of anisotropy to properly represent the spatial properties of the domain. Existing boreholes are typically not oriented in the anisotropy direction, and a transformation of borehole data to the orientation of the anisotropy of the system is therefore necessary. Geological information describing anisotropy was given as: (1) the trend and plunge of the mineral stretching orientation and (2) the strike and dip of the foliation. The orientation of rock units is a function of these.

A local coordinate system (x''' , y''' , z''') was developed for each subdomain, governed by the principal direction of anisotropy and an origin defined by minimum easting, minimum northing, and maximum elevation from positions in borehole records. The local coordinate system was obtained through rotations:

1. To the trend direction of the mineral orientation, i.e. rotation of the x-y plane around the z-axis. This produces the principal axes x' , y' and z' .
2. To the plunge of the mineral orientation, i.e. rotation of the x' - z' plane around the y' -axis. This produces the principal axes x'' , y'' and z'' .
3. To the foliation of the rocks, i.e. rotation of the y'' - z'' plane around the x'' -axis. This produces the principal axes x''' , y''' and z''' .

This results in a transformed coordinate system with main axis (x''') parallel to the principal direction of anisotropy, see Figure 4-3.

A detailed mathematical description of the transformation of borehole data to a coordinate system orientated in the principal direction of anisotropy as a function of the mineral stretching and foliation plane is given in Appendix D.

3. Calculation of typical lengths of TRCs for the x''' , y''' or z''' directions of anisotropy was made on the transformed borehole data. To minimize errors due to borehole deviations from anisotropy directions, only the boreholes with orientation close to **one** of the axes x''' , y''' or z''' were used, see Table 4-7 above. The typical lengths in remaining directions were obtained from geometry relationship information for TRCs, given by the geological interpretations in Table 4-6.
4. The transition probability structure was calculated with respect to the typical lengths calculated for x''' , y''' and z''' . By adjusting the typical lengths, the transition probability matrix was updated for each direction x''' , y''' and z''' . The proportions of TRCs were assumed to be isotropic and thus identical to those calculated in Step 1.

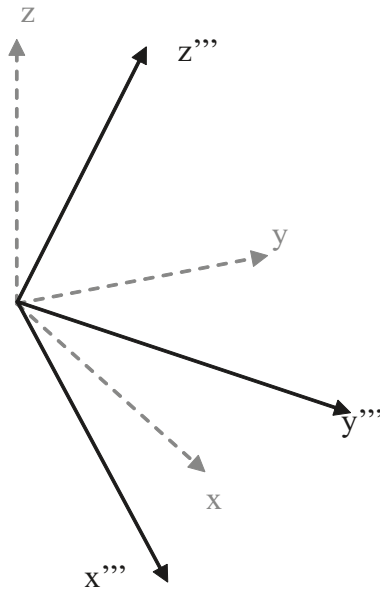


Figure 4-3. Principal directions x''' , y''' and z''' of the local transformed coordinate system, where x''' is parallel to the principal direction of anisotropy.

4.4.3 Spatial properties – results

The results of the spatial analysis by T-PROGS for each subdomain are given in Table 4-8 to Table 4-10.

Transition probabilities are presented as embedded probabilities. Most Markov chain analyses in geological applications have been performed in the form of so called embedded analyses /Carle 1999/, in which transition probabilities from one discrete occurrence of a category to another, is considered, irrespective of the lag distance; see /Davis 1986, Carle and Fogg 1997, Back and Sundberg 2007/ for more details. The embedded analysis thus provides the probabilities of entering the other categories when leaving a specific category and does not directly give information about the spatial dependencies of the categories. T-PROGS links the embedded Markov chain analysis to the development of continuous-lag (spatially dependent) Markov chain models. The reason this is important is that geologists are more inclined to think and work in the embedded framework /Carle 1999/.

Table 4-8. Proportions, transition probabilities and typical lengths for subdomain A1. Transition probabilities are shown as embedded probabilities of going from one TRC to other TRCs. Diagonal terms show the typical lengths of TRCs based on all boreholes and without consideration of anisotropy. “Typical TRC lengths” show the typical anisotropic lengths for directions x''' , y''' and z''' calculated from transformed borehole data and geological interpretations.

TRC	Proportion	Isotropic transition probabilities to TRCs (embedded) and typical lengths (m). (Lengths shown in bold)				Typical TRC lengths (m)		
		TRC 17	TRC 51	TRC 58	TRC 61	x'''	y'''	z'''
TRC 17	0.02	1.13	0.00	0.88	0.12	1.13	0.56	0.28
TRC 51	0.06	0.00	2.33	0.50	0.50	2.33	1.17	0.58
TRC 58	0.81	0.13	0.29	9.65	0.57	b.g.	b.g.	b.g.
TRC 61	0.12	0.03	0.03	0.93	1.83	1.83	1.83	0.37

b.g. = background material, not calculated for anisotropy directions.

Table 4-9. Proportions, transition probabilities and typical lengths for subdomain A2. See also text in Table 4-8.

TRC	Proportion	Isotropic transition probabilities to TRCs (embedded) and typical lengths (m). (Lengths shown in bold)				Typical TRC lengths (m)		
		TRC 17	TRC 51	TRC 57	TRC 61	X'''	Y'''	Z'''
TRC 17	0.02	1.67	0.00	1.00	0.00	3.33	1.67	0.83
TRC 51	0.06	0.00	3.21	0.57	0.43	6.43	3.21	1.61
TRC 58	0.81	0.10	0.08	8.68	0.82	b.g.	b.g.	b.g.
TRC 61	0.12	0.00	0.14	0.86	1.36	1.36	1.36	0.27

b.g. = background material, not calculated for anisotropy directions.

Table 4-10. Proportions, transition probabilities and typical lengths for subdomain B. See also text in Table 4-8.

TRC	Proportion	Isotropic transition probabilities to TRCs (embedded) and typical lengths (m). (Lengths shown in bold)				Typical TRC lengths (m)		
		TRC 17	TRC 51	TRC 57	TRC 61	X'''	Y'''	Z'''
TRC 17	0.18	6.29	0.07	0.29	0.64	12.57	6.29	3.14
TRC 51	0.19	0.07	3.37	0.56	0.37	6.74	3.37	1.69
TRC 58	0.44	0.10	0.37	5.40	0.53	b.g.	b.g.	b.g.
TRC 61	0.19	0.21	0.28	0.51	2.33	2.33	2.33	0.47

b.g. = background material, not calculated for anisotropy directions.

4.5 Stochastic simulation of lithology (TRC)

4.5.1 Introduction

Stochastic unconditional simulations of TRCs (step 8 in Figure 3-1) were performed using the spatial properties derived from the analysis described in section 4.4.3. Each realisation has a volume of $50 \times 50 \times 50 \text{ m}^3$ with a grid cell size of $1 \times 1 \times 1 \text{ m}$. Five hundred (500) realisations were produced. The numbers of realisations performed for each of the two subdomains reflect their volumetric importance, which in turn corresponds to the borehole lengths characterising each subdomain. Therefore, two-thirds (334) of the realisations are based on subdomain A, and one-third (166) on subdomain B. Subdomain A is further divided into A1 (105 realisations) and A2 (229 realisations).

Rock type proportions for domain RFM045 are presented in Table 4-11. Proportions determined from the output of the simulations are slightly different to the proportions estimated by geological modelling team /Stephens et al. 2007/. The reasons for the discrepancies are discussed in section 6.1.

4.5.2 Examples and visualisation of results

Figure 4-4 gives two examples of visualisations of realisations of the different thermal subdomains in domain RFM045. Figure 4-5 gives examples of realisations for domain RFM029 (internal) for comparison. The anisotropy in the shape of the subordinate rocks (TRCs) can be clearly seen in these visualisations. Additional 2D visualisations are presented in Appendix B.

Table 4-11. Quantitative estimates in volume % of different TRCs in domain RFM045.

TRC	Proportions of TRCs in 500 realisations (%)	Proportions from geological model v. 2.2 /Stephens et al. 2007/ (%)*	Comment
58	68.4	67.3	Comprises Granite to granodiorite, 101057, and Granite, aplitic, 101058
51	10.4	10.2	Comprises Granite, granodiorite and tonalite, 101051, and Felsic to intermediate volcanic rock, 103076
61	14.0	15.2	Comprises Pegmatite, pegmatitic granite, 101061, and Granite, 111058
17	7.1	6.5	Comprises Amphibolite, 102017, and Diorite, quartz diorite and gabbro, 101033

* Other rock types not belonging to any of the defined TRCs make up less than 1% of the rock volume /Stephens et al. 2007/.

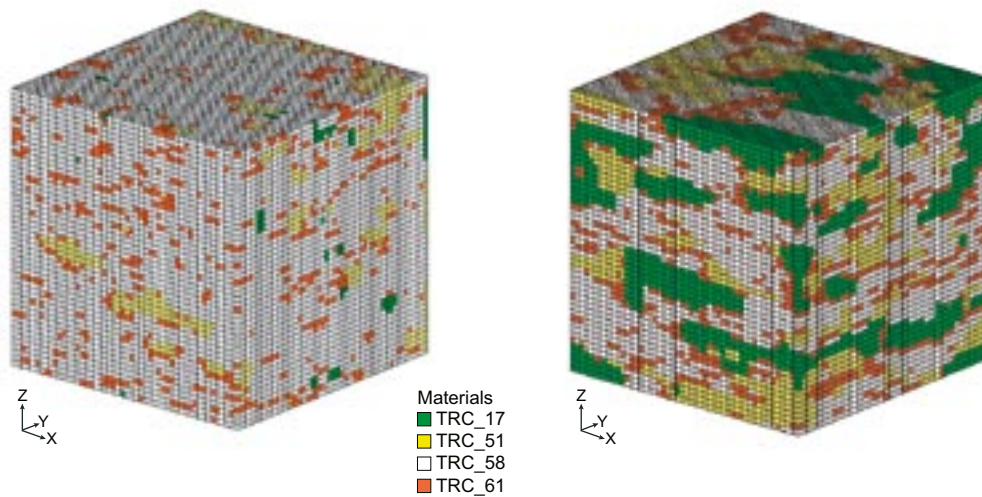


Figure 4-4. Two visualisations of realisations of thermal subdomains in domain RFM045: sub-domain A1 (left) and subdomain B (right). The simulated rock volume has dimensions 50×50×50 metres. The simulated TRCs are TRC 58 (white), TRC 51 (yellow), TRC 61 (orange) and TRC 17 (green).

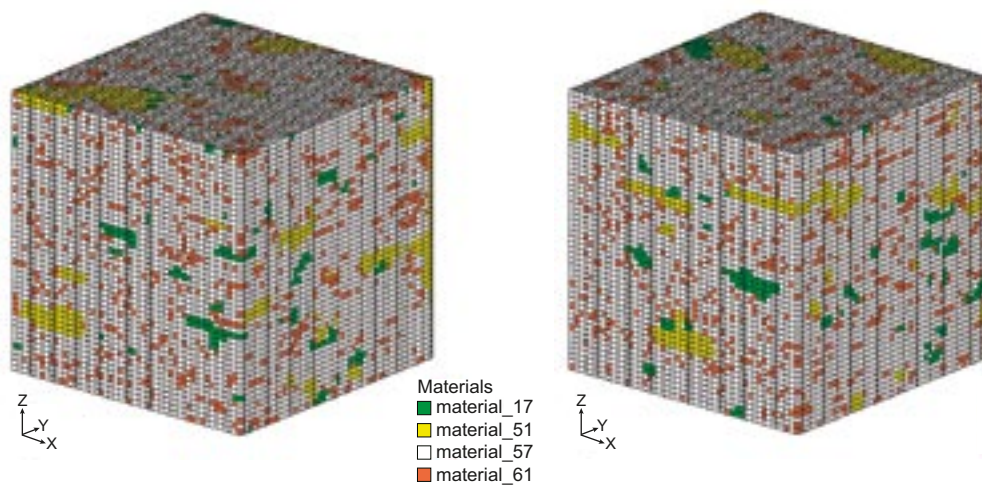


Figure 4-5. Two visualisations of realisations of domain RFM029 (internal). The simulated rock volume has dimensions 50×50×50 metres. From simulations made in /Back et al. 2007/. For explanation, see Figure 4-4.

4.5.3 Analysis and verification of results

Methodology

The statistical properties, i.e. the proportions of categories (TRCs), the typical lengths of categories, and the spatial properties of categories are assumed to be stationary for all realisations within a subdomain. The relevance of the results of the simulations have been analysed and verified by means of statistical analysis with respect to the ability of T-PROGS to reproduce:

- The proportions of the TRCs.
- Typical (mean) lengths of TRCs calculated by transition probability analysis.
- The distribution of TRC lengths observed in borehole data.

As input into the T-PROGS modelling, the proportions and typical TRC lengths were calculated through transition probability analysis of borehole data. The typical lengths for different directions of the model volume were then calculated from the relative length information provided by the geological interpretations of anisotropy.

Realisations of the three subdomains were used for the verification analysis, which was made for each subdomain as follows:

- The proportions of TRCs were calculated for 10 randomly selected realisations and compared to the proportions calculated from borehole data.
- The typical lengths were calculated from 36 “borings” along each direction (x, y and z) for each of 10 randomly selected realisations. Typical lengths were calculated for x, y and z directions for TRCs 17, 51 and 61.
- Histograms of the lengths of the TRCs were produced from the 36 “borings” along each direction (x, y and z) for each of the 10 randomly selected realisations.
- Histograms of the lengths of the TRCs observed in boreholes were produced.
- A qualitative comparison was made between the histograms produced from the simulations and the histograms produced from the borehole data.

Results of simulations – proportions

Table 4-12 shows the proportions of TRCs in 10 randomly selected realisations for subdomain A1.

Table 4-13 shows the proportions of TRCs in 10 randomly selected realisations for subdomain A2.

Table 4-14 shows the proportions of TRCs in 10 randomly selected realisations for subdomain B.

As can be seen from Table 4-12 to Table 4-14, T-PROGS nearly exactly reproduces the proportions of the TRCs for all realisations and for all subdomains.

Table 4-12. Proportions of TRCs in 10 randomly selected realisations for subdomain A1.

TRC	Proportions from borehole (%) [*]	Proportions of 10 randomly selected realisation (%)									
		1	2	3	4	5	6	7	8	9	10
TRC17	1.51	1.52	1.51	1.52	1.52	1.52	1.51	1.52	1.52	1.52	1.52
TRC51	6.23	6.23	6.23	6.26	6.25	6.24	6.25	6.24	6.23	6.24	6.24
TRC58	80.76	80.73	80.74	80.7	80.71	80.72	80.72	80.72	80.73	80.72	80.72
TRC61	11.51	11.51	11.51	11.52	11.51	11.52	11.52	11.52	11.52	11.51	11.52

^{*} Calculated in T-PROGS.

Table 4-13. Proportions of TRCs in 10 randomly selected realisations for subdomain A2.

TRC	Proportions from borehole (%)*	Proportions of 10 randomly selected realisation (%)									
		1	2	3	4	5	6	7	8	9	10
TRC17	1.51	1.56	1.55	1.54	1.54	1.53	1.54	1.53	1.55	1.52	1.54
TRC51	6.23	6.34	6.27	6.32	6.28	6.3	6.28	6.3	6.27	6.27	6.26
TRC58	80.76	80.6	80.67	80.64	80.68	80.67	80.67	80.66	80.68	80.7	80.68
TRC61	11.51	11.51	11.51	11.5	11.5	11.51	11.5	11.51	11.5	11.51	11.51

* Calculated in T-PROGS.

Table 4-14. Proportions of TRCs in 10 randomly selected realisations for subdomain B.

TRC	Proportions from borehole (%)*	Proportions of 10 randomly selected realisation (%)									
		1	2	3	4	5	6	7	8	9	10
TRC17	18.1	18.5	18.3	18.6	18.5	18.4	18.3	18.6	18.3	18.2	18.2
TRC51	18.8	18.7	18.7	18.7	18.7	18.7	18.7	18.7	18.7	18.7	18.7
TRC58	43.9	43.7	43.8	43.7	43.8	43.8	43.9	43.7	43.9	43.9	43.9
TRC61	19.2	19.1	19.1	19.0	19.1	19.1	19.1	19.1	19.1	19.1	19.1

* Calculated in T-PROGS.

Results of simulations – typical lengths

For all subdomains a comparison was made between simulated typical lengths (mean values) and the typical lengths (mean values) estimated from the transition analysis of boreholes (referred to as “nominal” lengths below). The mean values of simulated TRC lengths were estimated assuming a geometric distribution, which is a fundamental assumption in the approach to geological simulation used here. The transitions between categories (TRCs) are assumed to follow a Markov process, in which the lengths of the categories have a geometric distribution. The geometric distribution is the discrete analogue of the continuous exponential distribution, and has a probability function $P(X = n) = (1 - p)^{n-1} p$. In the geological model application used here the probability function describes the probability of leaving TRC X after taking n steps, each step having a probability p for leaving X . The mean of the geometric distribution is $1/p$. For further description of geometric distributions see e.g. /Evans et al. 2000/. It can be seen in the histograms from both simulations and from boreholes that the geometric distribution is a relevant model in most cases (see Appendix C). The comparison of the mean simulated lengths and mean lengths (nominal) from the transition analysis – both estimated assuming geometric distribution – was therefore considered as a relevant measure of performance.”

Calculations of typical lengths of TRCs 17, 51 and 61 were made from “borings” through 10 randomly selected realisations for each of the subdomains. The “borehole length” of each borehole is 50 metres and 36 “borings” were made in each direction. The total “borehole length” for the statistical analysis were thus $50 \times 36 \times 10 = 18,000$ metres. TRC 58 constitutes the “background” in the simulations for all three subdomains and is therefore not relevant to include in the analysis.

The results of the calculations of the typical length (m) for directions x, y and z for subdomain A1 are presented in Table 4-15 to Table 4-17.

The results of the calculations of the typical length (m) for directions x, y and z for subdomain A2 are presented in Table 4-18 to Table 4-20.

Table 4-15. Typical lengths of TRC17 in subdomain A1.

Typical simulated length (m)*	Nominal value (m)*	Comment on simulated values
$\mu_x = 1.71$	1.13	Somewhat high
$\mu_y = 1.19$	0.56	High
$\mu_z = 1.01$	0.28	High

* The typical simulated length is the mean lengths estimated from “borings” through the simulated rock volumes. The nominal value is the typical length estimated from the transition analysis in T-PROGS.

Table 4-16. Typical lengths of TRC51 in subdomain A1.

Typical simulated length (m)*	Nominal value (m)*	Comment on simulated values
$\mu_x = 2.74$	2.33	Somewhat high
$\mu_y = 1.70$	1.17	Somewhat high
$\mu_z = 1.25$	0.58	High

* The typical simulated length is the mean lengths estimated from “borings” through the simulated rock volumes. The nominal value is the typical length estimated from the transition analysis in T-PROGS.

Table 4-17. Typical lengths of TRC61 in subdomain A1.

Typical simulated length (m)*	Nominal value (m)*	Comment on simulated values
$\mu_x = 2.41$	1.83	Somewhat high
$\mu_y = 2.44$	1.83	Somewhat high
$\mu_z = 1.18$	0.37	High

* The typical simulated length is the mean lengths estimated from “borings” through the simulated rock volumes. The nominal value is the typical length estimated from the transition analysis in T-PROGS.

Table 4-18. Typical lengths of TRC17 in subdomain A2.

Typical simulated length (m)*	Nominal value (m)*	Comment on simulated values
$\mu_x = 3.55$	3.33	OK
$\mu_y = 2.03$	1.67	Somewhat high
$\mu_z = 1.36$	0.83	High

* The typical simulated length is the mean lengths estimated from “borings” through the simulated rock volumes. The nominal value is the typical length estimated from the transition analysis in T-PROGS.

Table 4-19. Typical lengths of TRC51 in subdomain A2.

Typical simulated length (m)*	Nominal value (m)*	Comment on simulated values
$\mu_x = 5.61$	6.43	OK
$\mu_y = 3.45$	3.21	OK
$\mu_z = 2.11$	1.61	Somewhat high

* The typical simulated length is the mean lengths estimated from “borings” through the simulated rock volumes. The nominal value is the typical length estimated from the transition analysis in T-PROGS.

Table 4-20. Typical lengths of TRC61 in subdomain A2.

Typical simulated length (m)*	Nominal value (m)*	Comment on simulated values
$\mu_x = 2.01$	1.36	Somewhat high
$\mu_y = 1.92$	1.36	Somewhat high
$\mu_z = 1.14$	0.27	High

* The typical simulated length is the mean lengths estimated from “borings” through the simulated rock volumes. The nominal value is the typical length estimated from the transition analysis in T-PROGS.

It can be seen from the analysis that T-PROGS reproduces the relative anisotropy between different directions in subdomain A (A1 and A2) reasonably well. T-PROGS overestimates shorter typical lengths, but for longer lengths, more than approximately 2 metres, estimations are closer to the nominal values. Typical lengths for TRCs 17, 51 and 61 are generally short in subdomain A, in several cases less than 1 metre, which results in estimations of typical simulated lengths that are longer than nominal values. The reason for overestimation of shorter lengths is the discretisation of the model, where 1 metre is the shortest length that can be represented.

The results of the calculations of the typical length (m) for directions x, y and z for subdomain B are presented in Table 4-21 to Table 4-23.

Table 4-21. Typical lengths of TRC17 in subdomain B.

Typical simulated length (m)*	Nominal value (m)*	Comment on simulated values
$\mu_x = 9.31$	12.57	Low
$\mu_y = 5.96$	6.29	OK
$\mu_z = 3.14$	3.14	OK

* The typical simulated length is the mean lengths estimated from “borings” through the simulated rock volumes. The nominal value is the typical length estimated from the transition analysis in T-PROGS.

Table 4-22. Typical lengths of TRC51 in subdomain B.

Typical simulated length (m)*	Nominal value (m)*	Comment on simulated values
$\mu_x = 6.77$	6.74	OK
$\mu_y = 3.71$	3.37	OK
$\mu_z = 2.35$	1.69	Somewhat high

* The typical simulated length is the mean lengths estimated from “borings” through the simulated rock volumes. The nominal value is the typical length estimated from the transition analysis in T-PROGS.

Table 4-23. Typical lengths of TRC61 in subdomain B.

Typical simulated length (m)*	Nominal value (m)*	Comment on simulated values
$\mu_x = 2.87$	2.33	Somewhat high
$\mu_y = 2.82$	2.33	Somewhat high
$\mu_z = 1.29$	0.47	High

* The typical simulated length is the mean lengths estimated from “borings” through the simulated rock volumes. The nominal value is the typical length estimated from the transition analysis in T-PROGS.

Again T-PROGS reproduces the relative anisotropy between different directions in subdomain B reasonably well. T-PROGS overestimates shorter typical lengths, but for longer lengths, more than approximately 2 metres, estimations are closer to the nominal values. An exception is the long nominal length of TRC17 in the x-direction which was underestimated in the simulations. However, simulations reproduce typical lengths in the y and z directions. This means that anisotropy is not as pronounced in the simulations as predicted by the model parameters. The reason for the underestimation of the relatively long typical lengths of TRC17 in the x-direction is tentatively suggested to be an effect of the limited simulation volume.

Typical lengths for TRCs 17, 51 and 61 are in general longer in subdomain B than in subdomains A1 and A2, which results in estimations of typical lengths that are closer to nominal values. Again, the reason for overestimation of shorter lengths is the discretisation of the model, where 1 metre is the shortest length that can be represented.

Results of simulations – distribution of lengths

In Appendix C, histograms of simulated lengths of TRCs, based on the “borings” in the 10 randomly selected realisations for each subdomain, and histograms of lengths observed in the actual borehole are presented. Due to the large number of “borings” in the simulated volumes it is assumed that the histograms in Appendix C give a good representation of the simulated lengths of TRCs. A visual comparison was made of the histograms from the “borings” with lengths observed in the actual borehole data. The borehole information is rather limited compared to the number of data used for the simulation histograms. The visual comparison indicates, however, that T-PROGS is able to reproduce – for all TRCs – the TRC lengths registered in the borehole data.

5 Thermal domain model

5.1 Modelling results – domain RFM045

Stochastic simulations of thermal conductivity for each TRC in domain RFM045 were performed in model stage 2.2 /Back et al. 2007/ and are not repeated here (step 10 in Figure 3-1). The new realisations of TRCs (geology) for domain RFM045 and the realisations of thermal conductivity produced in model stage 2.2 /Back et al. 2007/ are merged, so that each position in space in the geological realisation is assigned a thermal value from the corresponding position in the appropriate thermal realisation (step 11 in Figure 3-1). The result of this merging operation is a set of 500 realisations of thermal conductivity at the simulation scale of 1 m (example 2D visualisations in Figure 5-1). These realisations were scaled up (step 12 in Figure 3-1) to a cell size of 5 m using the self-consistent approximation approach /Back and Sundberg 2007/.

Histograms of thermal conductivity for the combined 500 realisations are presented in Figure 5-2 for the 1 m scale and in Figure 5-3 for the 5 m scale. Summary statistics of all 500 realisations are presented in Table 5-1. For the 1 m scale simulations, the pronounced lower tail and its strange shape is a result of the presence of low-conductive rock, mainly amphibolite (TRC17) and granite, granodiorite and tonalite (TRC51).

Table 5-1. Summary statistics for domain RFM045 based on simulations at the 1 m scale and upscaling to 5 m.

Statistical parameter	1 m	5 m	Unit
Mean	3.57	3.56	W/(m·K)
Variance	0.18	0.08	[W/(m·K)] ²
Standard deviation	0.42	0.28	W/(m·K)
Min	2.10	2.16	W/(m·K)
Max	4.25	4.18	W/(m·K)
0.1-percentile (0.001-quantile)	2.24	2.36	W/(m·K)
1-percentile (0.01-quantile)	2.31	2.56	W/(m·K)
2.5-percentile (0.025-quantile)	2.36	2.73	W/(m·K)

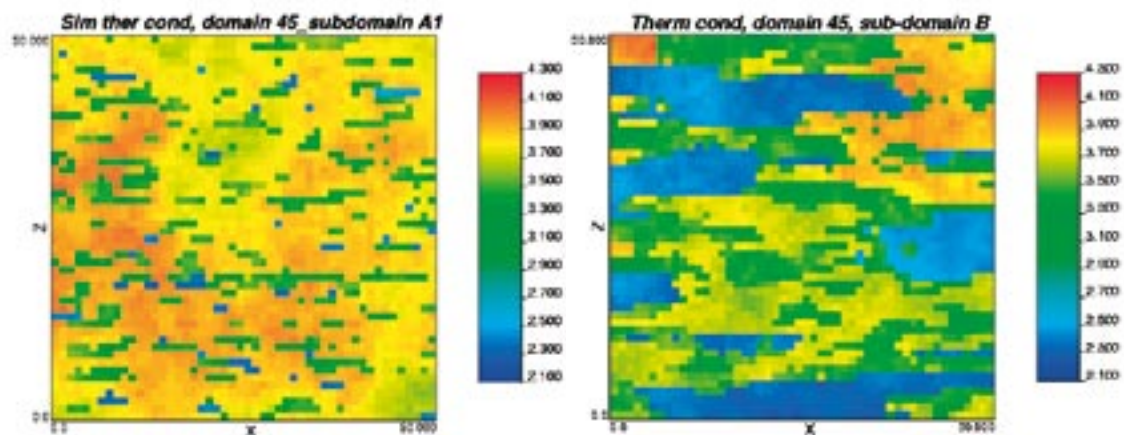


Figure 5-1. Example realisations of thermal conductivity (slices in xz-plane) for domain RFM045 simulated at the 1 m scale. Left: subdomain A1; Right: subdomain B. The simulation volume has dimensions 50 × 50 × 50 m.

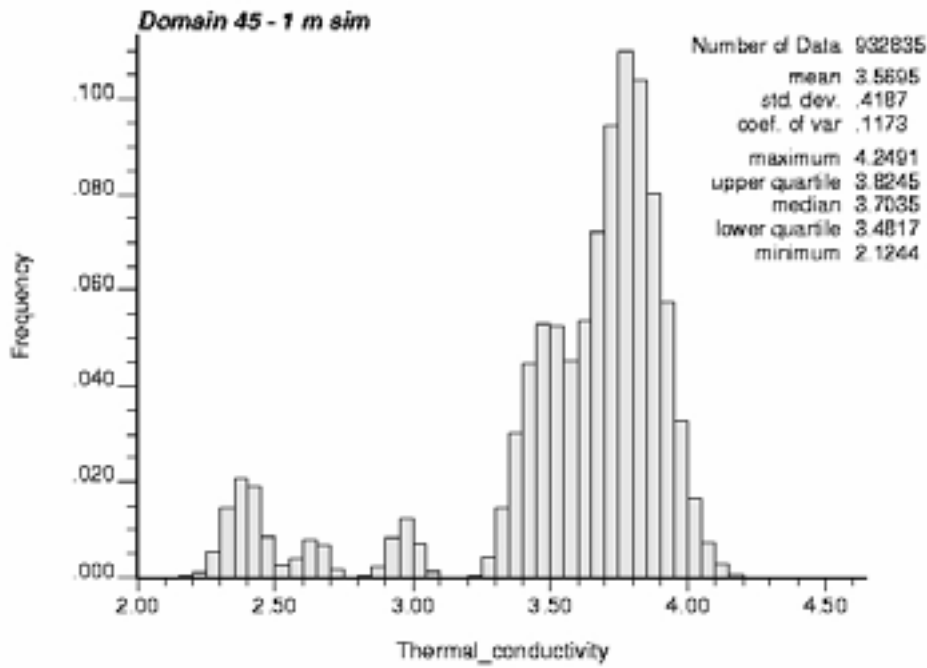


Figure 5-2. Histogram of thermal conductivity for domain RFM045 simulated at the 1 m scale.

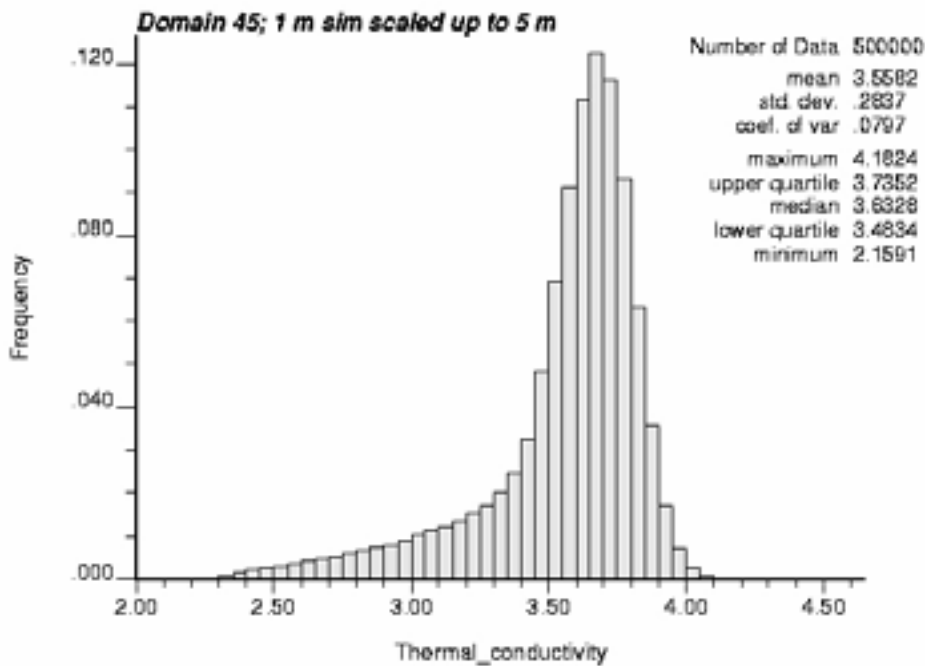


Figure 5-3. Histogram of thermal conductivity for domain RFM045 simulated at the 1 m scale followed by upscaling to 5 m.

Upscaling of the realisations has a smoothing effect of the histogram, as illustrated in Figure 5-3 for the scale 5 m. However, even at this scale there is a pronounced lower tail of thermal conductivity values, which reflects the presence of large bodies of low-conductive rock in domain RFM045; see Appendix B. This can be compared with the results for domain RFM029 in which large bodies of amphibolite have not been observed /Back et al. 2007/.

Simulation results have also been compiled for the individual thermal subdomains. Histograms of thermal conductivity for the 333 realisations representing subdomain A (A1 and A2) are presented in Figure 5-4 and for the 167 realisations of subdomain B in Figure 5-5. Results at both 1 m and 5 m scales are shown. Summary statistics of the individual subdomains are presented in Table 5-2 and Table 5-3. The lower tail is much more pronounced in subdomain B due to the presence of large amphibolite (TRC17) bodies. 2D visualisations of realisations of thermal conductivity are exemplified in Appendix B for each subdomain. Visualisations of the corresponding lithological (TRC) realisations are also presented in Appendix B to aid interpretation.

In the geological model /Stephens et al. 2007/, domain RFM045 has not been divided into two subdomains. Therefore, the statistics for the modelled thermal subdomains do not relate to any specific volume of rock. Rather, they apply to one possible scenario regarding the make-up of domain RFM045. Here, it is assumed that two-thirds of the domain is dominated by granite (101058) and granite to granodiorite (101057) with subordinate amounts of thin amphibolites, and one-third is characterised by greater lithological heterogeneity including the presence of large bodies of amphibolite.

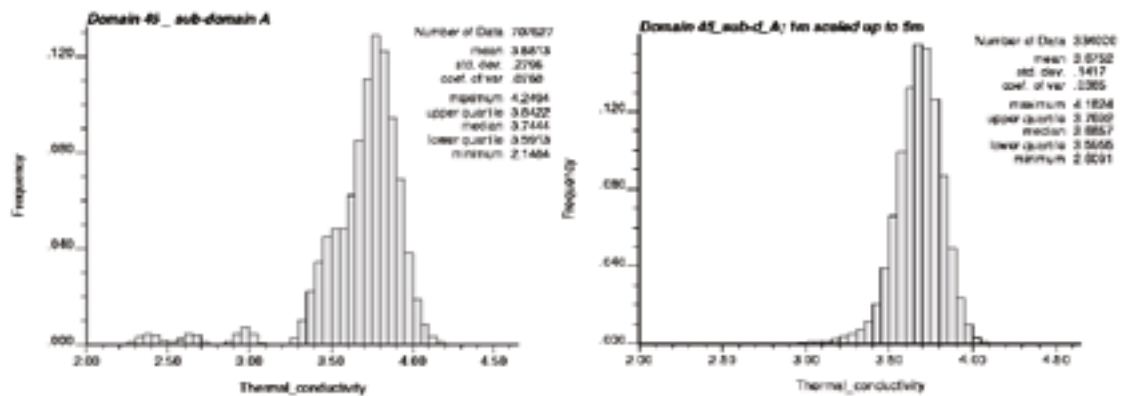


Figure 5-4. Histogram of thermal conductivity for subdomain A in RFM045 at 1 m and 5 m scales.

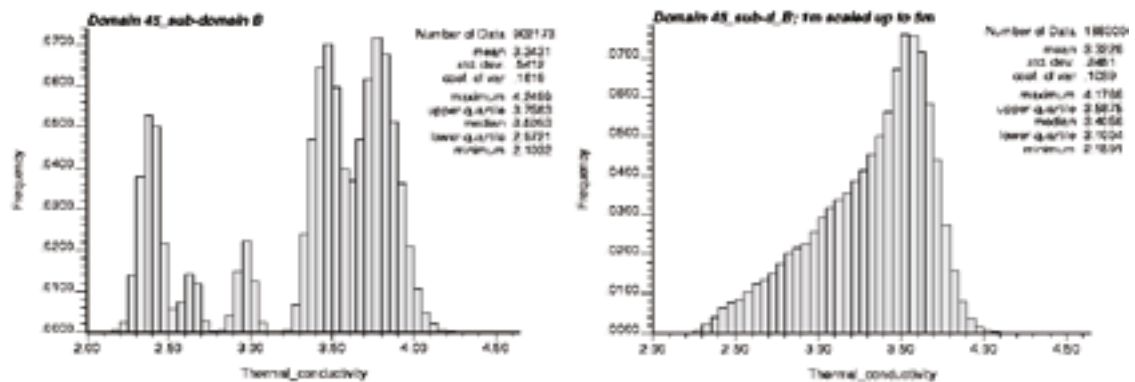


Figure 5-5. Histogram of thermal conductivity for subdomain B in RFM045 at 1 m and 5 m scales.

Table 5-2. Summary statistics for subdomain A in domain RFM045 based on simulations at the 1 m scale and upscaling to 5 m.

Statistical parameter	1 m	5 m	Unit
Mean	3.68	3.68	W/(m·K)
Variance	0.08	0.02	[W/(m·K)] ²
Standard deviation	0.28	0.14	W/(m·K)
Min	2.13	2.61	W/(m·K)
Max	4.25	4.18	W/(m·K)
0.1-percentile (0.001-quantile)	2.29	2.98	W/(m·K)
1-percentile (0.01-quantile)	2.41	3.24	W/(m·K)
2.5-percentile (0.025-quantile)	2.67	3.36	W/(m·K)

Table 5-3. Summary statistics for subdomain B in domain RFM045 based on simulations at the 1 m scale and upscaling to 5 m.

Statistical parameter	1 m	5 m	Unit
Mean	3.34	3.32	W/(m·K)
Variance	0.29	0.12	[W/(m·K)] ²
Standard deviation	0.54	0.35	W/(m·K)
Min	2.10	2.16	W/(m·K)
Max	4.25	4.18	W/(m·K)
0.1-percentile (0.001-quantile)	2.21	2.32	W/(m·K)
1-percentile (0.01-quantile)	2.28	2.43	W/(m·K)
2.5-percentile (0.025-quantile)	2.31	2.53	W/(m·K)

5.2 Modelling results – heat capacity

A relationship, described by a second order equation (Figure 2-3), between heat capacity (C) from direct measurements and thermal conductivity was established in the thermal modelling, stage 2.2 /Back et al. 2007/. It is also possible to include a random error component in prediction of C from λ using the regression equation; see Equation 2-3 in section 2.6. Using this relationship, together with the output from simulation of thermal conductivity, heat capacity realisations can be created. One example of such a realisation is illustrated in 2D in Figure 5-6. Heat capacity distributions at domain level can be created from these realisations. Distributions for the 1 m scale for rock domains RFM029 and RFM045 are presented in Figure 5-7 and Figure 5-8, respectively. Summary statistics are presented in Table 5-4.

Table 5-4. Statistics of heat capacity at scale 1 m for domains RFM029 and RFM045 based on simulations of thermal conductivity at the 1 m scale.

Statistical parameter	RFM029, MJ/(m ³ ·K)	RFM045, MJ/(m ³ ·K)
Mean	2.06	2.12
Standard deviation	0.10	0.15

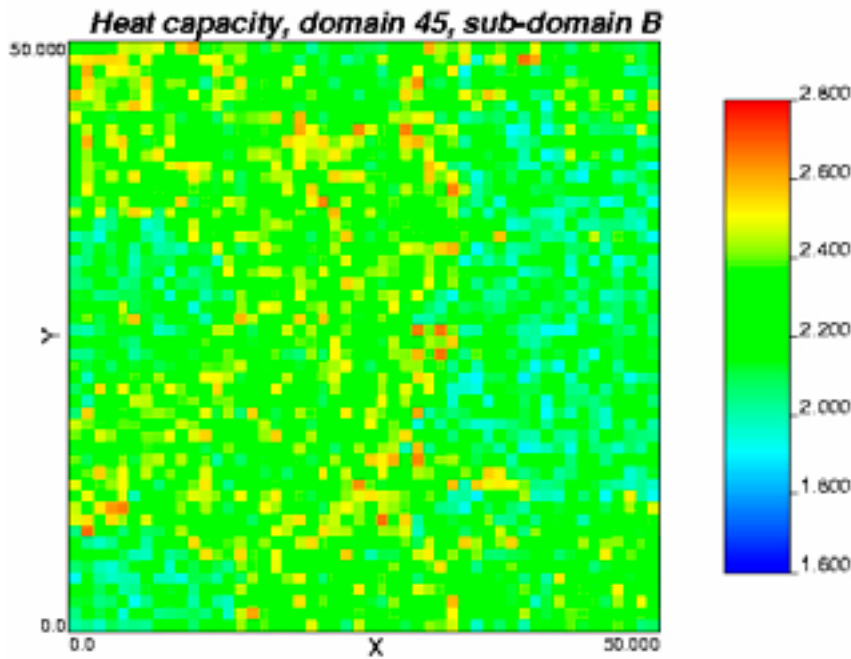


Figure 5-6. An example of a slice through a realisation showing the spatial distribution of heat capacity for domain RFM45 based on simulations of thermal conductivity at the 1 m scale and subsequent calculation of heat capacity. Subdomain B, xy plane. The simulation volume has dimensions 50 x 50 x 50 m.

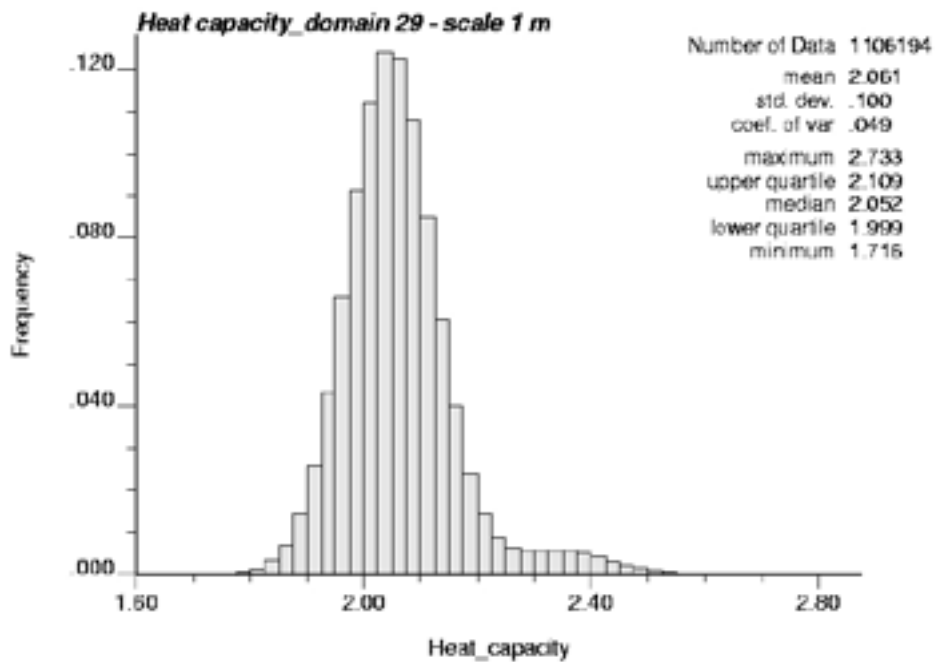


Figure 5-7. Histogram of heat capacity for domain RFM29 based on simulations of thermal conductivity at the 1 m scale. Calculated from simulation results in /Back et al. 2007/.

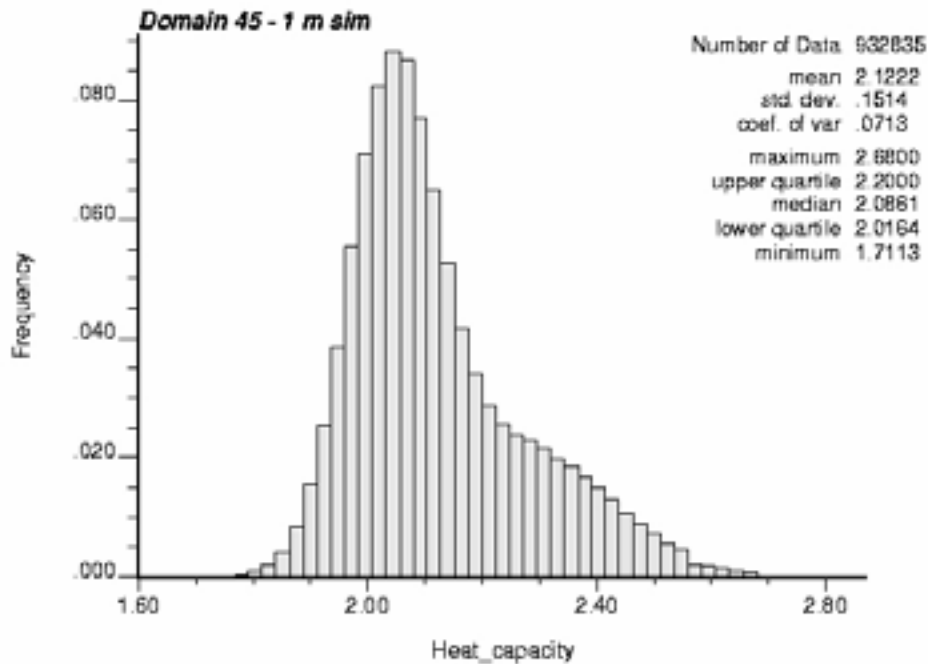


Figure 5-8. Histogram of heat capacity for domain RFM045 based on simulations of thermal conductivity at the 1 m scale.

5.3 Evaluation of modelling results – domain RFM045

The lower tail of the thermal conductivity distribution is of importance for the design of a repository. Therefore, the 0.1-percentile, 1-percentile and 2.5-percentile of the thermal conductivity distribution were estimated from the modelling results. These percentiles were estimated for two scales, 1 m and 5 m, for the domain as a whole, as well as for the separate thermal subdomains. The results are presented in Table 5-1, Table 5-2 and Table 5-3. The results illustrate how the lower percentiles increase when the scale increases from 1 m to 5 m.

Occurrences of rock types smaller than the smallest cell size are modelled as if they occur at this size. In other words, they are modelled at a size that is too large. At the same time, the modelled occurrences are less frequent than the number of small bodies occurring in reality. Since the smallest cell size in the simulations is 1 m, the proportion of TRC 17 equal to, or close to, the simulation scale is almost certainly overestimated in the simulations. This discretisation error was considered to be significant for the 1 m scale for domain RFM029 /Back et al. 2007/, since amphibolite commonly occurs as thin bodies with a borehole length less than 1 m /Stephens et al. 2007/. In Domain RFM045, however, most of the amphibolite is present as larger bodies, so the discretisation error is judged to be small. Moreover, any discretisation error decreases rapidly with upscaling, and is believed to have disappeared at the 5 m scale.

The new lithological simulations of domain RFM045 have underestimated the lengths of amphibolite bodies in the direction of maximum extension compared to the typical length indicated by the model, see section 4.5.3. This may have a slight effect on the distribution of thermal conductivity values at the 5 m scale, but is probably significant only at larger scales. It should be kept in mind that the models on which the lithological simulations are based are in themselves quite uncertain.

Table 5-5 and Figure 5-9 to Figure 5-11 compare the modelling results presented here for domain RFM045 with results reported in model stage 2.2 /Back et al. 2007/. Whereas the lower tail percentiles are almost identical for the 1 m scale, the same percentiles are significantly higher for the 5 m scale in the revised 2.3 model.

Figure 5-9, Figure 5-10 and Figure 5-11 show how the lower percentiles change with scale for both stage 2.2 results and the new stage 2.3 results. The lower percentiles increase more during upscaling in the thermal model stage 2.3 than was the case in stage 2.2. The reason is that large bodies of the low-conductive amphibolite are less common in stage 2.3 than in stage 2.2. Large bodies of low-conductive rock tend to maintain the lower tail even after upscaling but this effect is reduced in model stage 2.3.

Table 5-5. Comparison of modelling results for domain RFM045 for model stage 2.2 and model stage 2.3.

Statistical parameter	Stage 2.2 1 m scale, W/(m·K)	Stage 2.3 1 m scale, W/(m·K)	Stage 2.2 5 m scale, W/(m·K)	Stage 2.3 5 m scale, W/(m·K)
Mean	3.50	3.57	3.49	3.56
Standard deviation	0.44	0.42	0.30	0.28
0.1-percentile	2.25	2.24	2.33	2.36
1-percentile	2.31	2.31	2.48	2.56
2.5-percentile	2.35	2.36	2.64	2.73

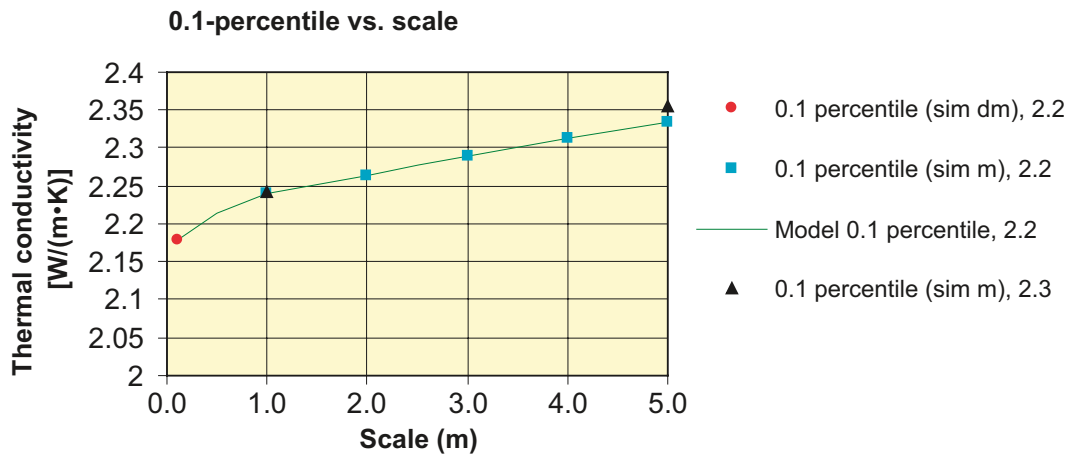


Figure 5-9. The 0.1-percentile (0.001 quantile) versus scale for domain RFM045. The black dots represent the 1 m simulation results in stage 2.3 and the blue dots the corresponding results in stage 2.2 /Back et al. 2007/. Upscaling was performed on simulated values at the 1 m scale.

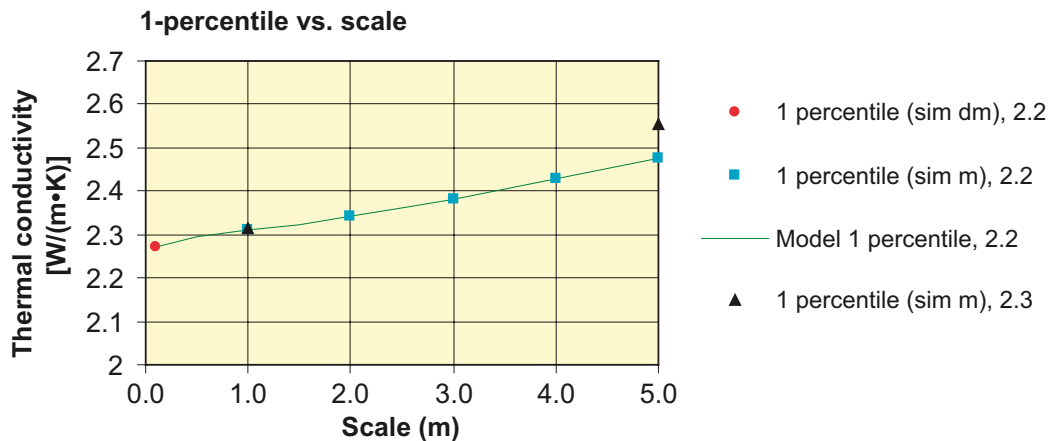


Figure 5-10. The 1-percentile (0.01 quantile) versus scale for domain RFM045. The black dots represent the 1 m simulation results in stage 2.3 and the blue dots the corresponding results in stage 2.2 /Back et al. 2007/. Upscaling was performed on simulated values at the 1 m scale.

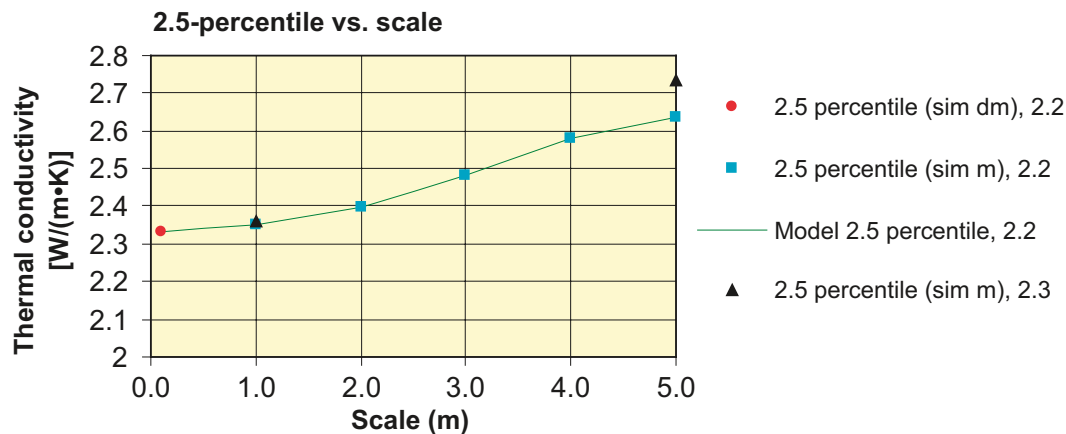


Figure 5-11. The 2.5-percentile (0.025 quantile) versus the scale for domain RFM045. The black dots represent the 1 m simulation results in stage 2.3 and the blue dots the corresponding results in stage 2.2 /Back et al. 2007/. Upscaling was performed on simulated values at the 1 m scale.

5.4 Quality control of thermal modelling – domain RFM029

5.4.1 Uncertainties

Stochastic simulations of TRCs (geology) and thermal conductivity for each TRC in domain RFM029 was performed in the Thermal Site Descriptive Model for Forsmark, stage 2.2 /Back et al. 2007/ and are not repeated here. However, quality control has been performed of the thermal modelling results for Domain RFM029. The control focused on the model uncertainties identified in model stage 2.2 /Back et al. 2007/. The thermal simulations were evaluated regarding scale issues, reproduction of variance in simulations, and the spatial statistical thermal models used in the simulation.

The simulation scale of 1 m was previously believed to have caused a discretisation error due to the inability to properly capture the small-scale rock occurrences of low-conductive rock types. This conclusion is maintained. However, the discretisation error is believed to be eliminated at the 5 m scale.

The simulation volume was limited to 5×5×5 m in the first simulation stage (upsampling from measurement scale), and to 50×50×50 m in the second simulation stage. It can be concluded that the limited simulation volumes have resulted in problems of reproducing the total variance in the realisations resulting from stochastic simulation of thermal conductivity for each TRC, i.e. the variance was slightly underestimated. The main reason for this problem has been identified: the Gaussian simulation software sometimes has difficulties in reproducing the variance, especially when the range of the variogram is close to, or larger than, the simulation volume. However, this effect has had no significant impact on the thermal modelling results. Primarily, this is because the main contribution to the total variance comes from the variability between different TRCs, whereas the problem of reproducing the variance concerns individual TRCs. In addition, the potential error or bias is additionally reduced during upscaling.

An evaluation was also performed of the spatial statistical thermal models that were used in the simulation. The evaluation focused on the variograms for the different TRCs. The reason for the uncertainty was the difference in total variance observed between the model and the simulation results (see discussion above). Standardised variograms (spherical and exponential models) are used in the modelling strategy, and the standardisation is achieved by normalising the variance against the total variance, as defined by the model variance. It is concluded that standardisation was performed against the correct variance for all TRCs.

5.4.2 Comparison of results after upscaling

An important conclusion in the Thermal Site Descriptive Model for Forsmark, stage 2.2 /Back et al. 2007/ was that the domain modelling results for the simulation performed at the scale of 0.1 m (cell size) were unreliable after upscaling because of a too small simulation volume ($5 \times 5 \times 5 \text{ m}^3$). This conclusion is still valid. The results from the simulation at the scale 1 m are much more reliable after upscaling. However, one remaining uncertainty is the discretisation error at the 1 m scale. This error is believed to be small after upscaling to scales larger than 2 m (cell size), and is believed to have disappeared at the 5 m scale.

6 Thermal rock class proportions and size distributions

6.1 Uncertainties in thermal rock class proportions

6.1.1 Introduction

Since thermal properties are closely correlated to rock type, the uncertainties in the estimated proportions of different rock types in rock domains are directly translated into uncertainties in the resulting thermal models. For thermal modelling purposes, rock types have been grouped into thermal rock classes (TRCs) and stochastic simulations of the spatial distribution of TRCs in rock domains RFM029 /Back et al. 2007/ and RFM045 (Chapter 4) were performed. The uncertainties associated with the estimates of volume proportions of different TRCs for domains RFM029 and RFM045 are quantified below.

The proportions of thermal rock classes (TRC) estimated in the thermal model differ somewhat from the corresponding estimates given in the geological model /Stephens et al. 2007/. The reasons for these discrepancies are discussed below.

6.1.2 Data treatment and assumptions

The mean proportions of TRCs and their confidence intervals have been determined for two somewhat different sets of borehole data:

- A. boreholes/borehole sections selected for the lithological simulations (Table 6-1). As regards domain RFM029, boreholes/borehole sections with anomalous rock contact orientations were excluded /Back et al. 2007/. The resolution of the data is 1 m.
- B. all cored boreholes longer than 200 m in the volume that it is situated entirely in both the local model volume and the Forsmark tectonic lens, i.e. the volume selected as a potential repository. These boreholes are listed in Table 6-2. TRC proportions were calculated from borehole data with a resolution of 0.1 m. For domain RFM045, the same boreholes sections apply to both datasets A and B.

The way in which the borehole data has been processed (and the assumptions made) and how this differs from the method used by the geological modelling team in their volumetric estimates are described below:

- Rock types of very minor importance, e.g. quartz veins and calc-silicate rock, were not assigned to any TRC and were therefore omitted from the analysis /Back et al. 2007/. Together these rocks make up less than 1% of the borehole length belonging to a rock domain. TRC proportions were recalculated to 100%.
- Data from Sicada tables p_rock (> 1 m borehole length) and p_rock_occurrence (< 1 m borehole length) are merged. Each 0.1 m section of borehole is assigned a rock type and TRC code according to the dominant lithology. This means that occurrences less than 5 cm are excluded, which may lead to underestimation of the proportions of some rock types. The geological modelling team have used a somewhat different approach for merging the above mentioned tables and estimating volume proportions (see Appendix 4 in /Stephens et al. 2007/).

- For dataset A, the boreholes have been weighted so that they reflect the relative volumes of the different thermal subdomains based on expert judgements made by the geological modelling team /Back et al. 2007/. The marginal subdomain of domain RFM029 was considered to comprise one-third, and the internal subdomain two-thirds of the domain's total volume. The lengths of the boreholes in the internal subdomain (01D, 05A, 08B) have been weighted so that they make up 2/3 of the total adjusted borehole length. Within each subdomain, the data is weighted according to the lengths of each borehole. It should be noted that subdomains are not defined in the rock domain model /Stephens et al. 2007/.
- For dataset B, the data is weighted to take account of the different lengths of each borehole; longer boreholes contribute more data than short boreholes (this is consistent with the way the borehole data has been treated by the geological modelling team).

It can be argued that the borehole datasets of type B above give better estimates of the volumetric proportions of the different TRCs and their uncertainties for the following reasons:

- All available boreholes within the volume selected as a potential repository are included in dataset B. For domain RFM029, a total of 9,081 m is represented by these boreholes. The data used as input for the lithological simulations, dataset A, are based on fewer boreholes comprising c. 5,750 m. For domain RFM045, the boreholes in each dataset are identical.
- Borehole dataset B has a resolution of 0.1 m, whereas the lithological simulations were based on data with a resolution of 1 m.

However, since the thermal model uses lithological simulations based on 1 m data, and, in the case of domain RFM029, a limited number of boreholes, it is also important to estimate confidence intervals for the mean proportions of TRCs that are valid for the thermal model.

Table 6-1. Boreholes used to characterise domains RFM029 /Back et al. 2007/ and RFM045 (Chapter 4) in the lithological simulations (dataset A).

Rock domain	Borehole	Borehole length used as input for lithological simulations
Domain RFM029		
Marginal subdomain	KFM01A	102–380 m
	KFM01C	12–450 m
	KFM04A	500–1,001 m
	KFM07A	102–793 m
	KLX07B	5–298 m
	KLX07C	85–498 m
	KFM08C	102–300 m
	KFM09B	9–616 m
	KFM10A	63–500 m
	Internal subdomain	KFM01D
KFM05A		102–1,000 m
KFM08B		6–200 m
Domain RFM045		
	KFM06A	751–998 m
	KFM06C	411–898 m
	KFM08C	342–546 m
	KFM08D	395–935 m

Table 6-2. All cored boreholes longer than 200 m in domains RFM029 and RFM045 within the target volume (dataset B).

Domain RFM029	Domain RFM045
KFM01A	KFM06A
KFM01B	KFM06C
KFM01C	KFM08C
KFM01D	KFM08D
KFM04A	
KFM05A	
KFM06A	
KFM06C	
KFM07A	
KLX07B	
KLX07C	
KFM08A	
KFM08B	
KFM08C	
KFM09B	
KFM10A	
KFM08D	

The borehole lengths defining each borehole are based on the domain classification of boreholes (Table 4-4 and Appendix 13 in /Stephens et al. 2007/).

6.1.3 Method for estimating confidence intervals

Each borehole or borehole section is seen as a sample (random data value) with a certain proportion of a rock type or TRC. Assuming that there are 8 boreholes, we calculate 8 different proportions for each TRC, one for each borehole. In this calculation, the value for each borehole is weighted according to the length of the borehole. Then the bootstrapping method is applied to these data values. This involves randomly selecting 8 values with replacement from the original set of 8. The bootstrap resampling is performed many times, e.g. 50,000. For each resample a new mean proportion is calculated, and a distribution of mean proportions for each TRC can be generated. For each TRC, the confidence intervals for the statistic of interest can then be determined. No assumptions regarding the nature of the data distributions are required, as confidence limits can be determined directly from the simulated data. In the case presented below, the 95% two-sided confidence limits for the mean volume proportions of TRCs are estimated.

The confidence intervals estimated here are valid for the borehole scale.

6.1.4 Results

Domain RFM029

The mean volume proportions and the 95% upper and lower confidence limits for TRCs in domain RFM029 are presented for both borehole datasets A and B in Table 6-3. The results for dataset B (columns 1 and 2) are based on the 17 boreholes listed in Table 6-2. The proportions and confidence intervals of TRCs based on dataset A, i.e. the 9 boreholes selected for lithological simulations of domain RFM029, are given in columns 3 and 4. The proportions estimated from the output of the simulations are shown in column 5. A comparison of the mean proportions for the different datasets (columns 1 and 3) show only minor differences. The confidence intervals are generally larger for dataset A than for dataset B. This is because of the fewer boreholes in dataset A.

The distributions generated by the bootstrap method for dataset B can be found in Appendix E.

Table 6-3. Proportions and confidence intervals for TRCs in domain RFM029. Proportions based on geological model are from /Stephens et al. 2007/.

TRC	Rock name/code	1	2	3	4	5	6
		Proportion of TRC in domain RFM029. From dm data (all boreholes > 200 m). [%]	95% confidence intervals. Calculated from bootstrapping results of dm data in (1). [%]	Proportions of TRCs in boreholes selected for 1 m lithological simulations, 1 m data. [%]*	95% confidence intervals. Calculated from bootstrapping results of m data in (3). [%]	Proportions of TRCs in 1,000 realisations, 1 m lithological simulations. [%]	Proportions in domain RFM029 based on geological model 2.2. [%]
57	Granite to granodiorite, 101057 Granite, aplitic, 101058	78.8	76.3–81.3%	78.9	76.4–82.4	78.9	74.8
51	Granite, granodiorite and tonalite, 101051 Felsic to intermediate volcanic rock, 103076	4.1%	2.5–5.8%	3.8	1.2–4.8	3.8	5.0
61	Pegmatite, pegmatitic granite, 101061 Granite, 111058	13.2%	11.0–15.6%	13.1	9.6–16.7	13.1	14.8
17	Amphibolite, 102017 Diorite, quartz diorite and gabbro, 101033	4.0%	3.3–4.6%	4.2	2.5–5.6	4.2	4.6
							0.8 (other)

* These percentages are based on boreholes used for geological simulations. First, the proportions for internal and marginal subdomains were calculated separately. Then the overall proportions were arrived at after consideration of the weights given to the subdomains: internal 2/3; marginal 1/3.

The proportions based on the estimates made by the geological modelling team (column 6) differ somewhat from the proportions estimated here (columns 1 and 3). For example, the volume proportion of rock types making up TRC 57 estimated by the geological modelling team does not fall within the 95% certainty limits quoted above. Possible reasons for the discrepancies between the estimates presented here and those calculated by the geological modelling team are:

- Different methods were used for merging rock type intervals mapped in boreholes from Sicada tables p_rock.xls and p_rock-occurrence.xls. Borehole occurrences shorter than 5 cm are excluded from our calculations but have been included in the determinations made by the geological modelling team. The effect of this has been evaluated by calculating the percentage of borehole length excluded from 12 boreholes (in both domain RFM029 and RFM045). The total length excluded amounts to about 2%, most of which (1.5%) is comprised of rock types 101061 or 111058 (TRC 61).

- The set of boreholes used in the different calculations are not identical. For example, the calculations described here for dataset B include borehole KFM08D (not included in the estimates made by the geological modelling team). The reverse is the case for boreholes 6B and 9A.
- Rock types not falling into one or other of the defined TRCs make up, according to /Stephens et al. 2007/, c. 0.8% of the rock volume. On normalising to 100%, most of this 0.8% is assigned to TRC 57, the dominant TRC.

The confidence intervals for the TRC proportions in domain RFM029 are relatively narrow because of the large number of boreholes combined with the rather homogenous geology.

Domain RFM045

The mean volume proportions and the 95% upper and lower confidence limits for TRCs in domain RFM045 are presented in Table 6-4. Both datasets are based on the same four boreholes listed in Table 6-1 and Table 6-2. The results for the 0.1 m data are given in columns 1 and 2, and those for the 1 m data used for lithological simulations of domain RFM045 are given in columns 3 and 4. The proportions estimated from the output of the simulations are shown in column 5. It could be argued that the higher resolution 0.1 m data is more accurate than the 1 m data used in the lithological simulations. However, a comparison of the mean proportions for the 0.1 m (column 1) and 1 m (column 3) datasets show only minor differences. The confidence intervals are slightly larger for the 1 m data than for the 0.1 m data.

Table 6-4. Proportions and confidence intervals for TRCs in domain RFM045. Proportions based on geological model are from /Stephens et al. 2007/.

TRC	Rock name/code	1	2	3	4	5	6
		Proportion of TRC in From dm data (4 boreholes) [%]	95% confidence intervals. Calculated from bootstrapping results of dm data in (1). [%]	Proportions of TRCs in boreholes selected for lithological simulations, 1 m data. [%]	95% confidence intervals. Calculated from bootstrapping results of m data in (3). [%]	Proportions of TRCs in 500 realisations, 1 m lithological simulations. [%]	Proportions in domain RFM045 based on geological model 2.2. [%]
58	Granite, aplitic, 101058 Granite to granodiorite, 101057	67.3%	62.8–77.6%	67.7	62.7–79.2%	68.4	67.3
51	Granite, granodiorite and tonalite, 101051 Felsic to intermediate volcanic rock, 103076	10.9%	6.0–13.1%	10.6	4.7–13.3%	10.4	10.2
61	Pegmatite, pegmatitic granite, 101061 Granite, 111058	14.7%	11.2–17.7%	14.6	9.3–18.2%	14.0	15.2
17	Amphibolite, 102017 Diorite, quartz diorite and gabbro, 101033	7.1%	1.8–9.4% (80% confidence intervals 4.7–8.6%)	7.0	2.4–9.1%	7.1	6.5
							0.8 (other)

The proportions estimated from the output of the simulations are shown in column 5. It was shown in section 4.5.3 that the simulations nearly exactly reproduce the proportions of the TRCs used as input. Therefore, the discrepancies between columns 3 and 5 are related to the way in which T-PROGS, the program used for lithological simulations, interpreted the borehole data. On calculating the proportions of TRCs from the borehole data, T-PROGS has interpreted short gaps in the data (brought about by removal of very minor rock types) incorrectly. The effect of this error is, however, very small.

The distributions generated by the bootstrap method for dataset B can be found in Appendix E.

The proportions based on the estimates made by the geological modelling team (column 6) differ only slightly from the proportions estimated here (columns 1 and 3). The former fall within the 95% certainty limits quoted above. The discrepancies can be explained by the different methods used for merging borehole data from Sicada tables `p_rock.xls` and `p_rock-occurrence.xls`, the treatment of very minor rock types, and differences in the number of boreholes used for the determinations. KFM08D was not included in the estimates made by the geological modelling team.

The confidence intervals for the TRC proportions in domain RFM045 are relatively large because of the small number of boreholes combined with the rather heterogeneous geology. The uncertainty for TRC 17 is particularly large due to the large variation in proportions from one borehole to another.

6.1.5 Conclusions

- The confidence intervals presented here for the TRCs are valid given the assumptions made in the preparation of the data for lithological simulations. Borehole occurrences shorter than 5 cm have been excluded, as have minor rock types not classified in any TRC. For domain RFM029, these account for 2.5–3% of the rock volume.
- The estimates of the TRC proportions in domain RFM029 are considerably more reliable than those for domain RFM045. For the latter, the small number of boreholes in combination with the high degree of lithological heterogeneity results in rather large uncertainties in the estimated proportions of TRCs.
- The same method can obviously be applied for estimating confidence intervals for rock type proportions.

6.2 Size distribution of TRCs

Based on the results of stochastic simulations of lithologies, it is possible to calculate the size distribution of subordinate rock types. However, a large number of simulations are required at several scales for this analysis. This work is on-going and will be reported in the near future.

To illustrate the information that can be obtained from a size-distribution analysis, the results of simulations at two scales, 0.1 m and 1 m, have been analysed for TRC 17 and TRC 61 in domain RFM029. This was performed by using an algorithm that calculates the volume of individual rock bodies in the lithological realisations created by the stochastic simulations. A set of rock volume classes were defined, and the number of TRC bodies belonging to each volume class were calculated. The statistics for the smaller scales are corrected for the smaller volumes so that the different scales can be compared.

According to the method used for determining the size distribution for a rock type, bodies in contact with the boundary of the simulation volume are removed. Retaining the boundary bodies would introduce a bias, since the volume of boundary bodies would be underestimated due

to truncation, and the number of bodies would be overestimated because the boundary bodies occur in two or more simulation volumes. An alternative approach to tackling this problem is to count all the bodies, even those truncated by the sides of the simulation cube, followed by applying correction factors to compensate for the bias mentioned above.

In Figure 6-1 and Figure 6-2, the size distributions of TRC 17 (mainly amphibolite) and TRC 61 (mainly pegmatite) are shown. In the first plot, the average number of bodies in each volume class per realisation is shown. A realisation is a cube with sides 50 m long corresponding to a rock volume of 125,000 m³. The second plot is a cumulative probability plot showing the relative volume of a TRC that is comprised of bodies with a size less than or equal to a volume class. As regards the cumulative graphs, each scale is normalised to the volume for the largest scale.

The figures for TRC 17 can usefully be compared with the true thickness distribution of amphibolite estimated from borehole data described in section 3.4.3 in /Stephens et al. 2007/. Both studies indicate a predominance of small bodies, e.g. in the case of borehole data true thickness less than 1 m.

Due to discretisation into 0.1 m and 1 m cells respectively, the size distribution results for the lower part of the curve for each scale are not well resolved. Even the data for the largest bodies, i.e. “the upper end”, are uncertain, due to limited simulation volumes, as well as the removal of boundary bodies. In future work, determining the type of distribution, e.g. power-law, that describes these data will be central to the understanding of the size distribution.

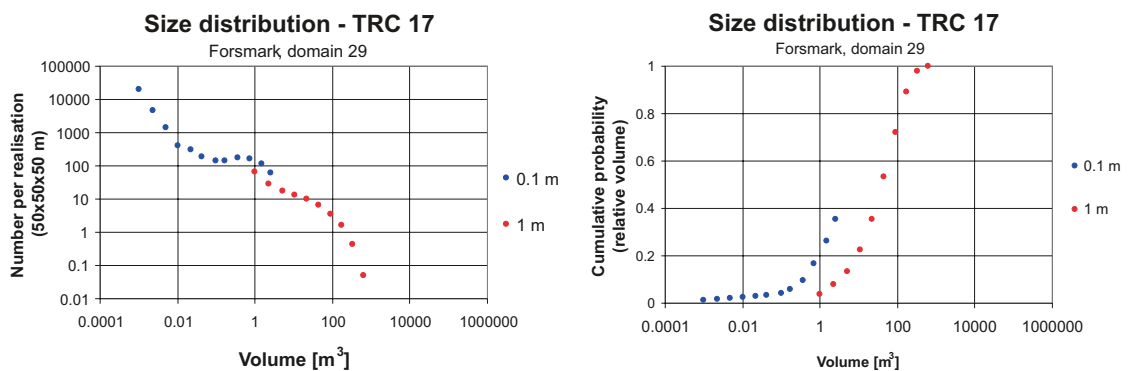


Figure 6-1. Size distribution of rock bodies of TRC17 in domain RFM029, based on stochastic simulation at 0.1 m and 1 m scales. A single realisation at 1 m scale represents a rock volume of 125,000 m³.

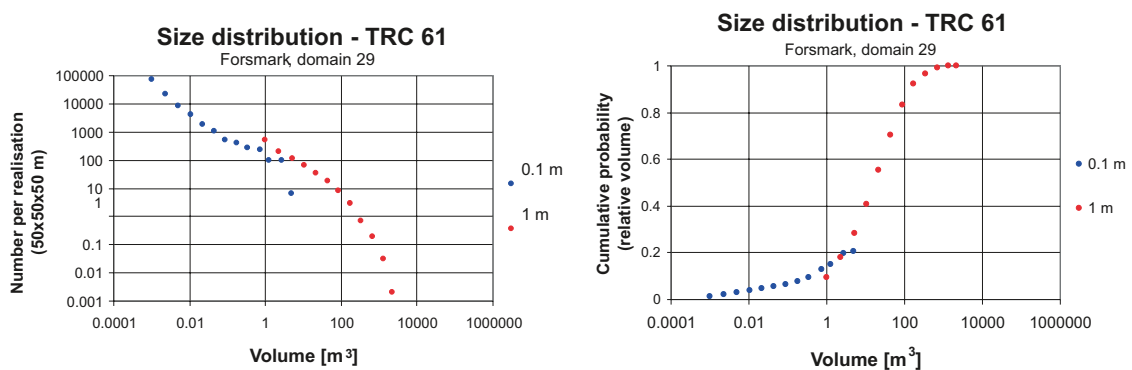


Figure 6-2. Size distribution Size distribution of rock bodies of TRC61 in domain RFM029, based on stochastic simulation at 0.1 m and 1 m scales. A single realisation at 1 m scale represents a rock volume of 125,000 m³.

7 Summary of domain thermal properties

The thermal conductivity for domain RFM045 is summarised in Table 7-1. The quoted values are valid at 20°C. With increasing temperature, the thermal conductivity of the dominant granitoid rock decreases by about 10 % per 100°C temperature increase, calculated as mean value. The impact of increasing temperature on other rock types may be lower. The corresponding results for rock domain RFM029 are given in /Back et al. 2007/.

The heat capacity results for the 1 m scale at domain level are summarised in Table 7-2 for domains RFM029 and RFM045. These values are valid at 20°C. With increasing temperature, the heat capacity of the dominant granite to granodiorite (101057) increases by about 29 % per 100°C temperature increase as a mean value.

The mean in situ temperatures measured at 400 m, 500 m and 600 m depth, based on 8 boreholes, are estimated at 10.5°C, 11.6°C, and 12.8°C respectively, which are identical to those presented in the thermal model report, stage 2.2 /Back et al. 2007/.

Table 7-1. Summary statistics for domain RFM045 based on simulations at the 1 m scale and upscaling to 5 m.

Statistical parameter	1 m	5 m	Unit
Mean	3.57	3.56	W/(m·K)
Standard deviation	0.42	0.28	W/(m·K)
0.1-percentile	2.24	2.36	W/(m·K)
1-percentile	2.31	2.56	W/(m·K)
2.5-percentile	2.36	2.73	W/(m·K)

Table 7-2. Statistics of heat capacity at scale 1 m for domains RFM029 and RFM045 based on simulations of thermal conductivity at the 1 m scale.

Statistical parameter	RFM029, MJ/(m ³ ·K)	RFM045, MJ/(m ³ ·K)
Mean	2.06	2.12
Standard deviation	0.10	0.15

8 Uncertainties

8.1 Major data uncertainties

The main uncertainties in the thermal data are described in the thermal model report, stage 2.2 /Back et al. 2007. These data include thermal conductivity determinations by the transient plane source (TPS) method and from mineral composition data (SCA method), heat capacity data determined by the calorimetric method, and fluid temperature borehole logging data. The uncertainties associated with the SCA thermal conductivity values are considered to be higher than for the TPS method, but no large bias is suspected. Only temperature logging data that fulfils certain requirements regarding calibration and the time between drilling and logging have been used to describe the in situ temperature conditions. For individual boreholes, the uncertainty is $\pm 0.25^{\circ}\text{C}$.

Boremap data

The uncertainties in the orientation of the boreholes and in the orientation of geological objects in the boreholes, documented by /Munier and Stigsson 2007/, are judged to have little or no effect on the results of thermal modelling.

8.2 Major model uncertainties

There are several model uncertainties to consider in the thermal modelling. The five most important uncertainties identified in model stage 2.2 were associated with (1) the simulation scale, (2) the simulation volume, (3) the spatial statistical structure of TRCs (lithology), (4) the spatial statistical thermal models, and (5) the simulation technique.

In model stage 2.3, special attention is given to the uncertainties in the spatial statistical structure of TRCs (lithology) and the simulation volume. These two types of model uncertainty are discussed below.

The spatial statistical structure of TRCs (lithology)

The models used for the lithological simulations of domains RFM029 /Back et al. 2007/ and RFM045 (section 4.4) are largely based on “best estimates” of uncertain parameters. There are several uncertainties associated with the developed models of the spatial statistical structure of the TRCs (lithology). Most of these are coupled to the lack of knowledge concerning detailed geological information, such as typical lengths of rock bodies in the three spatial directions, representativeness of the borehole information for the whole rock domain, and lithological heterogeneity within the rock domain.

There are also uncertainties linked to the degree to which geological heterogeneity has been reproduced in the lithological simulations. This is related to the variability in proportions of TRCs. In the simulation volume, the proportions of TRCs are held constant in each realisation (“best estimates” have been used). In reality, the proportions are variable at the scale of the realisation volume due to lithological heterogeneity. These uncertainties are largest for rock types with low proportions and heterogeneous rock domains.

Geological heterogeneities within domain RFM045 were dealt with in the complementary stochastic simulations in stage 2.3 by dividing the domain into two subdomains in the simulations, according to the strategy outlined in /Back and Sundberg 2007/. This is believed to have significantly reduced the uncertainty identified in model stage 2.2. The stage 2.3 lithological simulations honour the borehole data to a much higher degree, and therefore the lower tail percentiles of thermal conductivity are considered more reliable.

The estimates of the TRC proportions in domain RFM029 are considerably more reliable than those for domain RFM045. For the latter, the small number of number of boreholes in combination with the high degree of lithological heterogeneity results in rather large uncertainties. The impact of these uncertainties on the overall distribution of thermal conductivity are low for domain RFM029 but higher for domain RFM045 due to the greater lithological heterogeneity in the latter. However, for both domains, these uncertainties have only a minor effect on the lower thermal conductivity tail (the 1-percentile may vary by about 1%).

The simulation volume

The limited simulation volumes affect the simulation results, but the effect is not fully known. There are two situations when the limited volumes could be a problem for the objective of describing a rock domain statistically:

1. When the lithological simulation volume is so small that the statistics of this limited rock volume deviate from the true domain statistics. This is only a problem if upscaling to large blocks is performed, which is not the case in the model presented here. The limited simulation volumes also seem to be related to difficulties in fully reproducing anisotropy, as predicted by the model parameters, in the lithological simulations. This is exemplified by the underestimation of anisotropy of the geometry of TRC17.
2. When the correlation lengths of thermal properties are similar to or longer than the length of the simulation volume. The latter results in problems of reproducing the total variance in the realisations resulting from stochastic simulation of thermal conductivity for each TRC, i.e. the variance may be slightly underestimated. The main reason for this problem has been identified: experience indicates that the Gaussian simulation software sometimes has difficulties of reproducing the variance, especially when the range of the variogram is close to, or larger than, the simulation volume. However, this effect has had no significant impact on the thermal modelling results. Primarily, this is because the main contribution to the total variance comes from the variability between different TRCs, whereas the problem of reproducing the variance concerns individual TRCs. In addition, the potential error or bias is additionally reduced during upscaling.

It can be concluded that neither of the above uncertainties associated with the simulation volume is believed to have had any major impact on the thermal modelling results. There are two ways of reducing this uncertainty additionally: (1) to use a larger simulation volume, and (2) to use a different simulation algorithm for the first simulation stage (upscaling). The first method requires large computer capacity and is impractical. The second approach has a potential for the first simulation stage.

The results of the analysis of the size distribution of subordinate rock bodies are also influenced by the limited simulation volume, but even the choice of simulation scale. In order to describe the size distribution of subordinate rock types in an accurate way it is necessary to perform simulations at a number of different scales.

8.3 Summing up

Small uncertainties in the lower tail of the thermal conductivity distributions will have a significant impact on canister spacing in repository layout D2. For this reason, the uncertainties in the thermal model listed in this chapter and in /Back et al. 2007/ focus on the lower tail of the thermal conductivity distribution.

The thermal conductivity distribution for rock domain RFM045 is more uncertain than for domain RFM029. For domain RFM045, these uncertainties concern both the overall distribution and its lower tail, and are related to uncertainties associated with the output of the geological simulations, in particular the proportions of rock types, and the spatial and size distribution of amphibolite. Although the geological simulations performed have managed to model much of the heterogeneity observed in the boreholes, it is still somewhat unclear to what extent the borehole information is representative of the geology in domain RFM045. The reason for this is the small number of boreholes combined with the more heterogeneous distribution of amphibolite in rock domain RFM045.

Overall confidence in the thermal model is reinforced by the mutual consistency between understanding of the geology and the thermal properties description.

9 Conclusions

Although the differences are small, the complementary thermal modelling of rock domain RFM045 gave results that are more realistic and reliable than in model stage 2.2 /Back et al. 2007/.

Thermal modelling of domain RFM045 in Forsmark model stage 2.2 gave lower tail percentiles of thermal conductivity that were considered to be conservatively low, because geological simulations of domain RFM045 overestimated the importance/frequency of large bodies of amphibolite, the rock type with the lowest thermal conductivity of all rock types in Forsmark. Additional borehole data, made available as part of data freeze 2.3, together with the previously investigated boreholes /Stephens et al. 2007/ give an improved description of the lithological heterogeneity within domain RFM045. This heterogeneity was captured in the geological simulations to a large extent by dividing the borehole sections intersecting domain RFM045 into two more homogenous groups on the basis of their lithological characteristics, thereby defining two distinct thermal subdomains. A characteristic feature of one of the thermal subdomains is the presence of large amphibolite bodies.

The statistics of thermal properties at domain level are summarised in Table 7-1 for rock domain RFM045. The choice of scale has a profound influence on the distribution of thermal conductivity values. The variance decreases and the lower tail percentiles increase as the scale of observation increases from 1 to 5 m. The lower percentiles increase more during upscaling in the thermal model stage 2.3 than was the case in stage 2.2. The reason for this is that large bodies of the low-conductive amphibolite are less common in stage 2.3 than in stage 2.2.

Best estimates of the 0.1 percentile of thermal conductivity for domain RFM045 are 2.24 W/(m·K) for the 1 m scale and 2.36 W/(m·K) for the 5 m scale. This can be compared with corresponding values for domain RFM029 of 2.30 W/(m·K) for the 1 m scale and 2.87 W/(m·K) for the 5 m scale.

Domains RFM029 and RFM045 have a mean heat capacity of 2.06 MJ/(m³·K) and 2.12 MJ/(m³·K) respectively.

The mean in situ temperatures at 400 m, 500 m and 600 m depth are estimated at 10.5°C, 11.6°C, and 12.8°C respectively, and are therefore unchanged compared to model stage 2.2.

The estimates of the TRC proportions in domain RFM029 are considerably more reliable than those for domain RFM045. For the latter, the small number of boreholes in combination with the high degree of lithological heterogeneity results in rather large uncertainties in the estimated proportions.

The aspect of the thermal model with the highest confidence is the thermal properties of domain RFM029, because of its higher degree of lithological and thermal homogeneity compared to domain RFM045.


The aspect of the thermal model with the lowest confidence is the lower tail of the thermal conductivity distribution for rock domain RFM045. This uncertainty is related to the spatial and size distribution of amphibolite in domain RFM045.

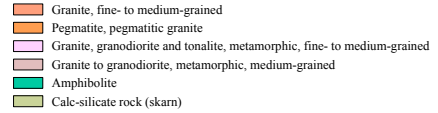



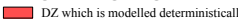
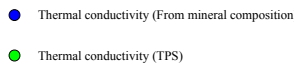
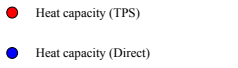
10 References

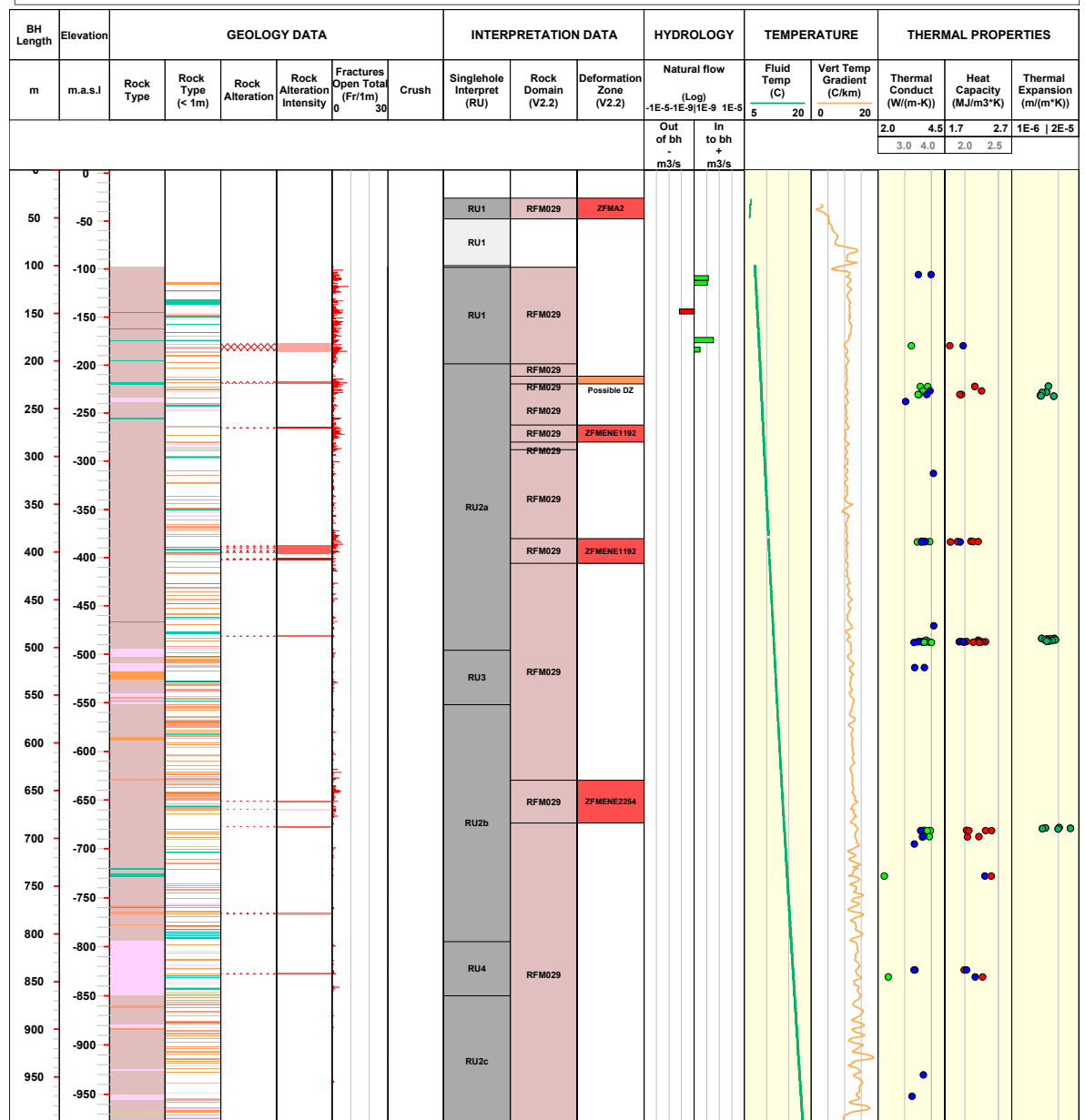
- Abdulagatov I M, Emirov S N, Abdulagatova Z Z, Askerov S Y, 2006.** Effect of Pressure and Temperature on the Thermal Conductivity of Rocks. *J. Chem. Eng. Data*, 51, 22–33.
- Back P-E, Sundberg J, 2007.** Thermal Site Descriptive Model. A Strategy for the Model Development during Site Investigations. Version 2.0. SKB R-07-42, Svensk Kärnbränslehantering AB.
- Back P E, Wrafter J, Sundberg J, Rosén L, 2007.** Thermal properties. Site descriptive modelling Forsmark – stage 2.2. SKB R-07-47, Svensk Kärnbränslehantering AB.
- Carle S F, Fogg G E, 1997.** Modeling spatial variability with one- and multi-dimensional Markov chains: *Mathematical Geology*, v. 28, no. 7.
- Carle S F, 1999.** T-PROGS: Transition Probability Geostatistical Software. Version 2.1. Hydrologic Sciences Graduate Group. University of California, Davis.
- Carlsten S, Gustafsson J, Samuelsson E, Stephens M, Thunehed H, 2007.** Geological single-hole interpretation of KFM08D. SKB R-07-108, Svensk Kärnbränslehantering AB.
- Davis J C, 1986.** Statistics and data analysis in geology. Wiley & Sons.
- Evans M, Hastings N, Peacock B, 2000.** Statistical distributions, third edition, John Wiley & Sons Inc. ISBN.
- Follin S, Levén J, Hartley L, Jackson P, Joyce S, Roberts D, Swift B, 2007.** Hydrogeological characterisation and modelling of deformation zones and fracture domains, Forsmark modelling stage 2.2. SKB R-07-48, Svensk Kärnbränslehantering AB.
- Johansson P-O, Werner K, Bosson E, Berglund S, Juston J, 2005.** Description of climate, surface hydrology, and near-surface hydrogeology. Preliminary site description Forsmark area – version 1.2. SKB R-05-06, Svensk Kärnbränslehantering AB.
- Munier R, Stigsson M, 2007.** Implementation of uncertainties in borehole geometries and geological orientation data in Sicada. SKB R-07-19, Svensk Kärnbränslehantering AB.
- Pöllänen J, Sokolnicki M, 2004.** Difference flow logging in borehole KFM03A – Forsmark site investigation. SKB R-04-189, Svensk Kärnbränslehantering AB.
- Rouhiainen P, Pöllänen J, 2004a.** Difference flow logging in borehole KFM02A – Forsmark site investigation. SKB R-04-188, Svensk Kärnbränslehantering AB.
- Rouhiainen P, Pöllänen J, 2004b.** Difference flow logging in borehole KFM04A – Forsmark site investigation. SKB R-04-190, Svensk Kärnbränslehantering AB.
- Seipold U, Huenges E, 1998.** Thermal properties of gneisses and amphibolites – high pressure and high temperature investigations of KTB-rock samples. *Tectonophysics* 291, 173–178.
- SKB, 2008.** Site description of Forsmark at completion of the site investigation phase (SDM-Site Forsmark). SKB TR-08-05, Svensk Kärnbränslehantering AB.
- Stephens M B, Fox A, Isaksson H, Öhman J, Simeonov A, 2007.** Geology – Site descriptive modelling, Forsmark stage 2.2. SKB R-07-45, Svensk Kärnbränslehantering AB.
- Sundberg J, Wrafter J, Back P E, Rosén L, 2008.** Thermal properties Laxemar. Site descriptive modelling. SDM-Site Laxemar. SKB R-08-61, Svensk Kärnbränslehantering AB.
- Walsh J B, Decker E R, 1966.** Effect of pressure and saturating fluid on the thermal conductivity of compact rock. *J. Geophys. Res.*, 71, 12.


WellCAD borehole plots

Geological, hydrological and thermal data relevant to the understanding of the thermal properties of the rock mass are presented for each cored borehole.

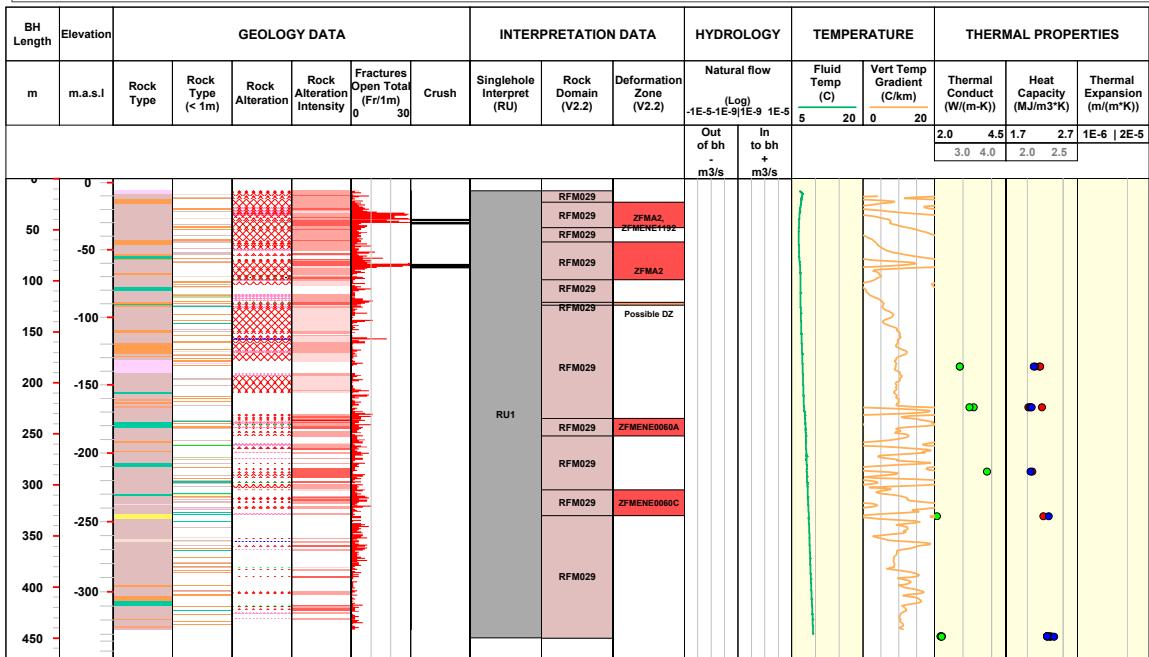
Title KFM01A		Site FORSMARK		Coordinate System RT90-RHB70	Elevation [m.a.s.l.] 3.13
	Borehole KFM01A	Coordinate System RT90-RHB70	Northing [m] 6699529.81	Drilling Start Date 2002-06-25 13:55:00	
	Diameter [mm] 76	Easting [m] 1631397.16	Drilling Stop Date 2002-10-28 14:39:00		
	Length [m] 1001.490	Inclination (at borehole collar) [°] -84.72	Surveying Date 2002-06-26 09:00:00		
	Bearing [°] 318.35	Date of mapping	Plot Date 2008-10-22 23:03:58		


ROCKTYPE FORSMARK  <ul style="list-style-type: none"> Granite, fine- to medium-grained Pegmatite, pegmatitic granite Granite, granodiorite and tonalite, metamorphic, fine- to medium-grained Granite to granodiorite, metamorphic, medium-grained Amphibolite Calc-silicate rock (skarn) 	ROCK ALTERATION  Oxidized	ROCK ALTERATION INTENSITY  <ul style="list-style-type: none"> Faint Weak Medium Strong
	ROCK DOMAIN V2.2  RFM029 Granite to granodiorite, metamorphic, medium-grained	DEFORMATION ZONE V2.2  DZ which is modelled deterministically
THERMAL CONDUCTIVITY  <ul style="list-style-type: none"> Thermal conductivity (From mineral composition) Thermal conductivity (TPS) 	HEAT CAPACITY  <ul style="list-style-type: none"> Heat capacity (TPS) Heat capacity (Direct) 	



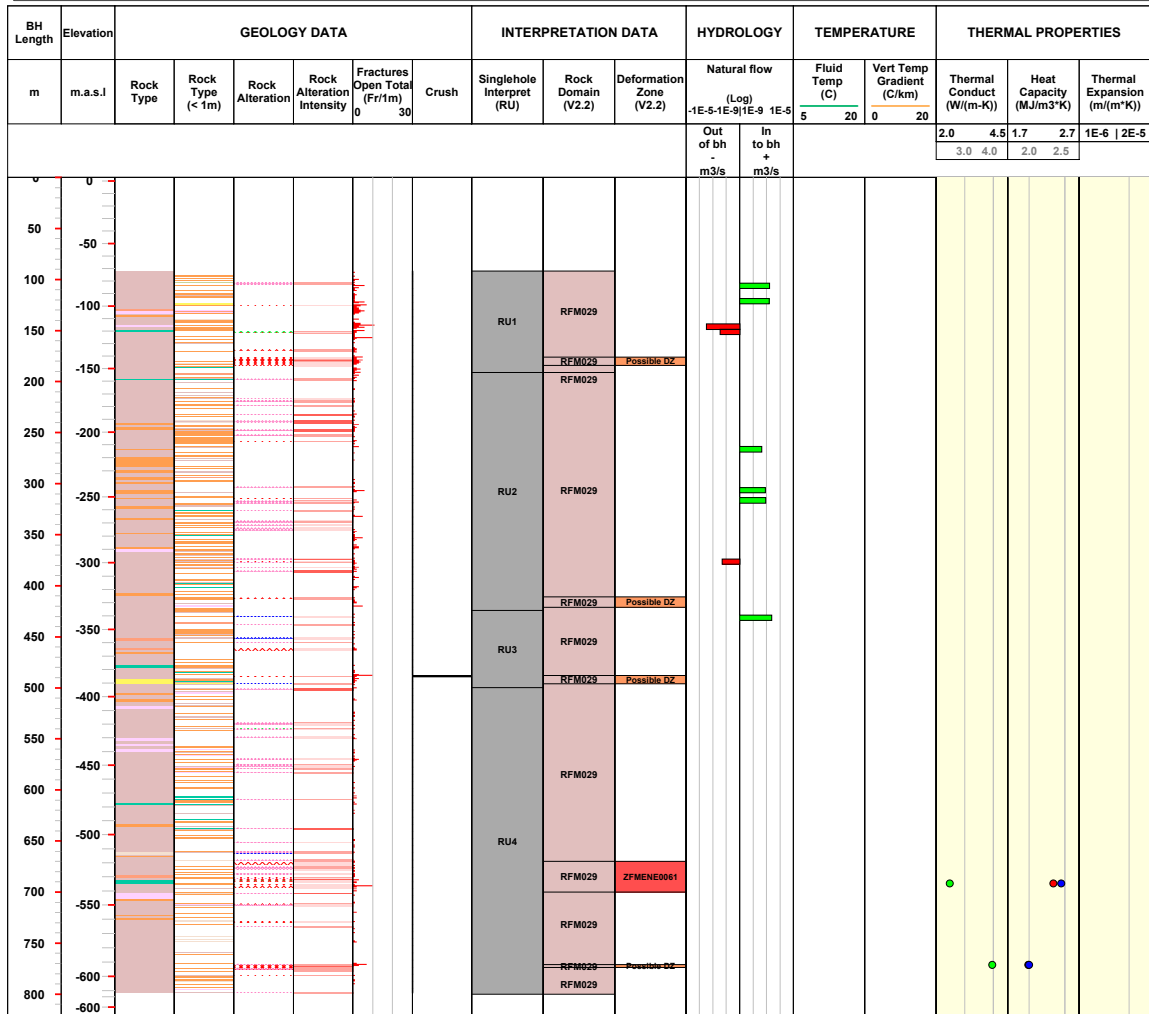
Title KFM01C		Site FORSMARK	Coordinate System RT90-RHB70	Elevation [m.a.s.l.] 2.91
	Borehole KFM01C	Northing [m] 6699526.14	Drilling Start Date 2005-11-05 13:56:00	
	Diameter [mm] 76	Easting [m] 1631403.75	Drilling Stop Date 2005-11-29 13:52:00	
	Length [m] 450.050	Inclination (at borehole collar) [°] -49.60	Surveying Date 2005-10-26 13:00:00	
	Bearing [°] 165.35	Date of mapping	Plot Date 2008-10-22 23:03:58	


ROCKTYPE FORSMARK Granite, fine- to medium-grained Pegmatite, pegmatitic granite Granite, granodiorite and tonalite, metamorphic, fine- to medium-grained Granite, metamorphic, aplitic Granite to granodiorite, metamorphic, medium-grained Amphibolite Felsic to intermediate volcanic rock, metamorphic	ROCK ALTERATION Oxidized Chloritized Epidotized Silicification Argillization Albitization Sausuritization Laumontitization ROCK DOMAIN V2.2 RFM029 Granite to granodiorite, metamorphic, medium-grained	ROCK ALTERATION INTENSITY Faint Weak Medium Strong DEFORMATION ZONE V2.2 DZ which is modelled deterministically
THERMAL CONDUCTIVITY Thermal conductivity (From mineral composition) Thermal conductivity (TPS)	HEAT CAPACITY Heat capacity (TPS) Heat capacity (Direct)	



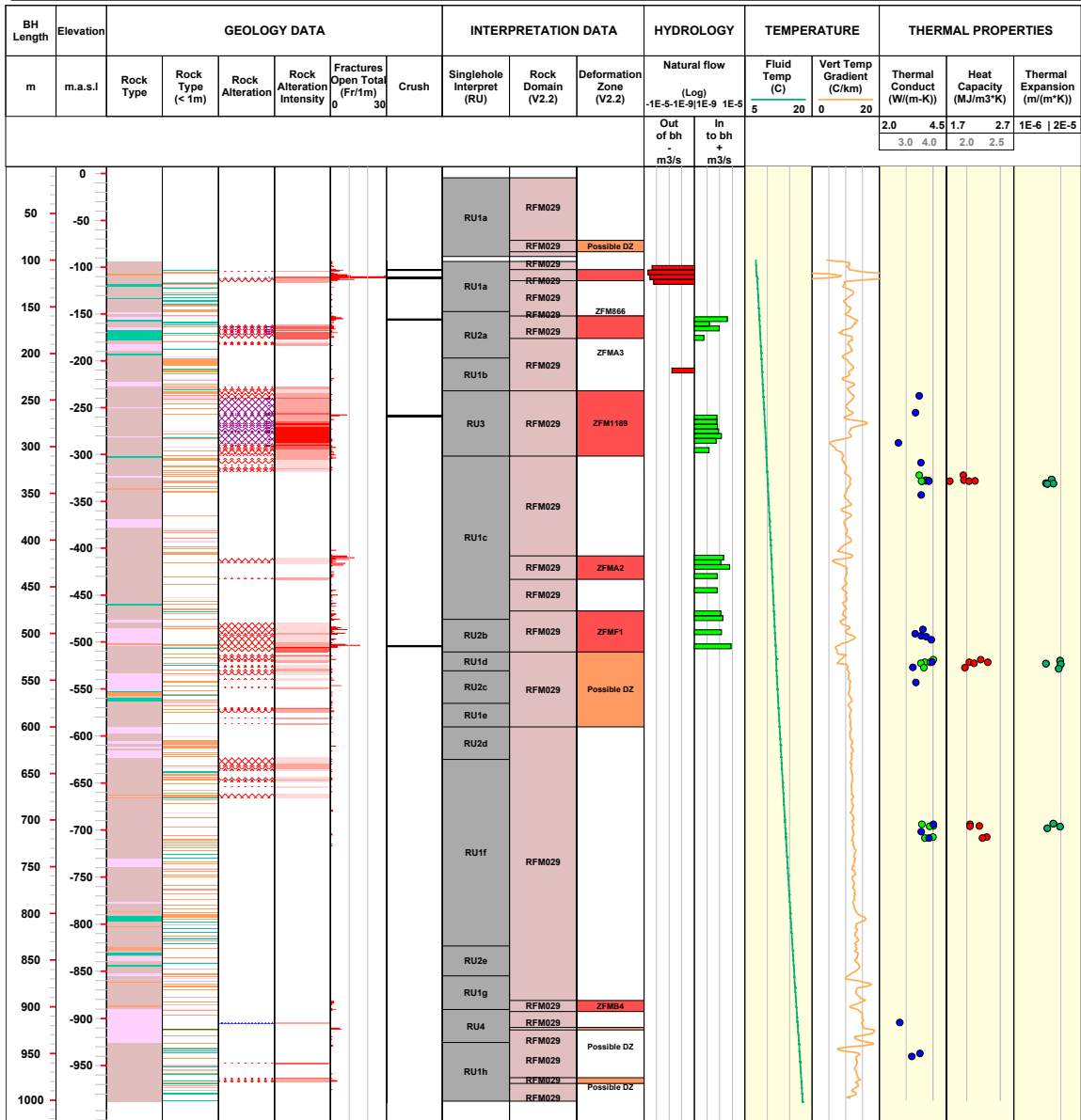
Title KFM01D		Site FORSMARK	Coordinate System RT90-RHB70	Elevation [m.a.s.l.] 2.95
	Borehole KFM01D	Northing [m] 6699542.07	Drilling Start Date 2005-12-18 13:44:00	
	Diameter [mm] 76	Easting [m] 1631404.52	Drilling Stop Date 2006-02-18 10:49:00	
	Length [m] 800.240	Inclination (at borehole collar) [°] -54.89	Surveying Date 2005-11-21 16:30:00	
	Bearing [°] 35.03	Date of mapping	Plot Date 2008-10-22 23:03:58	


ROCKTYPE FORSMARK Granite, fine- to medium-grained Pegmatite, pegmatitic granite Granite, granodiorite and tonalite, metamorphic, fine- to medium-grained Granite, metamorphic, aplitic Granite to granodiorite, metamorphic, medium-grained Amphibolite Felsic to intermediate volcanic rock, metamorphic	ROCK ALTERATION Oxidized Chloritized Epidotized Albitization Saussurization	ROCK ALTERATION INTENSITY Faint Weak Medium Strong DEFORMATION ZONE V2.2 DZ which is modelled deterministically
ROCK DOMAIN V2.2 RFM029 Granite to granodiorite, metamorphic, medium-grained		THERMAL CONDUCTIVITY Thermal conductivity (From mineral composition) Thermal conductivity (TPS)
		HEAT CAPACITY Heat capacity (TPS) Heat capacity (Direct)

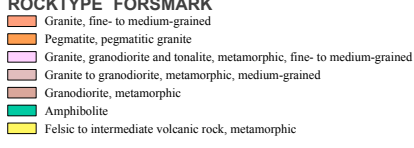
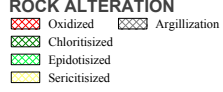
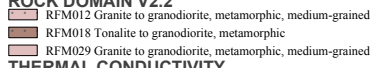


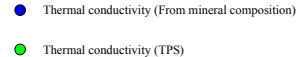
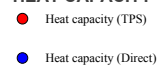


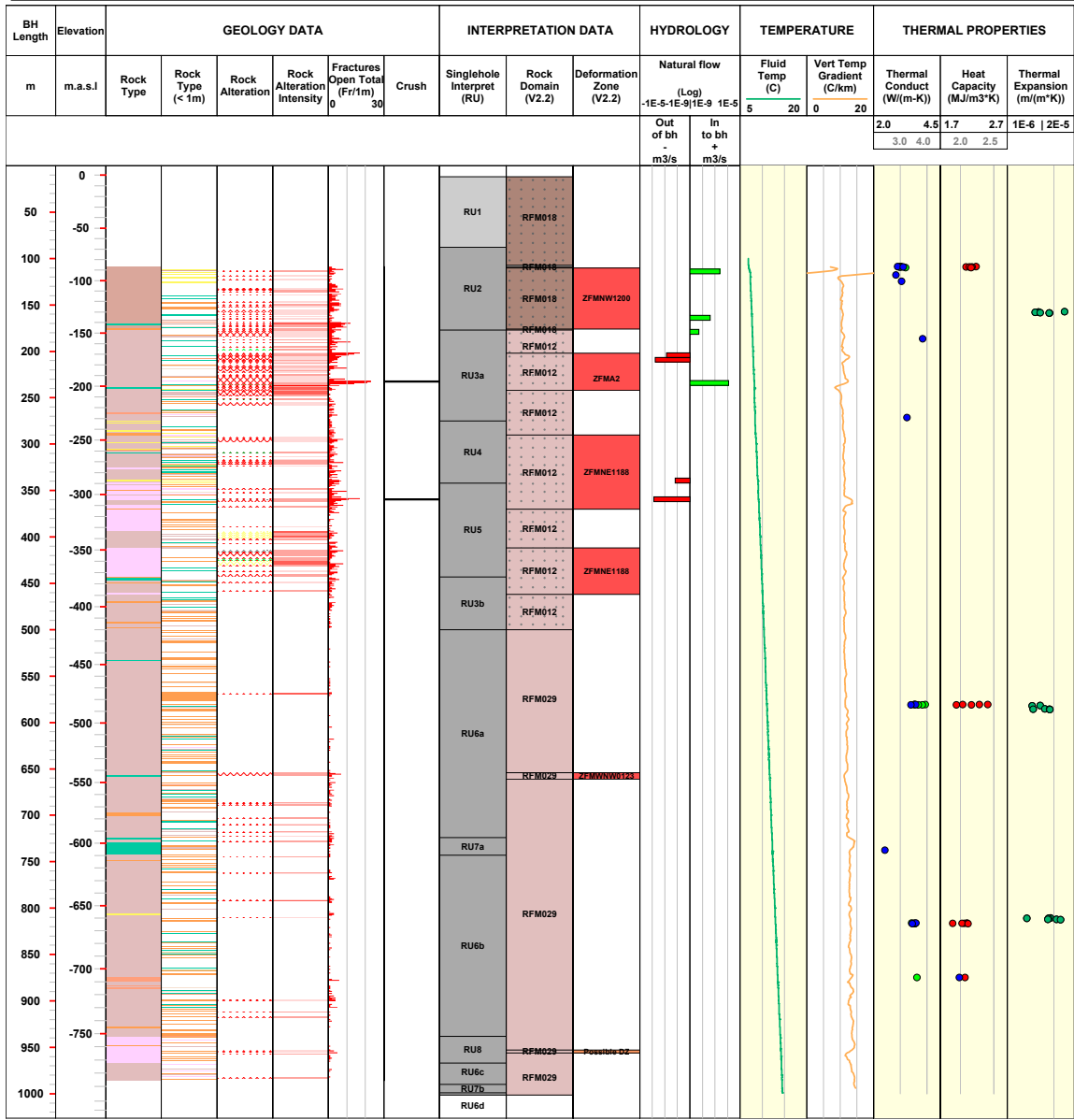
Title KFM02A		Site FORSMARK	Coordinate System RT90-RHB70	Elevation [m.a.s.l.] 7.35
	Borehole KFM02A	Northing [m] 6698712.50	Drilling Start Date 2003-01-08 14:23:00	
	Diameter [mm] 77	Easting [m] 1633182.86	Drilling Stop Date 2003-03-12 21:30:00	
	Length [m] 1002.440	Inclination (at borehole collar) [°] -85.37	Surveying Date 2002-12-17 14:40:00	
	Bearing [°] 275.76	Date of mapping	Plot Date 2008-10-22 23:03:58	


<p>ROCKTYPE FORSMARK</p> <ul style="list-style-type: none"> Granite, fine- to medium-grained Pegmatite, pegmatic granite Granite, granodiorite and tonalite, metamorphic, fine- to medium-grained Granite to granodiorite, metamorphic, medium-grained Amphibolite 	<p>ROCK ALTERATION</p> <ul style="list-style-type: none"> Oxidized Epidotized Quartz dissolution Argillization Albitization Sausuritization 	<p>ROCK ALTERATION INTENSITY</p> <ul style="list-style-type: none"> Faint Weak Medium Strong
<p>ROCK DOMAIN V2.2</p> <ul style="list-style-type: none"> RFM029 Granite to granodiorite, metamorphic, medium-grained 		<p>DEFORMATION ZONE V2.2</p> <ul style="list-style-type: none"> DZ which is modelled deterministically
<p>THERMAL CONDUCTIVITY</p> <ul style="list-style-type: none"> Thermal conductivity (From mineral composition) Thermal conductivity (TPS) 		<p>HEAT CAPACITY</p> <ul style="list-style-type: none"> Heat capacity (TPS) Heat capacity (Direct)

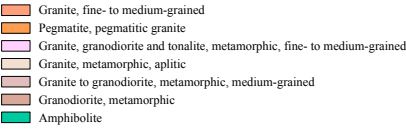
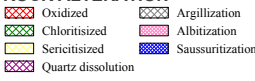

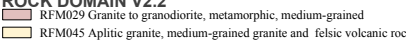
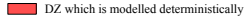
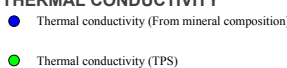
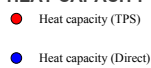


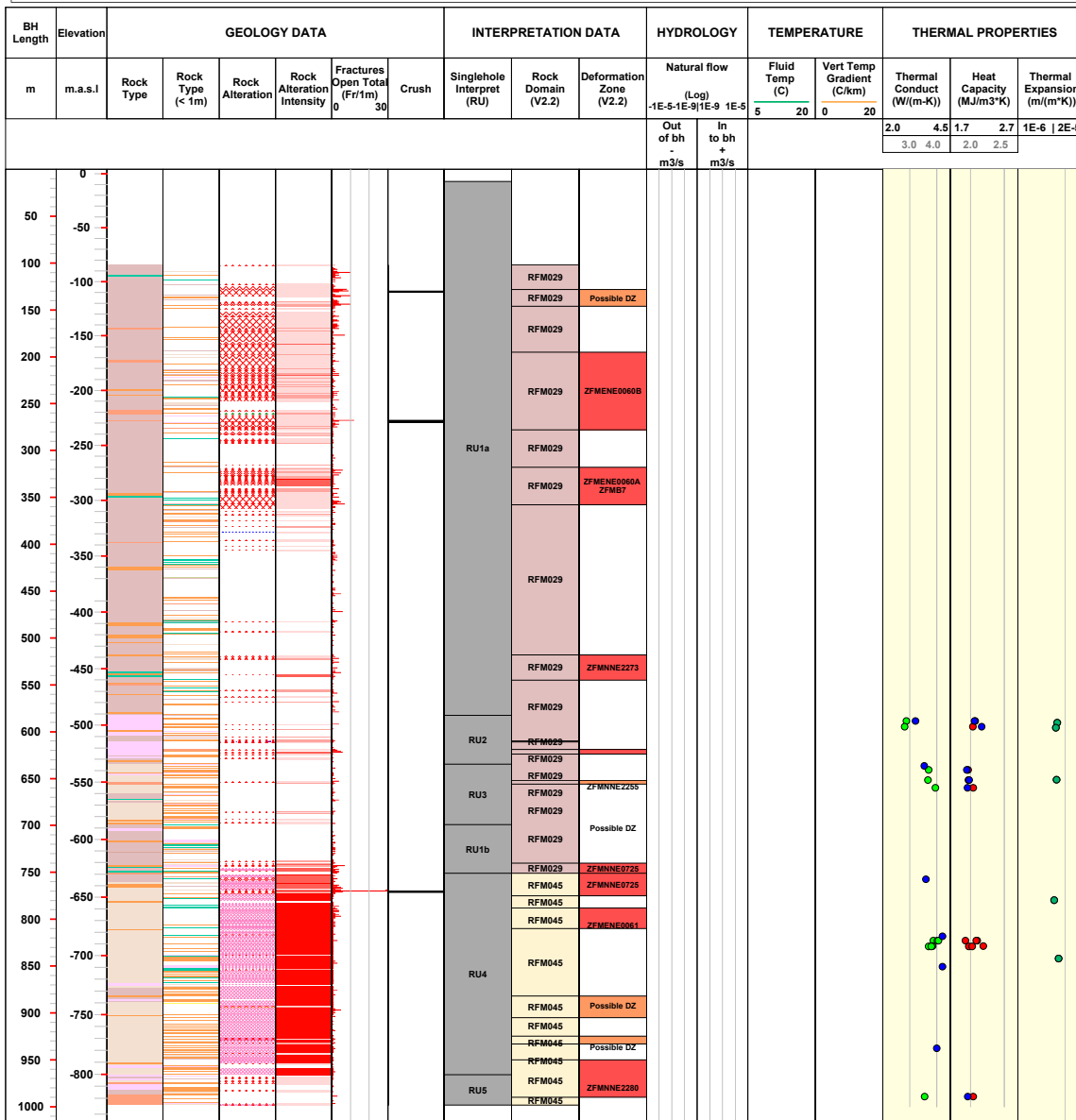
Title KFM04A		Site FORSMARK	Coordinate System RT90-RHB70	Elevation [m.a.s.l.] 8.77
	Borehole KFM04A	Northing [m] 6698921.74	Drilling Start Date 2003-08-25 11:17:00	
	Diameter [mm] 77	Easting [m] 1630978.96	Drilling Stop Date 2003-11-19 15:15:00	
	Length [m] 1001.420	Inclination (at borehole collar) [°] -60.07	Surveying Date 2003-09-04 12:05:00	
	Bearing [°] 45.24	Date of mapping	Plot Date 2008-10-22 23:03:58	


ROCKTYPE FORSMARK 	ROCK ALTERATION  ROCK DOMAIN V2.2 	ROCK ALTERATION INTENSITY  DEFORMATION ZONE V2.2 
THERMAL CONDUCTIVITY 		HEAT CAPACITY 

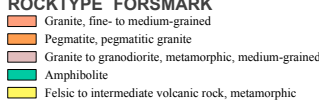


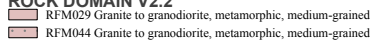
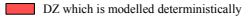
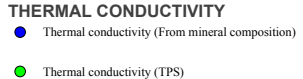
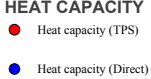


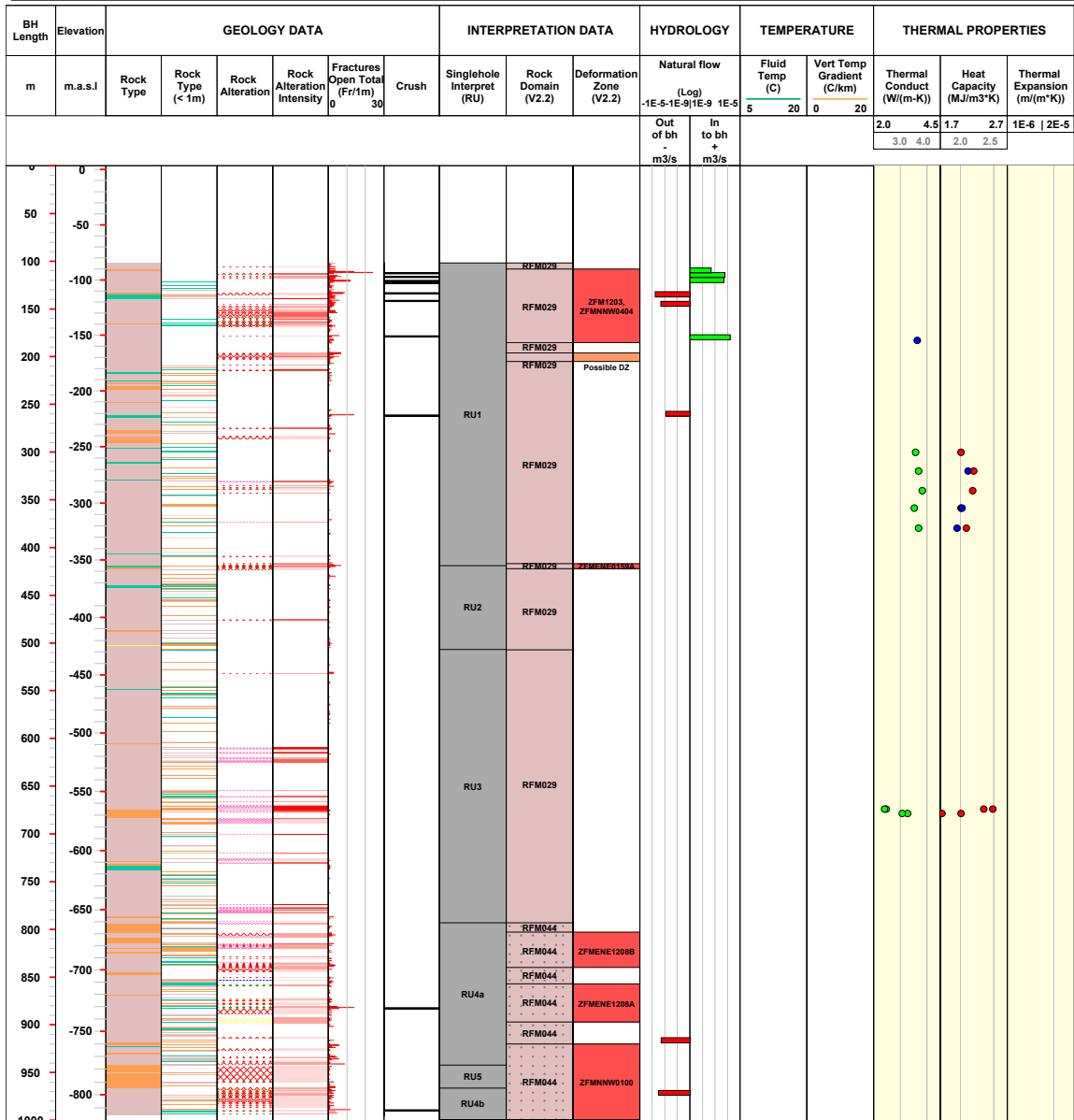
Title KFM06A		Site FORSMARK	Coordinate System RT90-RHB70	Elevation [m.a.s.l.] 4.10
	Borehole KFM06A	Northing [m] 6699732.88	Drilling Start Date 2004-06-14 14:00:00	
	Diameter [mm] 77	Easting [m] 1632442.51	Drilling Stop Date 2004-09-21 03:37:00	
	Length [m] 1000.640	Inclination (at borehole collar) [°] -60.24	Surveying Date 2003-11-11 15:15:00	
	Bearing [°] 300.92	Date of mapping	Plot Date 2008-10-22 23:03:58	


ROCKTYPE FORSMARK  <ul style="list-style-type: none"> Granite, fine- to medium-grained Pegmatite, pegmatitic granite Granite, granodiorite and tonalite, metamorphic, fine- to medium-grained Granite, metamorphic, aplitic Granite to granodiorite, metamorphic, medium-grained Granodiorite, metamorphic Amphibolite 	ROCK ALTERATION  <ul style="list-style-type: none"> Oxidized Chloritized Sericitized Quartz dissolution Argillization Albitization Saussurization 	ROCK ALTERATION INTENSITY  <ul style="list-style-type: none"> Faint Weak Medium Strong
ROCK DOMAIN V2.2  <ul style="list-style-type: none"> RFM029 Granite to granodiorite, metamorphic, medium-grained RFM045 Aplitic granite, medium-grained granite and felsic volcanic rock 		DEFORMATION ZONE V2.2  <ul style="list-style-type: none"> DZ which is modelled deterministically
THERMAL CONDUCTIVITY  <ul style="list-style-type: none"> Thermal conductivity (From mineral composition) Thermal conductivity (TPS) 		HEAT CAPACITY  <ul style="list-style-type: none"> Heat capacity (TPS) Heat capacity (Direct)



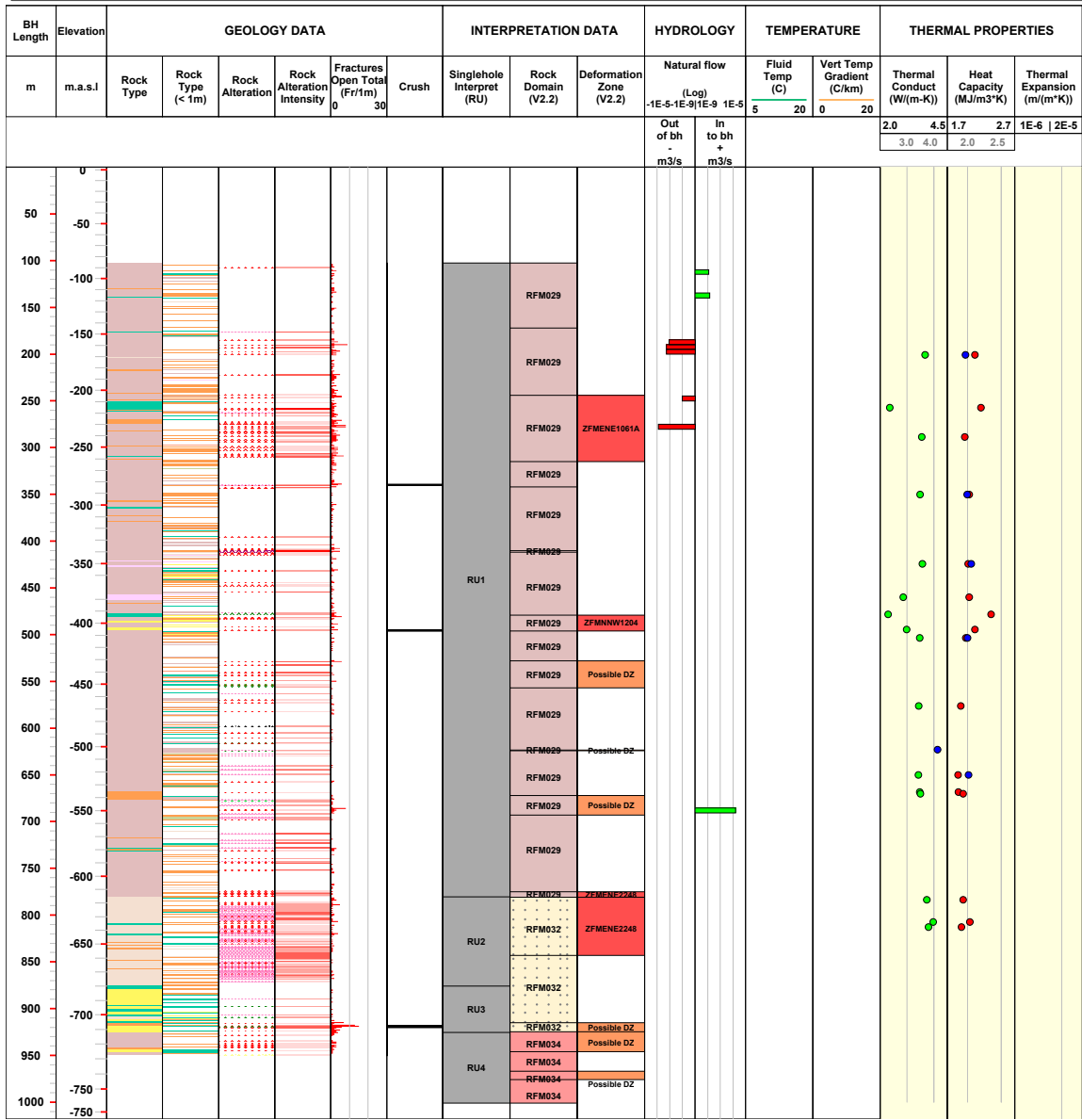
Title KFM07A		Site FORSMARK	Coordinate System RT90-RHB70	Elevation [m.a.s.l.] 3.33
	Borehole KFM07A	Northing [m] 6700127.08	Drilling Start Date 2004-10-14 08:00:00	
	Diameter [mm] 77	Easting [m] 1631031.57	Drilling Stop Date 2004-12-09 11:40:00	
	Length [m] 1002.100	Inclination (at borehole collar) [°] -59.28	Surveying Date 2004-06-07 16:10:00	
	Bearing [°] 261.47	Date of mapping	Plot Date 2008-10-22 23:03:58	


ROCKTYPE FORSMARK 	ROCK ALTERATION 	ROCK ALTERATION INTENSITY 
ROCK DOMAIN V2.2 		DEFORMATION ZONE V2.2 
THERMAL CONDUCTIVITY 		HEAT CAPACITY 



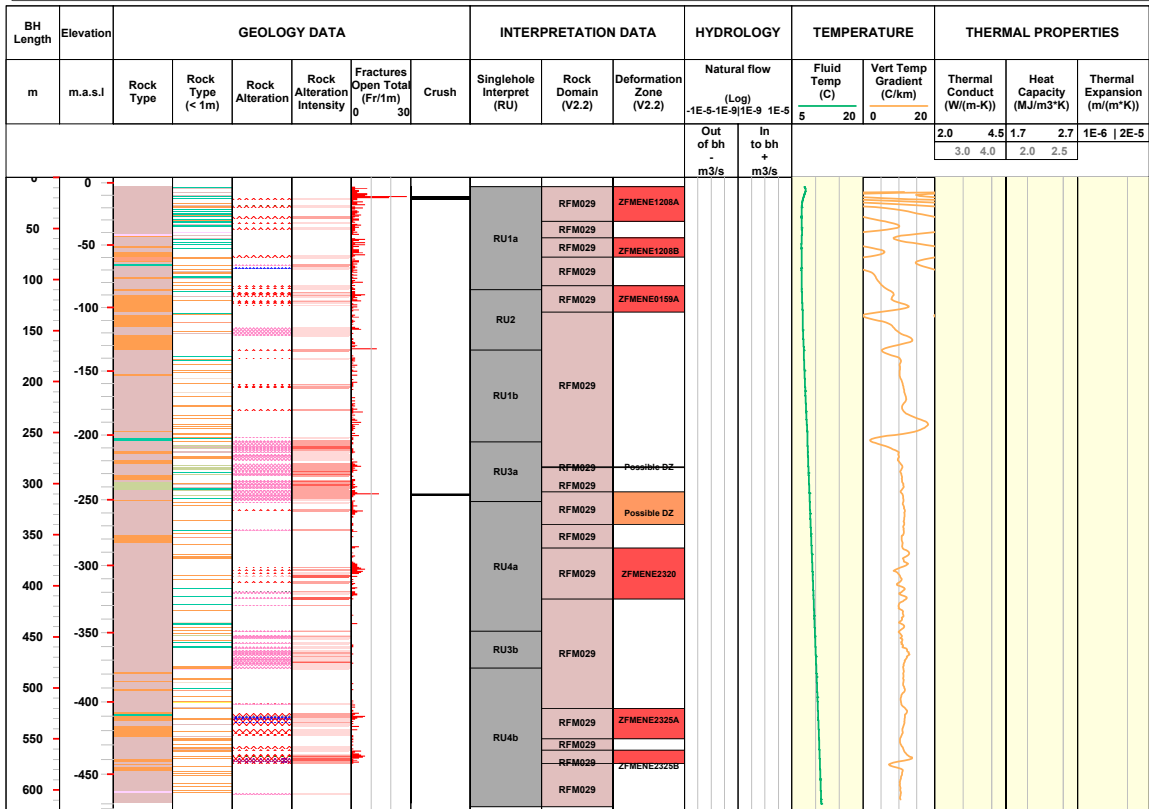
Title KFM08A		Site FORSMARK	Coordinate System RT90-RHB70	Elevation [m.a.s.l.] 2.49
	Borehole KFM08A	Northing [m] 6700494.49	Drilling Start Date 2005-01-25 01:00:00	
	Diameter [mm] 77	Easting [m] 1631197.06	Drilling Stop Date 2005-01-25 10:00:00	
	Length [m] 1001.190	Inclination (at borehole collar) [°] -60.84	Surveying Date 2004-09-13 13:50:00	
	Bearing [°] 321.00	Date of mapping	Plot Date 2008-10-22 23:03:58	

ROCKTYPE FORSMARK Pegmatite, pegmatitic granite Granite, granodiorite and tonalite, metamorphic, fine- to medium-grained Granite, metamorphic, aplitic Granite to granodiorite, metamorphic, medium-grained Amphibolite Felsic to intermediate volcanic rock, metamorphic	ROCK ALTERATION Oxidized Chloritised Epidotised Sericitised Quartz dissolution Silicification Albitization Saussurization	ROCK ALTERATION INTENSITY Faint Weak Medium Strong DEFORMATION ZONE V2.2 DZ which is modelled deterministically
ROCK DOMAIN V2.2 RFM029 Granite to granodiorite, metamorphic, medium-grained RFM032 Aplitic granite, medium-grained granite and felsic volcanic rock RFM034 Granite to granodiorite, metamorphic, medium-grained	THERMAL CONDUCTIVITY Thermal conductivity (From mineral composition) Thermal conductivity (TPS)	HEAT CAPACITY Heat capacity (TPS) Heat capacity (Direct)



Title KFM09B		Site FORSMARK	Coordinate System RT90-RHB70	Elevation [m.a.s.l.] 4.30
	Borehole KFM09B	Northing [m] 6700119.89	Drilling Start Date 2005-11-16 00:00:00	
	Diameter [mm] 77	Easting [m] 1630638.78	Drilling Stop Date 2005-12-19 00:00:00	
	Length [m] 616.450	Inclination (at borehole collar) [°] -55.07	Surveying Date 2005-10-27 09:00:00	
	Bearing [°] 140.83	Date of mapping	Plot Date 2008-10-22 23:03:58	

ROCKTYPE FORSMARK			ROCK ALTERATION			ROCK ALTERATION INTENSITY		
Granite, fine- to medium-grained	Oxidized	Albitization	Faint	Chloritized	Saussuritization	Weak	DEFORMATION ZONE V2.2	
Pegmatite, pegmatitic granite	Quartz dissolution	Laumontization	Medium	Argillization	RFM029 Granite to granodiorite, metamorphic, medium-grained	DZ which is modelled deterministically		
Granite, granodiorite and tonalite, metamorphic, fine- to medium-grained	ROCK DOMAIN V2.2							
Granite to granodiorite, metamorphic, medium-grained								
Amphibolite								
Calc-silicate rock (skarn)								
			THERMAL CONDUCTIVITY			HEAT CAPACITY		



Visualisations of TRC (lithology) and thermal conductivity realisations

In this appendix, example realisations are presented in 2D for simulation scale 1 m for rock domain RFM045. All 2D-realizations represent a slice in the centre of a 3D cube having a volume of 50×50×50 m. For example, the 25th slice of the xy-plane is the 25th slice that can be cut in the z-direction (there are 50 slices).

Realisations of the simulated TRCs and the corresponding thermal conductivity realisations are presented for each thermal subdomain, i.e. A1 and A2 (both subdomain A) and B.

Domain RFM045

Subdomain A – A1

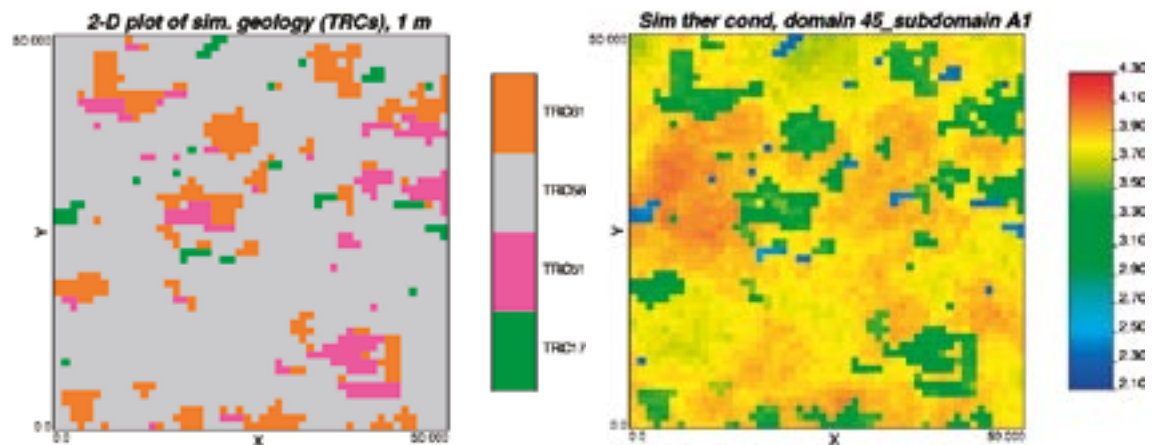


Figure B-1. 2D slice from one 3D realization (simulation scale = 1 m) illustrating the distribution of TRCs (left) and distribution of thermal conductivity values (right) for domain RFM045, subdomain A1. Realisation 1, slice 25, xy plane.

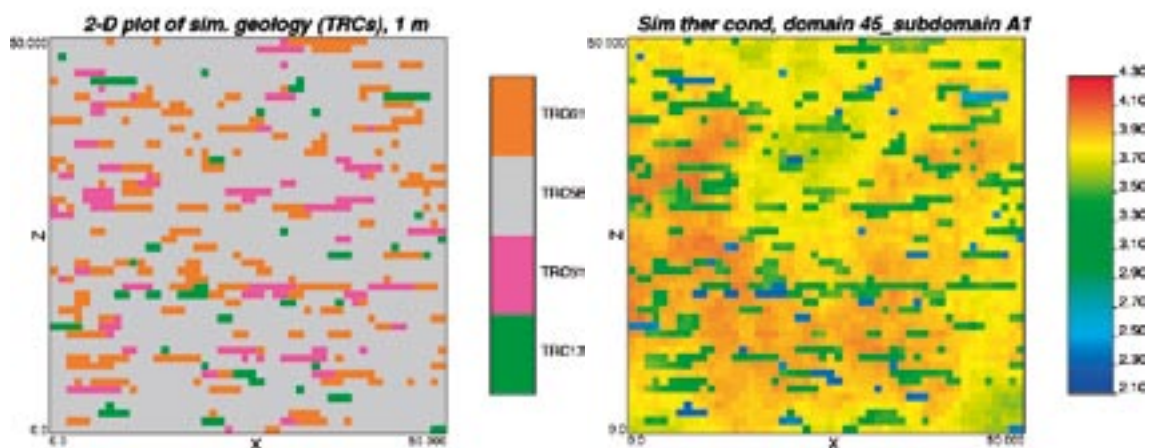


Figure B-2. 2D slice from one 3D realization (simulation scale = 1 m) illustrating the distribution of TRCs (left) and distribution of thermal conductivity values (right) for domain RFM045, subdomain A1. Realisation 1, slice 25, xz plane.

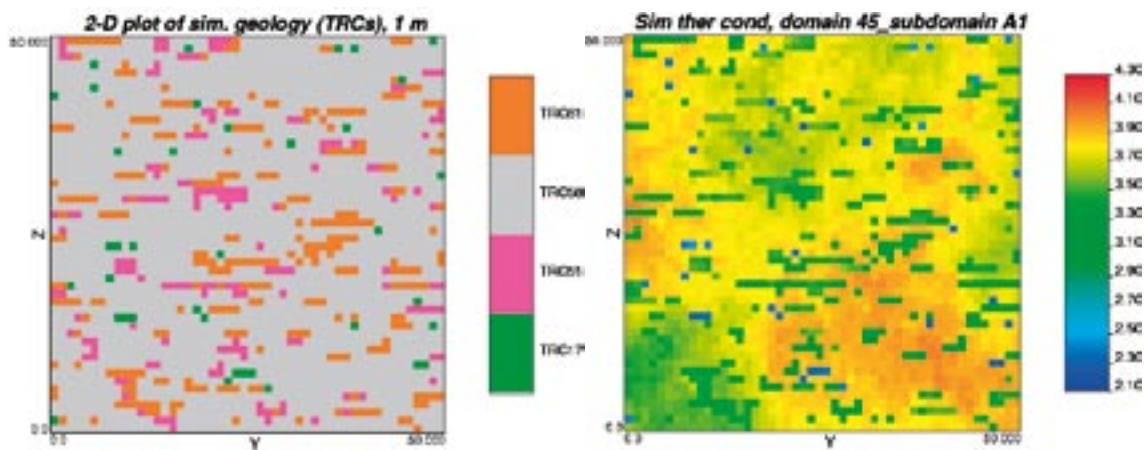


Figure B-3. 2D slice from one 3D realisation (simulation scale = 1 m) illustrating the distribution of TRCs (left) and distribution of thermal conductivity values (right) for domain RFM045, subdomain A1. Realisation 1, slice 25, yz plane.

Subdomain A – A2

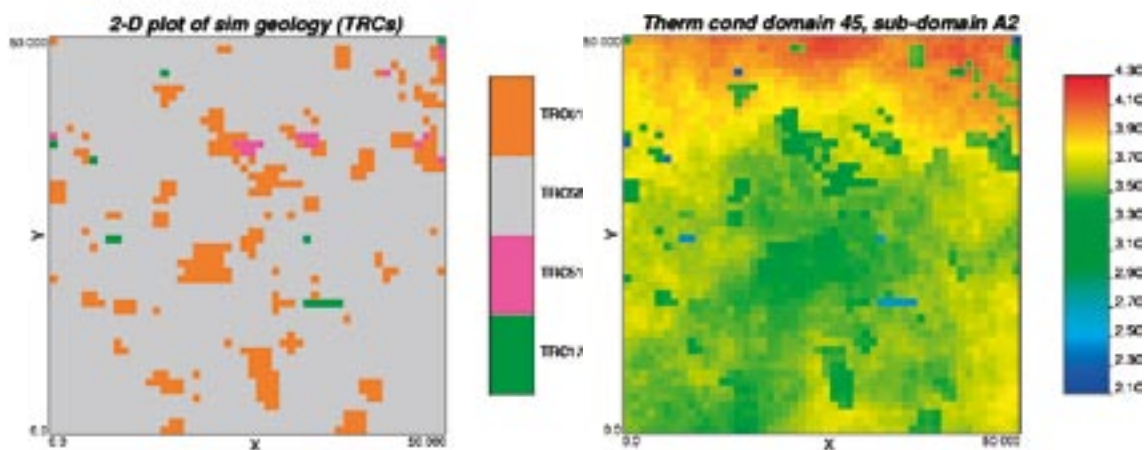


Figure B-4. 2D slice from one 3D realisation (simulation scale = 1 m) illustrating the distribution of TRCs (left) and distribution of thermal conductivity values (right) for domain RFM045, subdomain A2. Realisation 1, slice 25, xy plane.

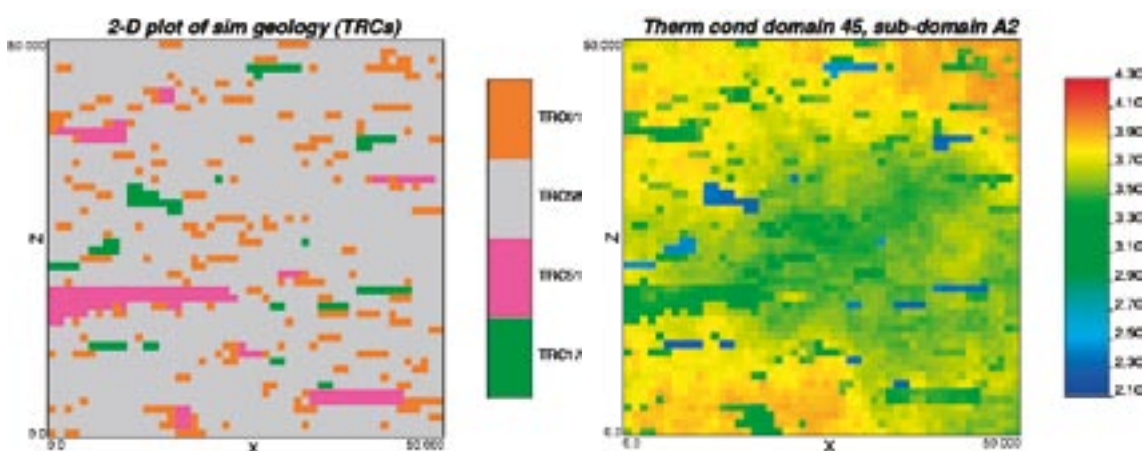


Figure B-5. 2D slice from one 3D realisation (simulation scale = 1 m) illustrating the distribution of TRCs (left) and distribution of thermal conductivity values (right) for domain RFM045, subdomain A2. Realisation 1, slice 25, xz plane.

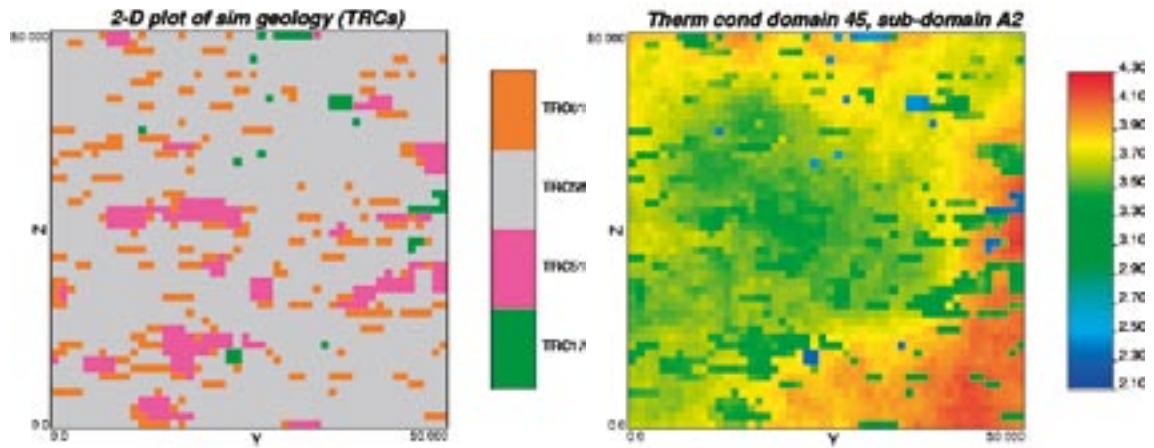


Figure B-6. 2D slice from one 3D realisation (simulation scale = 1 m) illustrating the distribution of TRCs (left) and distribution of thermal conductivity values (right) for domain RFM045, subdomain A2. Realisation 1, slice 25, yz plane.

Subdomain B

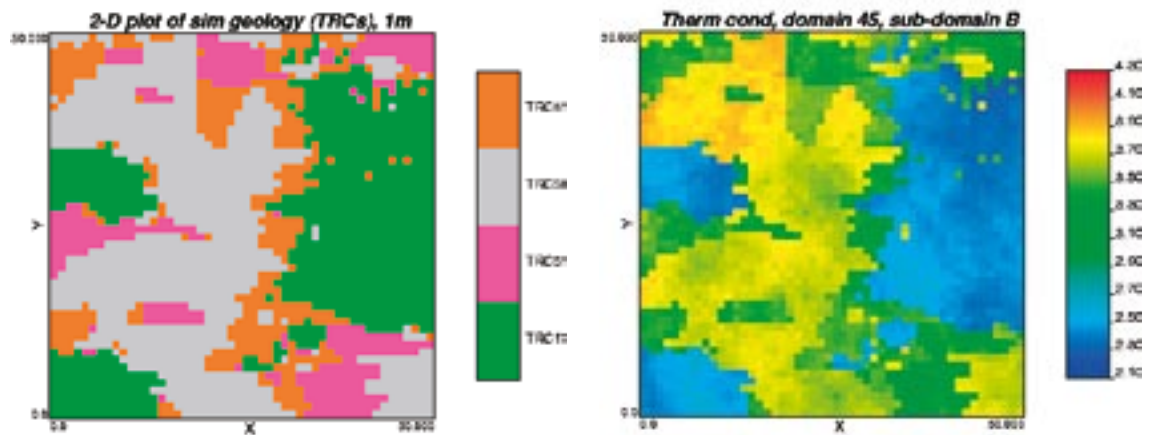


Figure B-7. 2D slice from one 3D realisation (simulation scale = 1 m) illustrating the distribution of TRCs (left) and distribution of thermal conductivity values (right) for domain RFM045, subdomain B. Realisation 1, slice 25, xy plane.

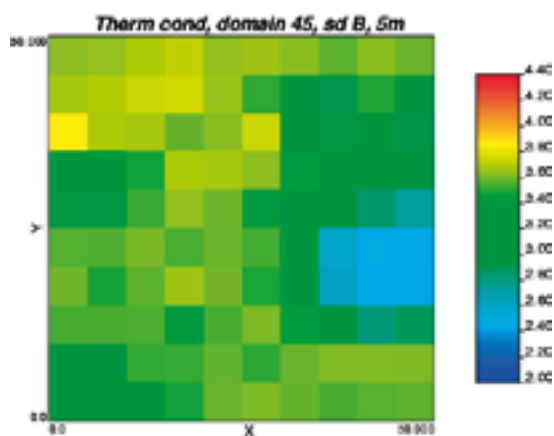


Figure B-8. 2D slice from one 3D realisation (1 m simulations upscaled to 5 m) illustrating the distribution of thermal conductivity values for domain RFM045, subdomain B. Realisation 1, slice 5, xy plane.

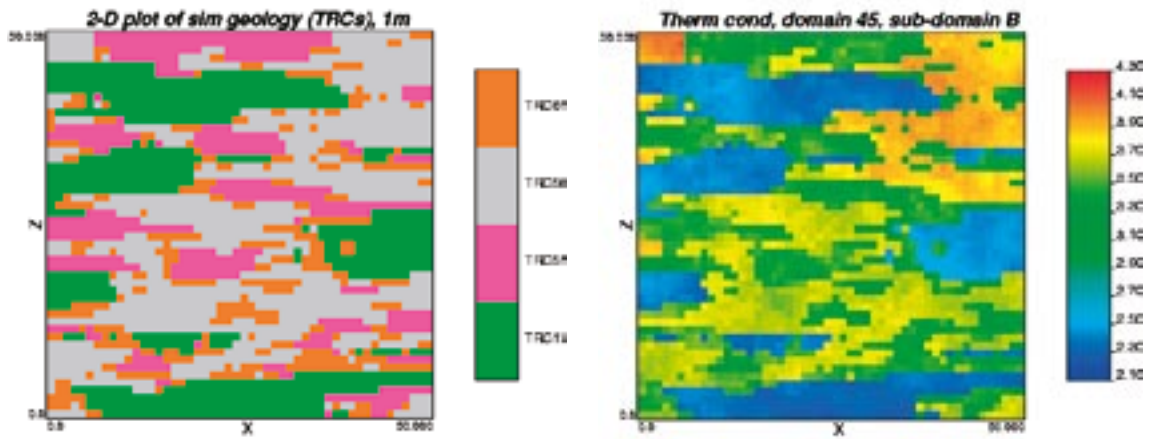


Figure B-9. 2D slice from one 3D realisation (simulation scale = 1 m) illustrating the distribution of TRCs (left) and distribution of thermal conductivity values (right) for domain RFM045, subdomain B. Realisation 1, slice 25, xz plane.

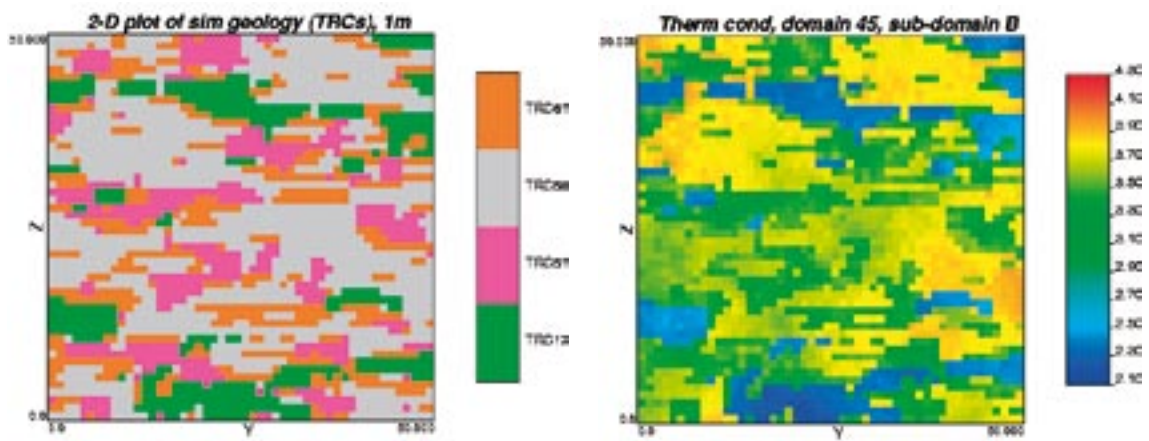


Figure B-10. 2D slice from one 3D realisation (simulation scale = 1 m) illustrating the distribution of TRCs (left) and distribution of thermal conductivity values (right) for domain RFM045, subdomain B. Realisation 1, slice 25, yz plane.

Histogram of simulated and observed lengths

Histograms of TRC length distributions in simulations and boreholes, Subdomain A1

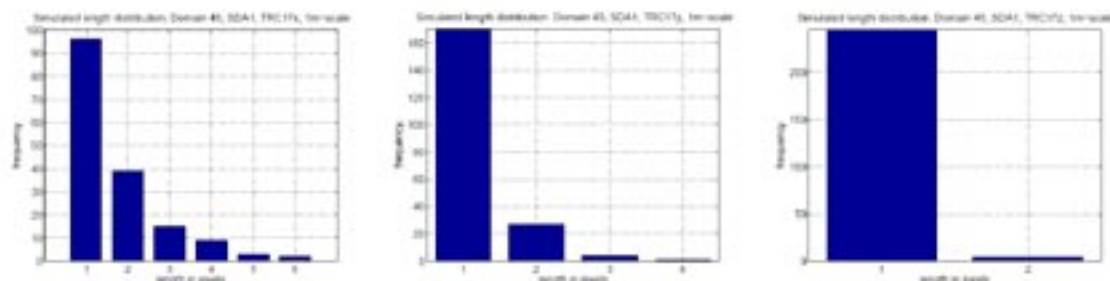


Figure 1. Histogram from 36 "borings" in 10 randomly selected realisations of TRC 17 in x -, y - and z -direction. Domain 45, SDA1. X-axis in pixels (px); 1px = 1m.

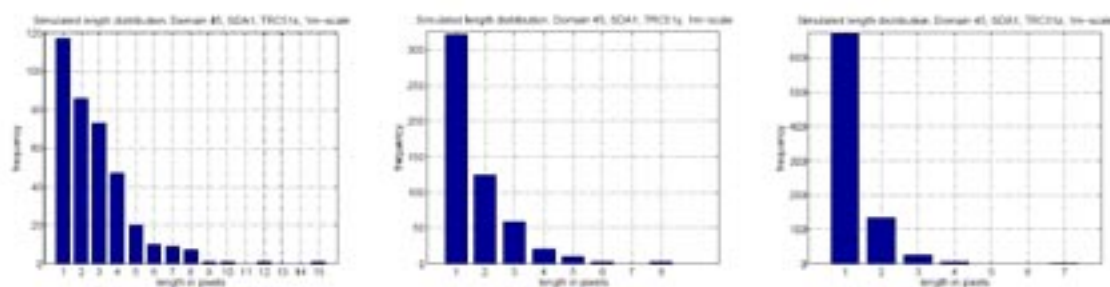


Figure 2. Histogram from 36 "borings" in 10 randomly selected realisations of TRC 51 in x -, y - and z -direction. Domain 45, SDA1. X-axis in pixels (px); 1px = 1m.

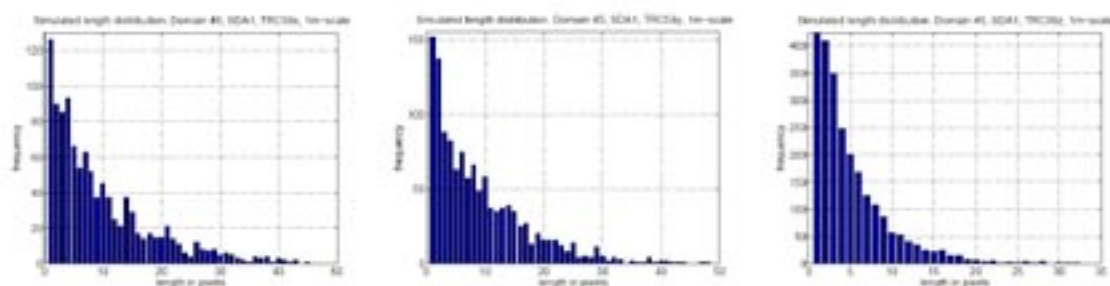


Figure 3. Histogram from 36 "borings" in 10 randomly selected realisations of TRC 58 in x -, y - and z -direction. Domain 45, SDA1. X-axis in pixels (px); 1px = 1m.

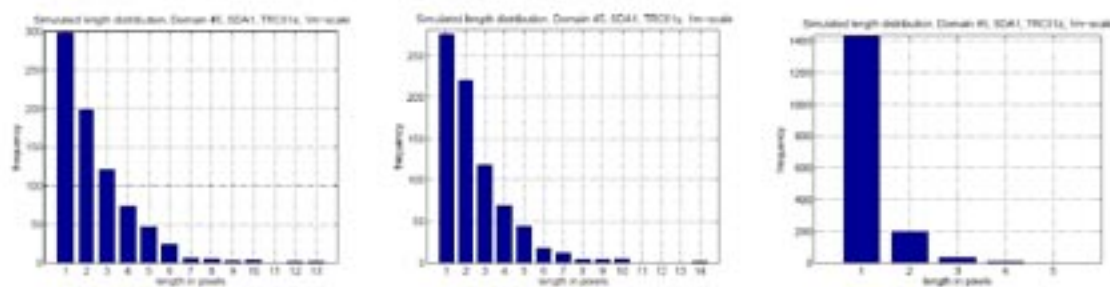


Figure 4. Histogram from 36 "borings" in 10 randomly selected realisations of TRC 61 in x -, y - and z -direction. Domain 45, SDA1. X-axis in pixels (px); 1px = 1m.

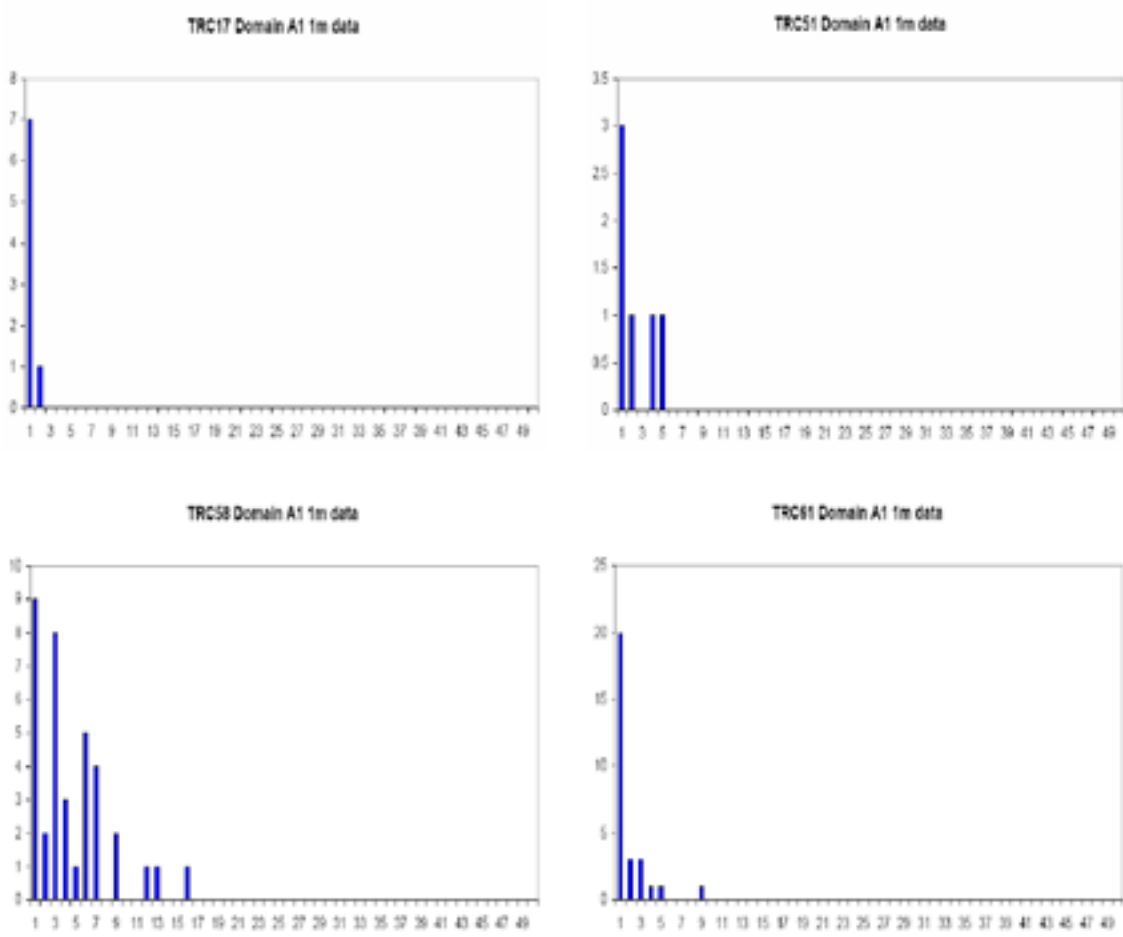


Figure 5. Histograms of TRC lengths observed in boreholes in subdomain A1. X-axis in meters (pixels).

Histograms of TRC length distributions in simulations and boreholes, Subdomain A2

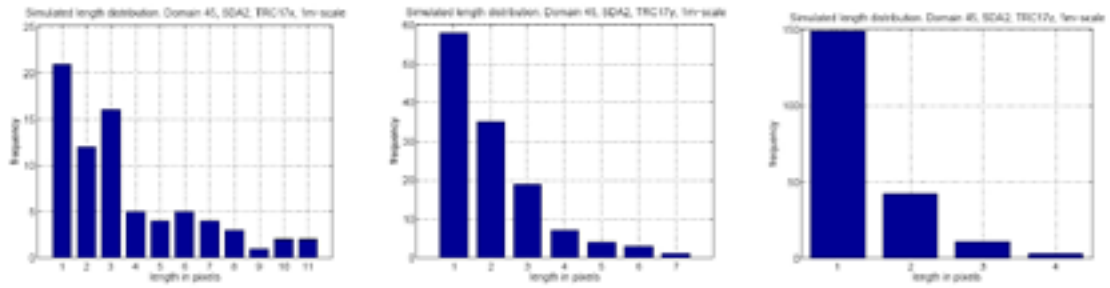


Figure 1. Histogram from 36 "borings" in 10 randomly selected realisations of TRC 17 in x -, y - and z -direction. Domain 45, SDA2. X -axis in pixels (px); 1px = 1m.

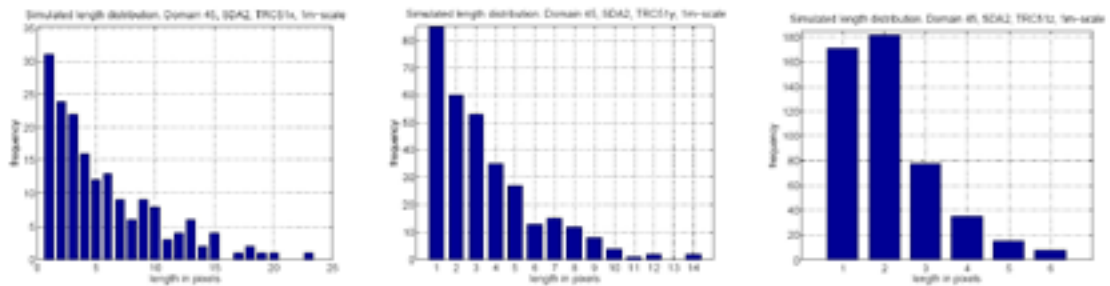


Figure 2. Histogram from 36 "borings" in 10 randomly selected realisations of TRC 51 in x -, y - and z -direction. Domain 45, SDA2. X -axis in pixels (px); 1px = 1m.

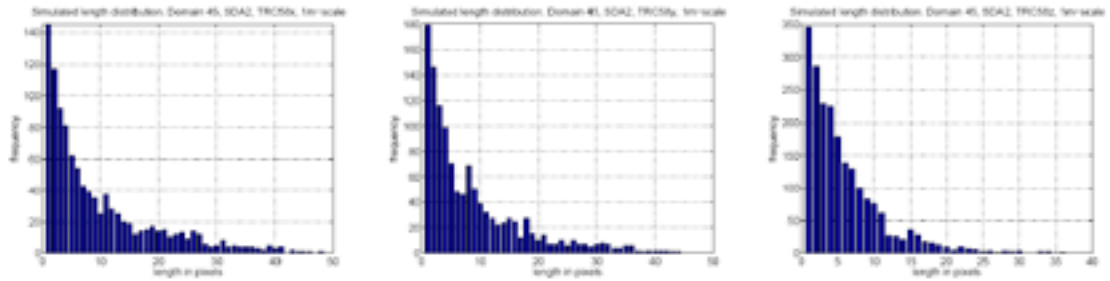


Figure 3. Histogram from 36 "borings" in 10 randomly selected realisations of TRC 58 in x -, y - and z -direction. Domain 45, SDA2. X -axis in pixels (px); 1px = 1m.

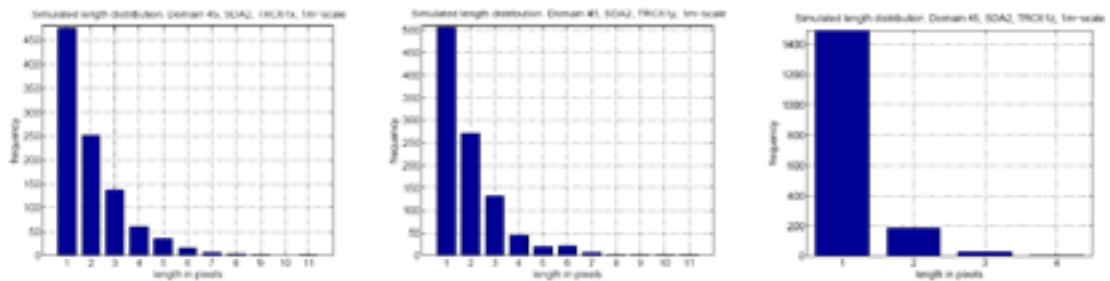


Figure 4. Histogram from 36 "borings" in 10 randomly selected realisations of TRC 61 in x -, y - and z -direction. Domain 45, SDA2. X -axis in pixels (px); 1px = 1m.

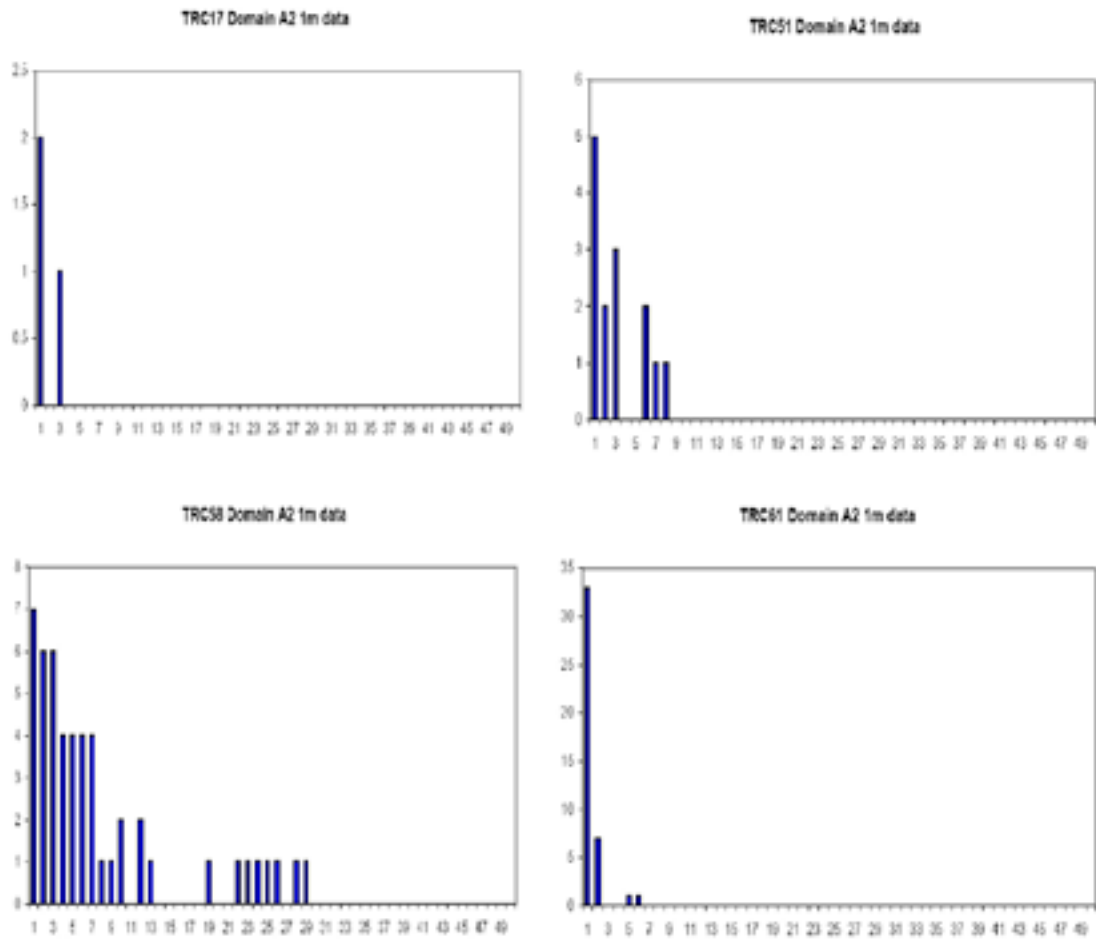


Figure 5. Histograms of TRC lengths observed in boreholes in subdomain A2. X-axis in meters (pixels).

Histograms of TRC length distributions in simulations and boreholes, Subdomain B

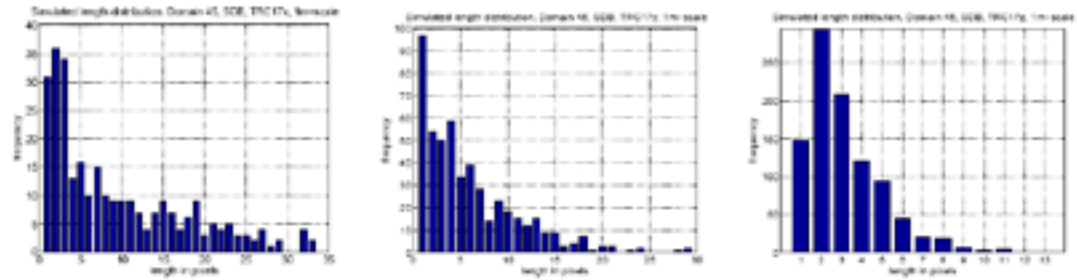


Figure 1. Histogram from 36 "borings" in 10 randomly selected realisations of TRC 17 in x -, y - and z -direction. Domain 45, SDB. x -axis in pixels (px); 1px = 1m.

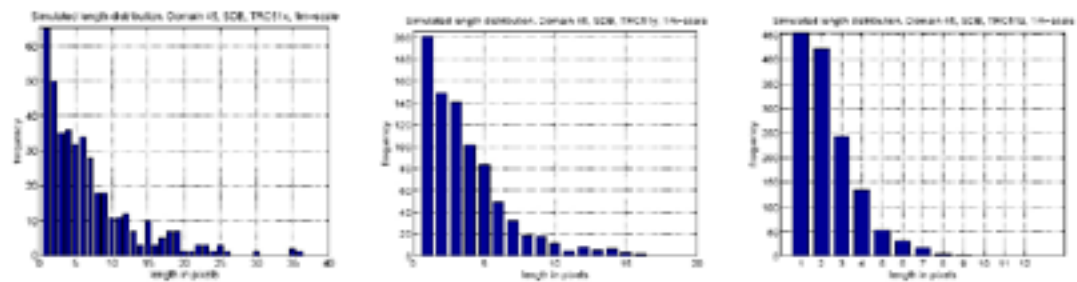


Figure 2. Histogram from 36 "borings" in 10 randomly selected realisations of TRC 51 in x -, y - and z -direction. Domain 45, SDB. x -axis in pixels (px); 1px = 1m.

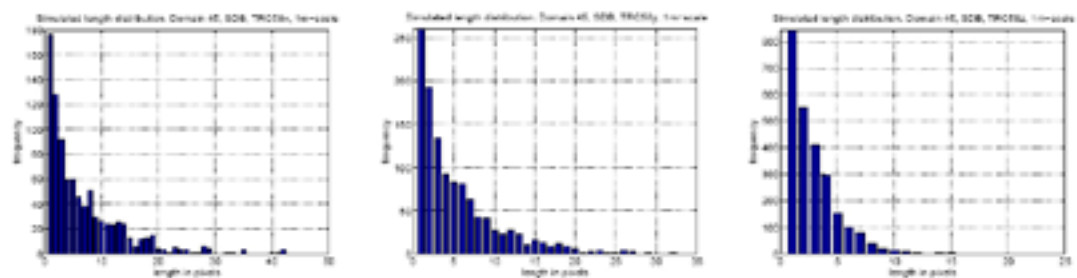


Figure 3. Histogram from 36 "borings" in 10 randomly selected realisations of TRC 58 in x -, y - and z -direction. Domain 45, SDB. x -axis in pixels (px); 1px = 1m.

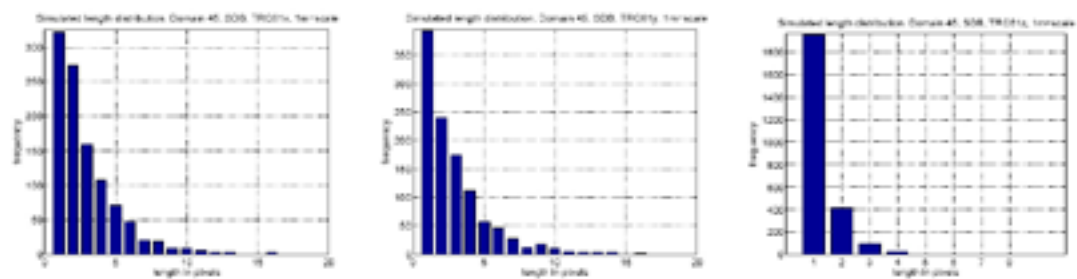


Figure 4. Histogram from 36 "borings" in 10 randomly selected realisations of TRC 61 in x -, y - and z -direction. Domain 45, SDB. x -axis in pixels (px); 1px = 1m.

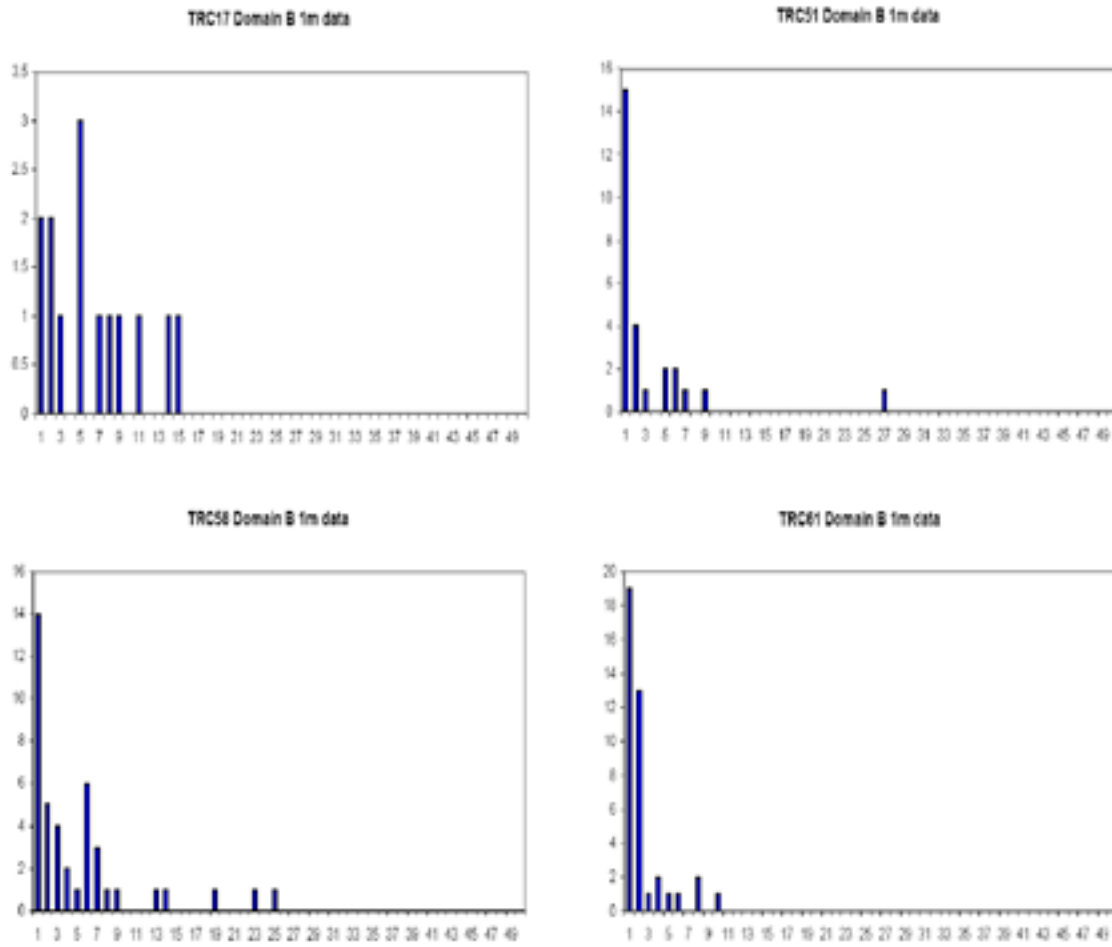


Figure 5. Histograms of TRC lengths observed in boreholes in subdomain B. X-axis in meters (pixels).

Mathematical description of the transformation of borehole data

Introduction

This memorandum describes the coordinate transformation procedure for setting up a model for the stochastic simulation of geology in T-PROGS. As input data, T-PROGS uses transition probabilities for the principal direction of anisotropy. To facilitate realistic modelling results the model volume therefore needs to be orientated in a transformed coordinate system, obtained through rotation of the main principal directions (Figure D-1) in three steps; $(x, y, z) \rightarrow (x', y', z') \rightarrow (x'', y'', z'') \rightarrow (x''', y''', z''')$, Figures D-3 to D-5.

Geological information describing anisotropy is given as: (1) the trend and plunge of the mineral stretching orientation and (2) the strike and dip of the foliation. The orientation of rock units is a function of these. The theoretical description of the transformation to a coordinate system orientated in the principal direction of anisotropy as a function of the mineral stretching and foliation plane is given below.

Coordinate transformation

The main principal directions are shown in Figure D-1.

Each domain has a local coordinate system (x''', y''', z''') governed by the principal direction of anisotropy and an origo defined by minimum easting, minimum northing, and maximum elevation from positions in borehole records supplied. The local coordinate system is obtained through rotations in three steps, as described below. This results in a transformed coordinate system with main axis (x''') parallel to the principal direction of anisotropy, see Figure D-2.

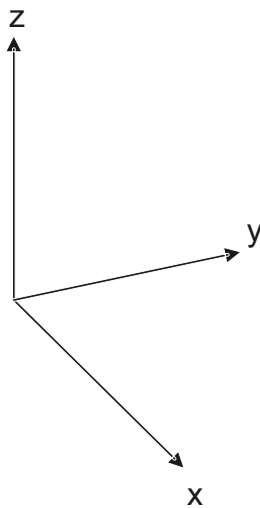


Figure D-1. Main principal directions (X = easting direction, y =northing direction, z =elevation direction).

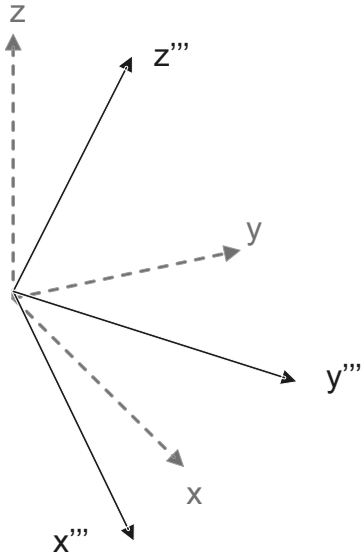


Figure D-2. Principal directions of the local transformed coordinate system where x''' is parallel to the principal direction of anisotropy.

For domain RFM045 origo ($x''' = y''' = z''' = x = y = z = 0$) is located at:

Northing 6699927.88, Easting 1631300.33, Elevation -319.27

The principal direction of anisotropy is parallel to the trend and plunge of the mineral stretching lination ($145^\circ/42^\circ$ for boreholes KFM06A and KFM06C; $145^\circ/60^\circ$ for borehole KFM08C; $145^\circ/42^\circ$ for boreholes KFM08D). Two unit vectors (x_1, y_1, z_1) and (x_2, y_2, z_2) can be defined as:

$$x_1 = \cos \alpha_1 \cos \beta_1$$

$$y_1 = \sin \alpha_1 \cos \beta_1 \quad ; (x_1, y_1, z_1) \text{ in principal direction of anisotropy}$$

$$z_1 = \sin \beta_1$$

and

$$x_2 = \cos \alpha_2 \cos \beta_2$$

$$y_2 = \sin \alpha_2 \cos \beta_2 \quad ; (x_2, y_2, z_2) \text{ in direction of foliation and TRC contacts}$$

$$z_2 = \sin \beta_2$$

where

$$\alpha_1 = \text{trend} - 90^\circ = 145^\circ - 90^\circ = 55^\circ, \beta_1 = \text{plunge} = 42^\circ, \alpha_2 = \text{strike} - 90^\circ + 90^\circ = 112.5^\circ - 90^\circ + 90^\circ = 112.5^\circ, \beta_2 = \text{dip} = 60^\circ ; \text{ for boreholes KFM06A and KFM06C}$$

and

$$\alpha_1 = 145 - 90 = 55^\circ, \beta_1 = 60^\circ, \alpha_2 = 60 - 90 + 90 = 60^\circ, \beta_2 = 60^\circ ; \text{ for borehole KFM08C}$$

and

$$\alpha_1 = 145 - 90 = 55^\circ, \beta_1 = 42^\circ, \alpha_2 = 125 - 90 + 90 = 125^\circ, \beta_2 = 70^\circ ; \text{ for borehole KFM08D.}$$

The coordinate system is now rotated so that the x-axis points in the trend/plunge direction. The position (x_1, y_1, z_1) will then have the coordinates $(1, 0, 0)$. The first rotation is thus the x-y plane α_1 degrees clockwise around the z-axis. The second rotation is the x'-z' plane β_1 degrees clockwise around the y'-axis. The final transformation is to rotate the y''-z'' plane γ_1 degrees around the x''-axis until $z_2=0$ for the position (x_2, y_2, z_2) . The unit vectors (x_1, y_1, z_1) and (x_2, y_2, z_2) will then be in the new x'''-y''' plane and z''' is perpendicular to this plane. The three rotations are defined as follows:

First rotation

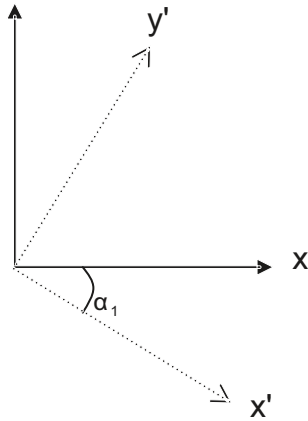


Figure D-3. First rotation, α_1 degrees around the z-axis.

$$\begin{bmatrix} x' \\ y' \\ z' \end{bmatrix} = \begin{bmatrix} \cos \alpha_1 & -\sin \alpha_1 & 0 \\ \sin \alpha_1 & \cos \alpha_1 & 0 \\ 0 & 0 & 1 \end{bmatrix} \begin{bmatrix} x \\ y \\ z \end{bmatrix}$$

Second rotation

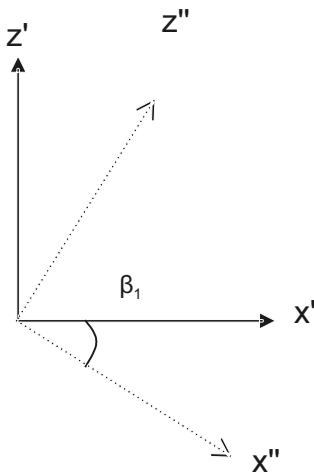


Figure D-4. Second rotation, β_1 degrees around the y'-axis.

$$\begin{bmatrix} x'' \\ y'' \\ z'' \end{bmatrix} = \begin{bmatrix} \cos \beta_1 & 0 & -\sin \beta_1 \\ 0 & 1 & 0 \\ \sin \beta_1 & 0 & \cos \beta_1 \end{bmatrix} \begin{bmatrix} x' \\ y' \\ z' \end{bmatrix}$$

Third rotation

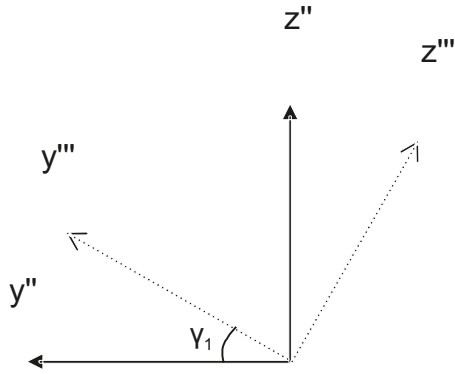


Figure D-5. Third rotation, γ_1 degrees around the x'' -axis.

$$\begin{bmatrix} x''' \\ y''' \\ z''' \end{bmatrix} = \begin{bmatrix} 1 & 0 & 0 \\ 0 & \cos \gamma_1 & \sin \gamma_1 \\ 0 & -\sin \gamma_1 & \cos \gamma_1 \end{bmatrix} \times \begin{bmatrix} x'' \\ y'' \\ z'' \end{bmatrix}$$

where the angle γ_1 is defined by:

$$\tan \gamma_1 = \frac{z_2''}{y_2''} \Leftrightarrow y_2'' \sin \gamma_1 = z_2'' \cos \gamma_1 \Leftrightarrow -y_2'' \sin \gamma_1 + z_2'' \cos \gamma_1 = 0$$

Verification

To verify that the unit vectors (x_1, y_1, z_1) and (x_2, y_2, z_2) are within the new x''' - y''' plane and that (x_1, y_1, z_1) will have the new coordinates $(1, 0, 0)$ the following can be set up:

$$\begin{bmatrix} x_1 \\ y_1 \\ z_1 \end{bmatrix} = \begin{bmatrix} \cos \alpha_1 \cos \beta_1 \\ -\sin \alpha_1 \cos \beta_1 \\ -\sin \beta_1 \end{bmatrix}$$

$$\begin{bmatrix} x_1' \\ y_1' \\ z_1' \end{bmatrix} = \begin{bmatrix} \cos \alpha_1 & -\sin \alpha_1 & 0 \\ \sin \alpha_1 & \cos \alpha_1 & 0 \\ 0 & 0 & 1 \end{bmatrix} \begin{bmatrix} \cos \alpha_1 \cos \beta_1 \\ -\sin \alpha_1 \cos \beta_1 \\ -\sin \beta_1 \end{bmatrix} = \begin{bmatrix} \cos^2 \alpha_1 \cos \beta_1 + \sin^2 \alpha_1 \cos \beta_1 \\ \sin \alpha_1 \cos \alpha_1 \cos \beta_1 - \cos \alpha_1 \sin \alpha_1 \cos \beta_1 \\ -\sin \beta_1 \end{bmatrix} = \begin{bmatrix} \cos \beta_1 \\ 0 \\ -\sin \beta_1 \end{bmatrix}$$

$$\begin{bmatrix} x_1'' \\ y_1'' \\ z_1'' \end{bmatrix} = \begin{bmatrix} \cos \beta_1 & 0 & -\sin \beta_1 \\ 0 & 1 & 0 \\ \sin \beta_1 & 0 & \cos \beta_1 \end{bmatrix} \begin{bmatrix} \cos \beta_1 \\ 0 \\ -\sin \beta_1 \end{bmatrix} = \begin{bmatrix} 1 \\ 0 \\ 0 \end{bmatrix}$$

$$\begin{bmatrix} x_1''' \\ y_1''' \\ z_1''' \end{bmatrix} = \begin{bmatrix} 1 & 0 & 0 \\ 0 & \cos \gamma_1 & \sin \gamma_1 \\ 0 & -\sin \gamma_1 & \cos \gamma_1 \end{bmatrix} \begin{bmatrix} 1 \\ 0 \\ 0 \end{bmatrix} = \begin{bmatrix} 1 \\ 0 \\ 0 \end{bmatrix} \dots \text{Q.E.D.}$$

$$\begin{bmatrix} x_2 \\ y_2 \\ z_2 \end{bmatrix} = \begin{bmatrix} \cos \alpha_2 \cos \beta_2 \\ -\sin \alpha_2 \cos \beta_2 \\ -\sin \beta_2 \end{bmatrix}$$

$$\begin{bmatrix} x_2' \\ y_2' \\ z_2' \end{bmatrix} = \begin{bmatrix} \cos \alpha_1 & -\sin \alpha_1 & 0 \\ \sin \alpha_1 & \cos \alpha_1 & 0 \\ 0 & 0 & 1 \end{bmatrix} \begin{bmatrix} \cos \alpha_2 \cos \beta_2 \\ -\sin \alpha_2 \cos \beta_2 \\ -\sin \beta_2 \end{bmatrix} = \begin{bmatrix} \cos \alpha_1 \cos \alpha_2 \cos \beta_2 + \sin \alpha_1 \sin \alpha_2 \cos \beta_2 \\ \sin \alpha_1 \cos \alpha_2 \cos \beta_2 - \cos \alpha_1 \sin \alpha_2 \cos \beta_2 \\ -\sin \beta_2 \end{bmatrix}$$

$$\begin{bmatrix} x_2'' \\ y_2'' \\ z_2'' \end{bmatrix} = \begin{bmatrix} \cos \beta_1 & 0 & -\sin \beta_1 \\ 0 & 1 & 0 \\ \sin \beta_1 & 0 & \cos \beta_1 \end{bmatrix} \begin{bmatrix} \cos \alpha_1 \cos \alpha_2 \cos \beta_2 + \sin \alpha_1 \sin \alpha_2 \cos \beta_2 \\ \sin \alpha_1 \cos \alpha_2 \cos \beta_2 - \cos \alpha_1 \sin \alpha_2 \cos \beta_2 \\ -\sin \beta_2 \end{bmatrix} =$$

$$\begin{bmatrix} \cos \beta_1 \cos \alpha_1 \cos \alpha_2 \cos \beta_2 + \cos \beta_1 \sin \alpha_1 \sin \alpha_2 \cos \beta_2 + \sin \beta_1 \sin \beta_2 \\ \sin \alpha_1 \cos \alpha_2 \cos \beta_2 - \cos \alpha_1 \sin \alpha_2 \cos \beta_2 \\ \sin \beta_1 \cos \alpha_1 \cos \alpha_2 \cos \beta_2 + \sin \beta_1 \sin \alpha_1 \sin \alpha_2 \cos \beta_2 - \cos \beta_1 \sin \beta_2 \end{bmatrix}$$

It can now be noted that:

$$\tan \gamma_1 = \frac{\sin \beta_1 \cos \alpha_1 \cos \alpha_2 \cos \beta_2 + \sin \beta_1 \sin \alpha_1 \sin \alpha_2 \cos \beta_2 - \cos \beta_1 \sin \beta_2}{\sin \alpha_1 \cos \alpha_2 \cos \beta_2 - \cos \alpha_1 \sin \alpha_2 \cos \beta_2}$$

and that:

$$\begin{bmatrix} x_2''' \\ y_2''' \\ z_2''' \end{bmatrix} = \begin{bmatrix} 1 & 0 & 0 \\ 0 & \cos \gamma_1 & \sin \gamma_1 \\ 0 & -\sin \gamma_1 & \cos \gamma_1 \end{bmatrix} \begin{bmatrix} \cos \beta_1 \cos \alpha_1 \cos \alpha_2 \cos \beta_2 + \cos \beta_1 \sin \alpha_1 \sin \alpha_2 \cos \beta_2 + \sin \beta_1 \sin \beta_2 \\ \sin \alpha_1 \cos \alpha_2 \cos \beta_2 - \cos \alpha_1 \sin \alpha_2 \cos \beta_2 \\ \sin \beta_1 \cos \alpha_1 \cos \alpha_2 \cos \beta_2 + \sin \beta_1 \sin \alpha_1 \sin \alpha_2 \cos \beta_2 - \cos \beta_1 \sin \beta_2 \end{bmatrix}$$

$$= \begin{bmatrix} \cos \beta_1 \cos \alpha_1 \cos \alpha_2 \cos \beta_2 + \cos \beta_1 \sin \alpha_1 \sin \alpha_2 \cos \beta_2 + \sin \beta_1 \sin \beta_2 \\ \left\{ \begin{array}{l} \cos \gamma_1 \sin \alpha_1 \cos \alpha_2 \cos \beta_2 - \cos \gamma_1 \cos \alpha_1 \sin \alpha_2 \cos \beta_2 + \sin \gamma_1 \sin \beta_1 \cos \alpha_1 \cos \alpha_2 \cos \beta_2 + \\ + \sin \gamma_1 \sin \beta_1 \sin \alpha_1 \sin \alpha_2 \cos \beta_2 - \sin \gamma_1 \cos \beta_1 \sin \beta_2 \end{array} \right\} \\ \left\{ \begin{array}{l} -\sin \gamma_1 \sin \alpha_1 \cos \alpha_2 \cos \beta_2 + \sin \gamma_1 \cos \alpha_1 \sin \alpha_2 \cos \beta_2 + \cos \gamma_1 \sin \beta_1 \cos \alpha_1 \cos \alpha_2 \cos \beta_2 + \\ + \cos \gamma_1 \sin \beta_1 \sin \alpha_1 \sin \alpha_2 \cos \beta_2 - \cos \gamma_1 \cos \beta_1 \sin \beta_2 \end{array} \right\} \end{bmatrix}$$

$$\begin{aligned} z_2''' &= -\sin \gamma_1 (\sin \alpha_1 \cos \alpha_2 \cos \beta_2 - \cos \alpha_1 \sin \alpha_2 \cos \beta_2) + \cos \gamma_1 (\sin \beta_1 \cos \alpha_1 \cos \alpha_2 \cos \beta_2 + \\ &+ \sin \beta_1 \sin \alpha_1 \sin \alpha_2 \cos \beta_2 - \cos \beta_1 \sin \beta_2) = \\ &= -\sin \gamma_1 (\sin \alpha_1 \cos \alpha_2 \cos \beta_2 - \cos \alpha_1 \sin \alpha_2 \cos \beta_2) + \\ &+ \cos \gamma_1 \tan \gamma_1 (\sin \alpha_1 \cos \alpha_2 \cos \beta_2 - \cos \alpha_1 \sin \alpha_2 \cos \beta_2) = 0 \end{aligned}$$

...Q.E.D.

From $z_1''' = z_2''' = 0$ it follows that both vectors (x_1, y_1, z_1) and (x_2, y_2, z_2) are within the new $x'''-y'''$ plane.

Back transformation

When transforming back original coordinates, the procedure described above is performed in reverse order, α , β and γ angles represented with negative signs. The procedure is as described below:

Rotation 1:

$-\gamma_1$ degrees around the x''' -axis transforms (x''', y''', z''') back to (x'', y'', z'') .

Rotation 2:

$-\beta_1$ degrees around the y'' -axis transforms (x'', y'', z'') back to (x', y', z') .

Rotation 3:

$-\alpha_1$ degrees around the x' -axis transforms (x', y', z') back to (x, y, z) .

TRC proportions and confidence intervals

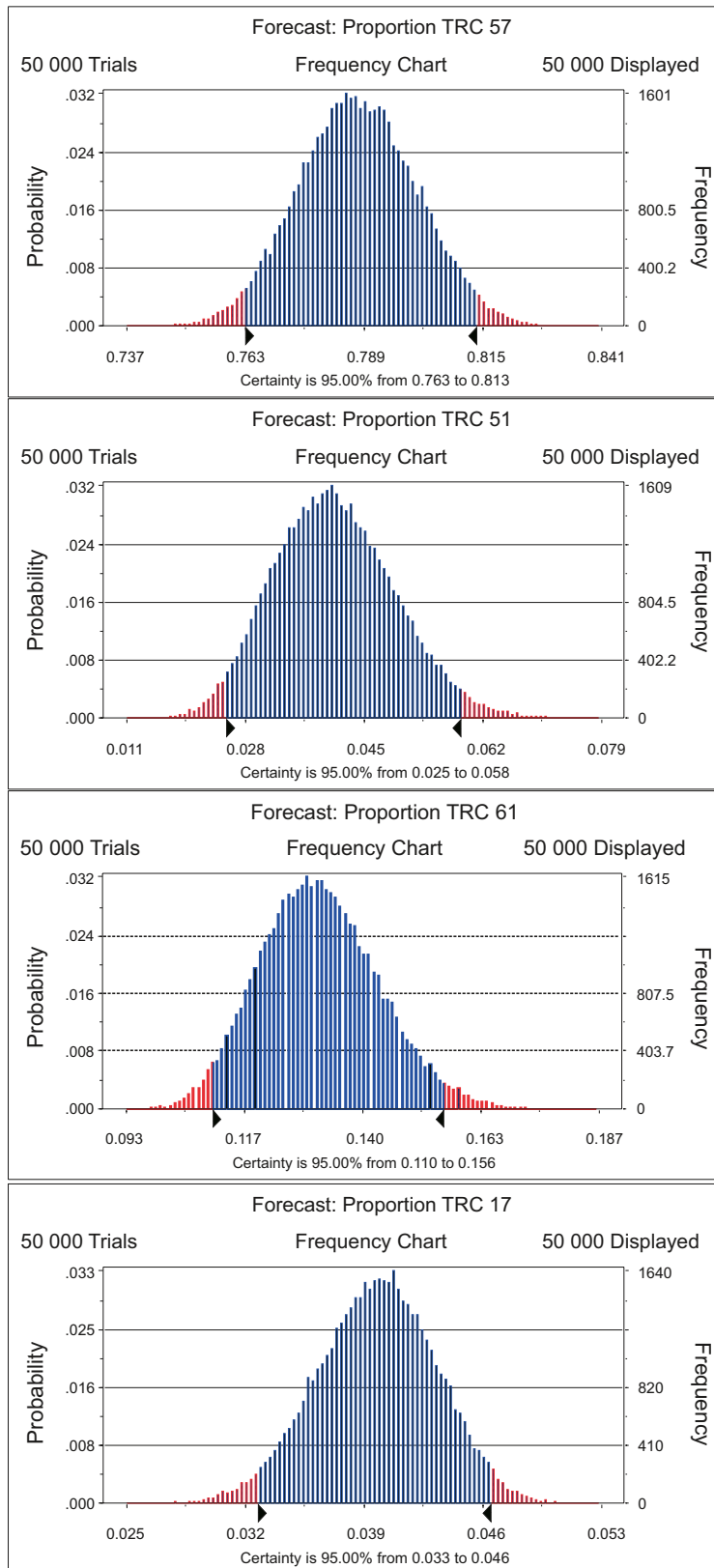


Figure E-1. Distributions of mean proportions of TRCs generated by the bootstrap method for domain RFM029 based on 0.1 m data from all boreholes within the target volume. 95% confidence intervals are indicated.

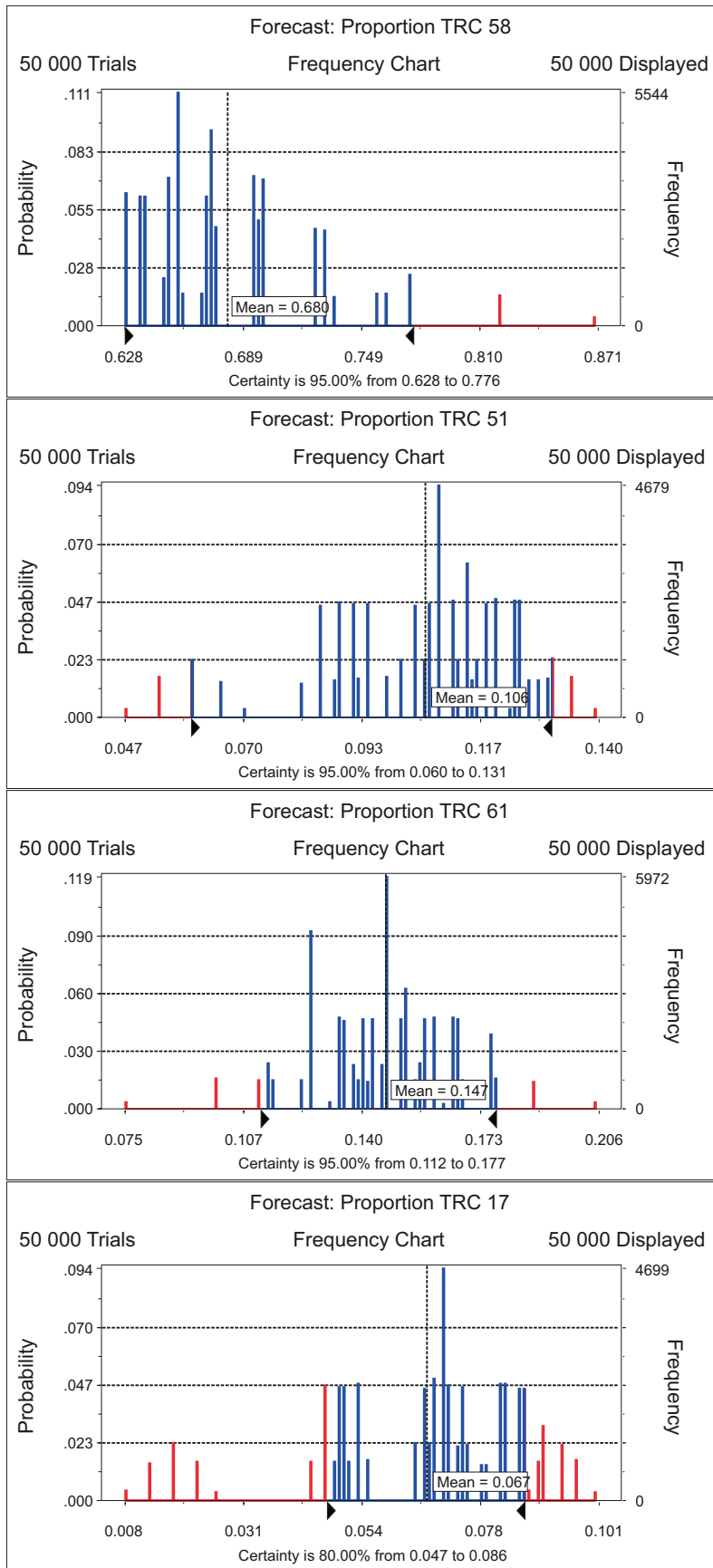


Figure E-2. Distributions of mean proportions of TRCs generated by the bootstrap method for domain RFM045 based on 0.1 m data from all boreholes within the target volume. 95% confidence intervals are indicated.